Modelling Scour Depth at Quay Walls due to Thrusters

MSc Thesis

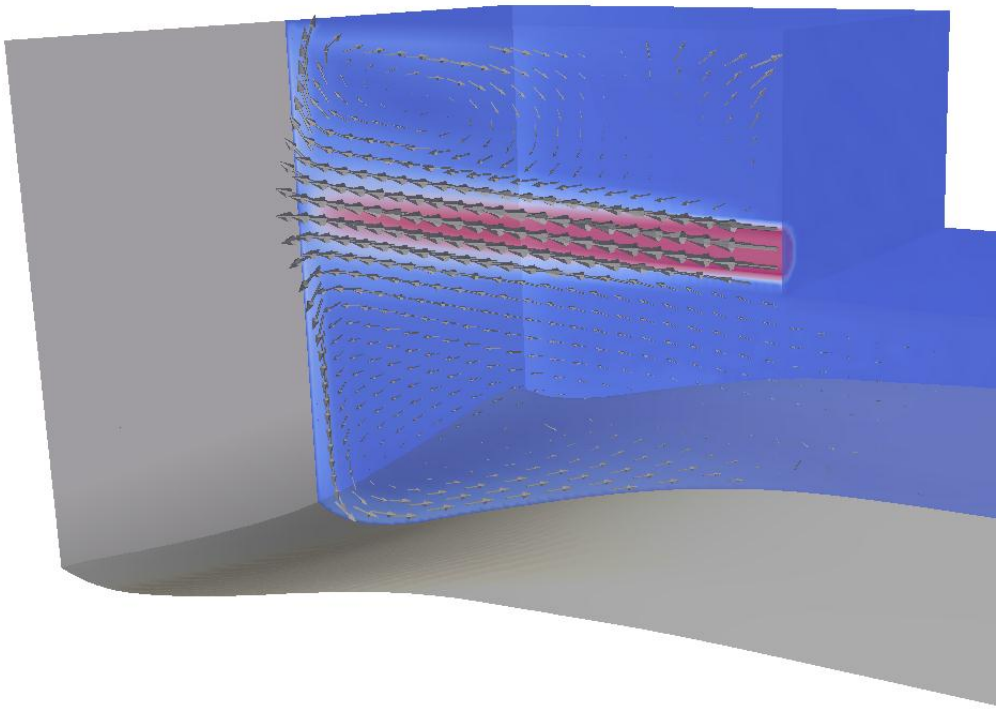

A.J.W. (Arjan) van den Brink

Delft University of Technology

Deltares

Modelling Scour Depth at Quay Walls due to Thrusters

A.J.W. (Arjan) van den Brink

Thesis submitted to the faculty of Civil Engineering of
Delft University of Technology in partial fulfilment of
the requirements of the degree

Master of Science

in

Hydraulic Engineering

Prof. ir. T. Vellinga	Delft University of Technology
Ir. H.J. Verheij	Delft University of Technology and Deltares
Ir. H.J. Verhagen	Delft University of Technology
Ir. T. Blokland	Rotterdam Municipality Engineering Department

Delft, 29 January 2014

Keywords: Scour, Bow Thruster, Soil Water Structure Interaction, CFD

Acknowledgments

This MSc Thesis is the final work of my master study Hydraulic Engineering at Delft University of Technology. In cooperation with the university and Deltares I studied, by means of a numerical model, the behaviour of local scour next to a vertical quay wall, caused by bow thrusters.

I would like to thank the members of the graduation committee Prof. ir. T. Vellinga, ir. H.J. Verheij, ir. H.J. Verhagen and ir. T. Blokland for their valuable advices and feedback. Especially I want to thank Henk Verheij and Teus Blokland for their adequate daily supervision and pleasant communication.

At last I want to thank my family and my fiancé Aliya, for their concern and great support during my full master study.

Delft, Januari 2014,

Arjan van den Brink

Summary

Inland and seagoing vessels are equipped with (bow) thrusters. The use of these thrusters can cause scour of the bed alongside a quay wall. In order to assess the consequences of local scour due to bow thrusters on the design of the structure and its bed protection it is desirable to know the dimensions of the scour holes and the behaviour of the scour development in time. Analytical relations for the calculation of scour, only determine the scour depth, but do not involve the remaining dimensions of the scour hole and the development of scour in time.

A three dimensional quasi-steady-state numerical model is developed which describes the scour development alongside a vertical quay wall induced by thrusters of a vessel that performs several departure manoeuvres at the same location. The flow simulations, using the Realizable k-ε Model in the Computational Fluid Dynamics package OpenFOAM, provide the flow properties near the bed in order to calculate the bed shear stress. In the flow simulation the influence of the rotation of the propeller is neglected. A boundary adjustment technique is applied in order to move the mesh near the bed. In case the critical shear stress is reached, the morphology plays a role and the bed changes. This critical shear stress and the bed change are calculated in Matlab, by applying an empirical relation for the erosion rate of sand, which is valid for both the high and low velocity regime of the flow. Every time step the bed level is updated and the hydrodynamics are calculated for the updated bed level, based on a steady state approach.

The hydrodynamics are validated separately from the model with erosion by applying a fixed (i.e. non-erodible) bed and comparing the results regarding flow velocity in the numerical model with physical experiments and analytical expressions. Several cases are elaborated with different distances between quay and ship, and keel clearances. It appears that for relative large distances between ship and quay the numerical model overestimates the near bed velocities. The erosion itself is validated with full scale tests regarding thruster induced scour, performed in the Port of Rotterdam. A maximum scour depth of 2.2 meter after 6 departures of the vessel is calculated with the numerical model, which is rather conservative compared to the measurements where a maximum depth of 1.75-1.85 meter is measured. The difference in results is probably due to presence of clay and silt in the Port of Rotterdam, however the numerical model is developed using an empirical relation for sand.

From a sensitivity analysis it appears that the maximum scour depth is sensitive for the amount of fine sediment which is present in the soil. Coherent with this the porosity of the soil and the dilatation of the soil during erosion plays an important role in the magnitude of the erosion velocity (i.e. velocity of the moving bed).

For further research it is recommended to improve the modelling of the propeller induced flow and to integrate this flow model with the current erosion model. Beside that an improved mesh near the bed is recommended. In this case flow properties, regarding flow velocity and turbulence, should most probably be averaged over the

water column in order to involve the higher order moments for the calculation of the extreme bed shear stresses. The length of this water column depends on the mixing length of the turbulence.

In addition, it is striking that the width of the scour hole in both calculations and measurements, are smaller than the width of common applied bed protections. From an economical point of view it might be interesting to assess whether the current bed protection design is not too conservative.

Table of Content

1 Introduction

1.1 Background and motivation

For several decades inland and seagoing vessels are equipped with (bow) thrusters in order to increase the manoeuvrability of vessels in ports. Due to the increasing dimensions of those vessels, the power of the thrusters is also increasing to ensure this manoeuvrability. This development is responsible for an increasing load on bed protections in ports. An important issue is the increasing load on the bed near inclined and vertical quay walls. This load might cause serious damage of the bed (protections), which endangers the stability of hydraulic structures like quay walls.

To ensure a stable quay wall, two design strategies are possible. (1) One way is to design a bed protection. (2) The other way is to allow scour and guarantee stability by sufficiently deep drilled sheet pile walls and monitoring the scour development. From an economical point of view it might be possible that a deeper drilled quay wall will be cheaper than constructing a (heavy) bed protection. To assess the economical equilibrium it is important to know how the scour hole develops in time and what the maximum scour depths are.

The flow field induced by (bow) thrusters in the vicinity of both vertical and sloped quay walls is studied before. [Van Blaaderen, 2006] compared the difference of results in his numerical model, using Computational Fluid Dynamics, with the physical model build by [Van Der Laan, 2005] and measured by [Nielsen, 2005]. In addition [Van Doorn, 2012] performed scale model tests of a container vessel (propeller) with a focus on hydraulic load due to bow thrusters on a non-erodible slope. The velocity field and the hydraulic loads are emphasized in the research of Van Doorn. The scour near the bed is not investigated.

Other researches like [Römisch, 2012], [Schmidt, 1998] and [Hamill et al. 1999] examined the scour near quay walls with physical models. Analytical expressions to estimate the maximum scour depth as function of amongst others the near bed velocity are derived for both bow- and stern thrusters. In the study of [Römisch, 2012] the scour depth is derived, but the development of the scour in time is not taken into account. It might be useful to know more about the development of scour in time for proper monitoring of the scour in ports.

Recently full scale tests have been performed with two inland vessels in the Port of Rotterdam [Blokland, 2013]. This is a unique research regarding this topic, since the scour development is usually only investigated by means of scale models with vessels on a fixed location. In these tests the scour depth is measured for different numbers of departures, i.e. as function of time. Furthermore, during the full scale test different vessels with different thrusters and applied power are used. The thruster induced scour is measured along the quay wall. Measurements of the flow velocity field are not performed.

In this thesis a three-dimensional (3D) numerical model for the scour development in time due to bow thrusters is elaborated, since the scour development in time is not studied by means of a numerical model before. The experiments in the Port of Rotterdam give the opportunity to validate the numerical model [Blokland, 2013].

This study is focused on the erosion process due to the high flow velocities near the bed. In order to do so a velocity field is required. However, the goal is not to develop a model which represents a detailed outflow of the jet induced by the bow thruster like [Van Blaaderen, 2006] did. The emphasis regarding the velocity field in this thesis is on the near bed velocities.

1.2 Problem formulation

The problem is formulated as a research question, which will be divided into sub-questions in section 1.4.

Problem formulation: *What are the dimensions of the scour hole due to thrusters near a vertical quay wall as a function of time and number of departures and particularly what is the maximum depth of this scour hole?*

1.3 Objective

The objective of this research is *to establish a three dimensional (3D) numerical model which describes the scour development induced by thrusters after a certain number of departures of a vessel near a vertical quay wall*.

1.4 Research questions

The research questions following from the problem definition are as follows:

1. What is the velocity field and the flow velocities near the non-erodible bed in the numerical model as function of keel clearance, distance between vessel and quay, and operation time?;
2. What are dimensions of the scour hole in the numerical model as function of time as result of the interaction between flow and sand bed, and is an equilibrium scour depth reached?;
3. Do the results of the numerical model regarding scour hole dimensions agree with the measurements of the full scale tests in the Port of Rotterdam?;
4. What is the interaction between flow and scour in the numerical model as function of different soil properties and applied power of the bow thruster?

1.5 Outline

In the numerical model the hydrodynamics are calculated with Computational Fluid Dynamics (CFD) software OpenFOAM, using a simplified jet and calibrating the model to obtain realistic near bed velocities. The calculation of the erosion is decoupled from the model in OpenFOAM. The flow properties near the bed are used to calculate the bed shear stress resulting in the displacements of the bed (i.e. the erosion) for a single time step with Matlab using an empirical formulation. The updated bed level is implemented in the next time step of the numerical model in OpenFOAM, to calculate the hydrodynamics for the deformed bed (see Figure 1.1).

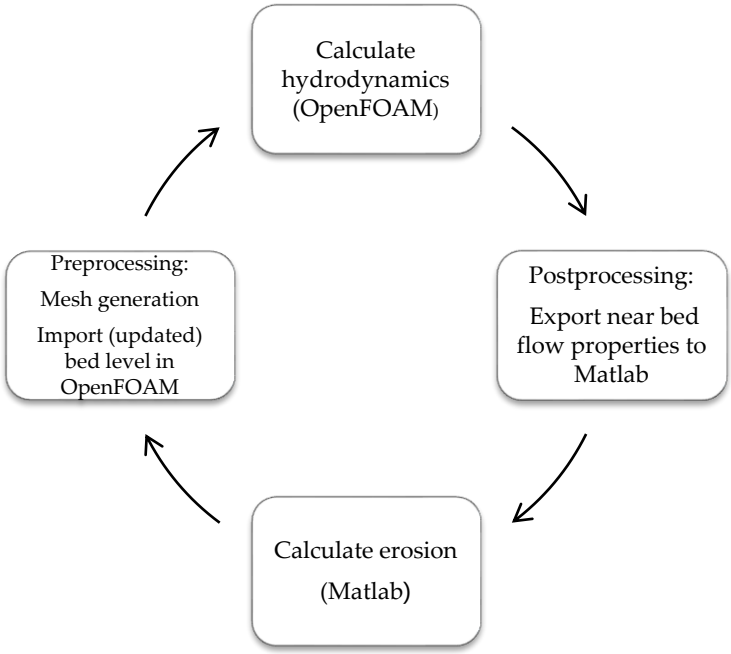

Figure 1.1 Calculation cycle of the numerical model

This thesis consists of three main parts. First of all an overview of the literature is presented which might be required to go through the calculation steps in Figure 1.1. The second part describes the model and assumptions. In the last part of the report an overview of the results is given by means of a sensitivity analysis.

In chapter 2 the literature is described which is used in this research. Background information which is not directly applied in the model is presented in Appendix A. In chapter 3 the flow field of the numerical model is described with a flat and fixed bed (i.e. no erosion). The reason for this is to validate the near bed velocities with help of physical scale tests of [Schmidt, 1998] and an analytical expression which estimates the maximum near bed velocity [PIANC, 2012]. In chapter 4 the numerical model with an erodible bed is described which is going through all the steps of the cycle in Figure 1.1. In addition calculation results are given after six departures of the vessel. After that in chapter 5 the sensitivity analysis is described with the results following from this analysis. The last chapter contains conclusions and recommendations in order to answer the research questions.

2 Literature

2.1 Introduction to elaborated literature

This chapter mainly describes the literature which is used for developing the numerical model, in order to model the 3D development of the scour hole in time due to thrusters. The literature study is divided in such a way, that it gradually walks through the loop which is made in order to compute the scour and to validate the model (Figure 2.2).

In most studies for local scour CFD based models are applied. [Melling, 2013] made a distinction between two fundamentally different types of CFD modelling in which morphological interactions are involved (Figure 2.1):

1. *Mesh deformation techniques*: In this method flow simulations are coupled with empirical morphological relations. The flow simulations provide the shear stress near the bed. In case the critical shear stress is reached the morphology plays a role and the bed changes. In this way, a moving bed mesh is developed. Another common method is based on sediment transport theory where bed load transport and/or suspended sediment transport plays a role.
2. *Multiphase models*: In these types of models fluid-solid and solid-solid interactions are taken into account and no empirical morphological relations have to be applied.

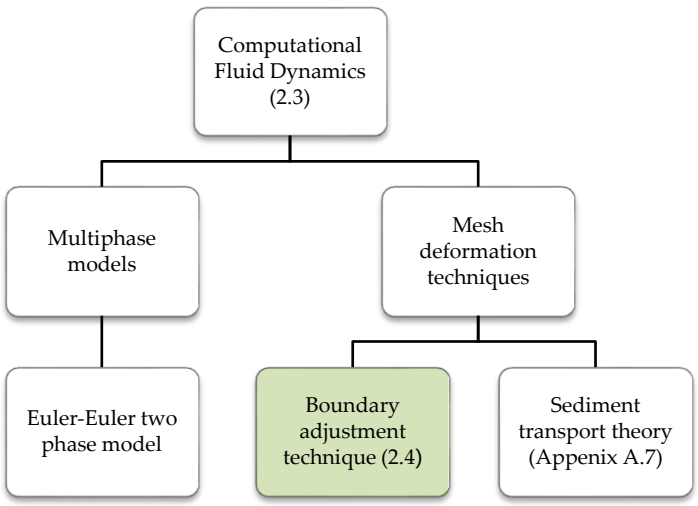

Figure 2.1 Approaches for CFD based scour modeling [Melling, 2013]

A similar method as the mesh deformation techniques is applied in this study. However, in this thesis the mesh deformation and the flow are not directly coupled within the CFD software. The flow is calculated using OpenFOAM and the mesh deformation is calculated with an empirical relation in Matlab using the flow parameters near the bed. Both models are connected.

The basic procedure to model scour by mesh deformation techniques is depicted in Figure 2.2 in the dashed block indicated with '*computational model for scour prediction*'. The outflow velocity due to the bow thruster is an important boundary condition which provides the input for the hydrodynamic model. A suitable formulation to calculate the efflux velocity and flow field of the bow thruster is presented in section 2.2. For the computation of the hydrodynamics, explanation is given regarding the applied turbulence model and software in section 2.3. The hydrodynamic calculation provides the flow properties in order to determine the bed shear stress and to calculate the scour, which is described in section 2.4. In order to validate the model, experimental data is used and elaborated in section 2.5. Finally, in section 2.6, conclusions following from this literature study are drawn regarding the applied theory for the hydraulic modelling, scour modelling and software.

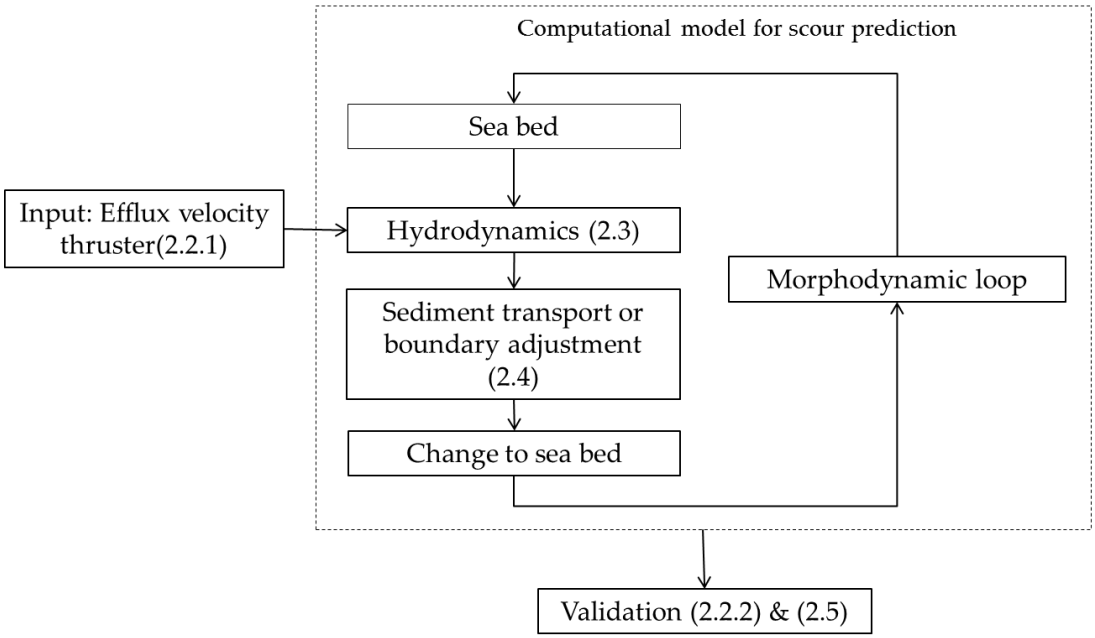

Figure 2.2 Overview of literature study, figure based on [Whitehouse, 1998]**.**

2.2 Velocity distribution due to thruster jets

There are different types of propulsion systems which also result in a diversity of behaviour of the velocity field. The most common propulsion systems are main propellers and bow thrusters, depending on the type of vessel.

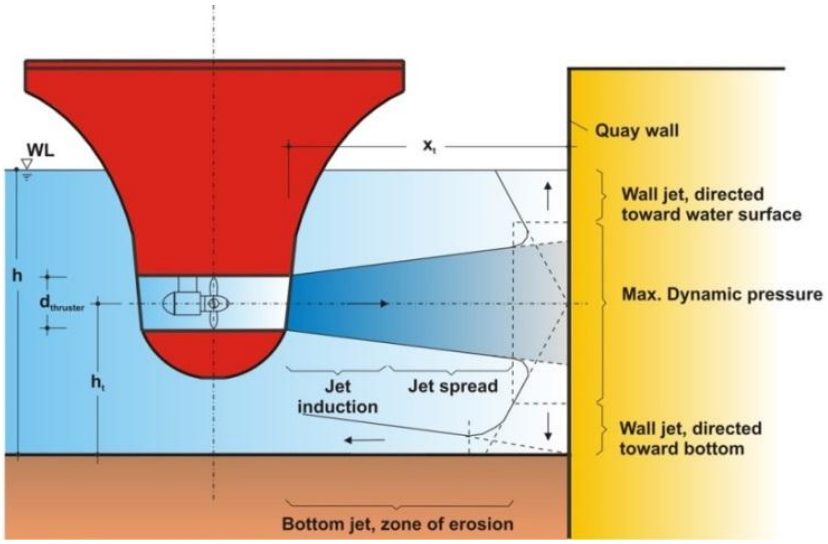

Figure 2.3 Relevant area in the flow field of a bow thruster

The propeller jet cause a turbulent and swirling flow velocity field which is influenced by the bed or quay wall. In this chapter the velocity distribution with and without lateral boundaries or walls are discussed. The influence of rudder and the turbulent flow induced by the propeller are neglected.

2.2.1 Free jet velocity distribution

The free velocity distribution due to the thruster is Gaussian or normal distributed around the axis as depicted in Figure 2.4. [PIANC, 2012] defines a free jet as follows: *"A free jet is defined as the water flowing out of an orifice into the surrounding water without any disturbance by lateral boundaries or walls that may hinder the spreading of the jet."*

The Gaussian distribution of the velocity profile can be used for a qualitative comparison of the flow velocity profile in the numerical model. The figure shows that the jet is spreading (i.e. the jet becomes wider) and the maximum velocity in the jet is decreasing with increasing distance from outflow opening of the thruster. The radial spreading is amplified for a jet by the presence of a propeller. In case of a pressure jet without a propeller, there will occur radial spreading, but this spreading is smaller.

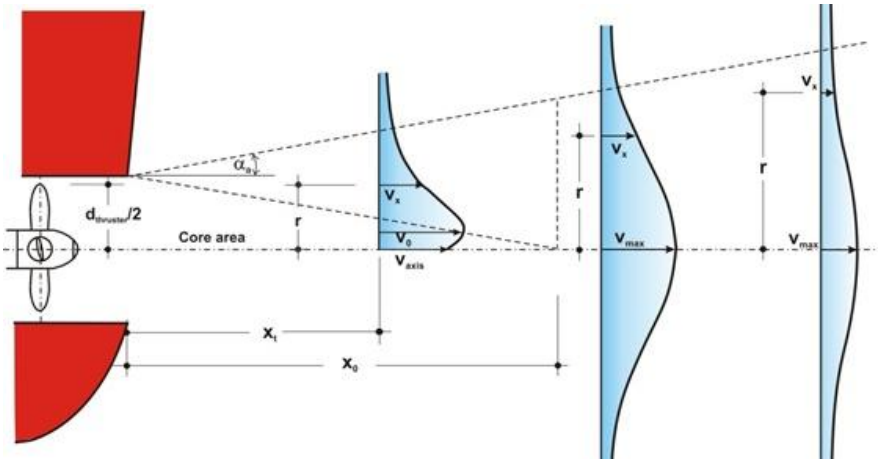

Figure 2.4 Velocity distribution induced by a bow thruster

[Van Doorn, 2012] cites Blaauw and Van der Kaa (1978) who presented formulations for the efflux velocity V_0 as a function of the (applied) power P_0 in [kW] and the diameter of the propeller duct D_0 in [m]. One of the expressions to determine the efflux velocity is eq. (2.1).

$$V_0 = \zeta \cdot 1.17 \left(\frac{P_0}{\rho D_0^2} \right)^{\frac{1}{3}} \quad (2.1)$$

Where ζ is a factor for energy loss in the channel system of the thruster.The advantage of this expression is that it is a function of the applied power and the diameter of the propeller duct. This simplifies the validation of the numerical model since those parameters are known for the full scale tests of [Blokland, 2013] in contrary to e.g. parameters for rotational speed and the propeller thrust coefficient which is, according to [Van Doorn, 2012], used in other expressions for the efflux velocity of Blaauw and Van der Kaa (1978).

2.2.2 *Bed velocity near vertical quay wall*

German and Dutch researchers developed expressions for the bed velocity near inclined and horizontal quay walls, to design the bed protection near quays. The Dutch method for vertical quay walls is applied for validation of the numerical model, beside other experimental data (section 2.5).

According to [PIANC, 2012] the Dutch method is based on research by Blaauw and Van de Kaa (1977), Verheij (1983), Blokland (1996) and Blokland (1997) and is formulated in eq. (2.2).

$$V_{b,max} = \begin{cases} 1.0 V_0 \left(\frac{D_0}{h_p} \right) for \frac{L}{h_p} < 1.8 \\ 2.8 V_0 \left(\frac{D_0}{L + h_p} \right) for \frac{L}{h_p} > 1.8 \end{cases} \quad (2.2)$$

Where $V_{b,max}$ is the maximum near bed velocity, V_0 is the outflow velocity of the jet, L is the distance between outflow opening and quay wall, D_0 is the diameter of the propeller duct and h_p is the distance from the propeller axis to the bed.

These equations are empirically determined for a free or ducted propeller. In case the flow of a bow thruster is going through a long channel, the characteristics of the jet after leaving the channel can deviate from these of a jet behind a free or ducted propeller: the characteristics of a channel bow thruster jet will probably be more like these of a pipe jet. This means that the thruster jet out of a long channel probably will show less radial spreading than a normal propeller jet. This means that eq. (2.2) in case of a thruster with a long channel possible gives no correct description of $V_{b,max}$.

The German method, which is elaborated in detail in Appendix A.2, is not used for validation of the maximum near bed velocity, since this method results in unrealistic values for the near bed velocities. For example for a quay clearance (i.e. distance between thruster and quay wall) of 5 meter, a keel clearance of 4 meter and applied power of the thruster of 320 kW (equivalent to an outflow velocity of the thruster of about 8 m/s) the near bed velocity of the German method is 3.4 m/s and for the Dutch method 1.6 m/s. This difference is significant and probably due to the fact that both the Dutch and the German method are developed in order to design the bed protection based on the near bed velocity, instead of giving realistic results for the near bed velocity itself. This means that the combination of formulas for the bed protection and the maximum near bed velocity lead to similar results for the bed protection design. That is why [PIANC, 2012] recommends to prevent interchanging the formulas in the Dutch and German method.

Also the Dutch method has its limitations since it only provides the maximum near bed velocity and not the velocity profile near the bed. However, this is the only method available for direct comparison and validation of a full scale numerical model. Experimental data regarding the velocity profile near the bed is available from physical scale models, which is explained in section 2.5.1.

2.3 Turbulence modelling and software

2.3.1 Turbulence models

The turbulence model is divided into two regions, the outer turbulent zone or core flow and the wall layer as depicted in Figure 2.5. For the modelling of the outer turbulent zone the Realizable k-ε model is applied. Near the wall the gradients of properties of the fluid are much higher compared to the core region of the flow, which requires wall functions to avoid a very fine mesh.

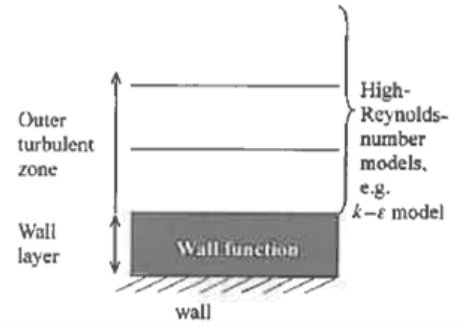

Figure 2.5 Two zones in the applied turbulence model [Andersson, 2012]

2.3.1.1 Core flow (outer turbulent zone)

In CFD an extended variety of models are available. The biggest part of those models are RANS-based (Reynolds Averaging Navier Stokes) and another way of modelling is LES (Large Eddy Simulation), which can be more accurate but is also more time consuming. A schematic overview of the available models is depicted in Figure 2.6.

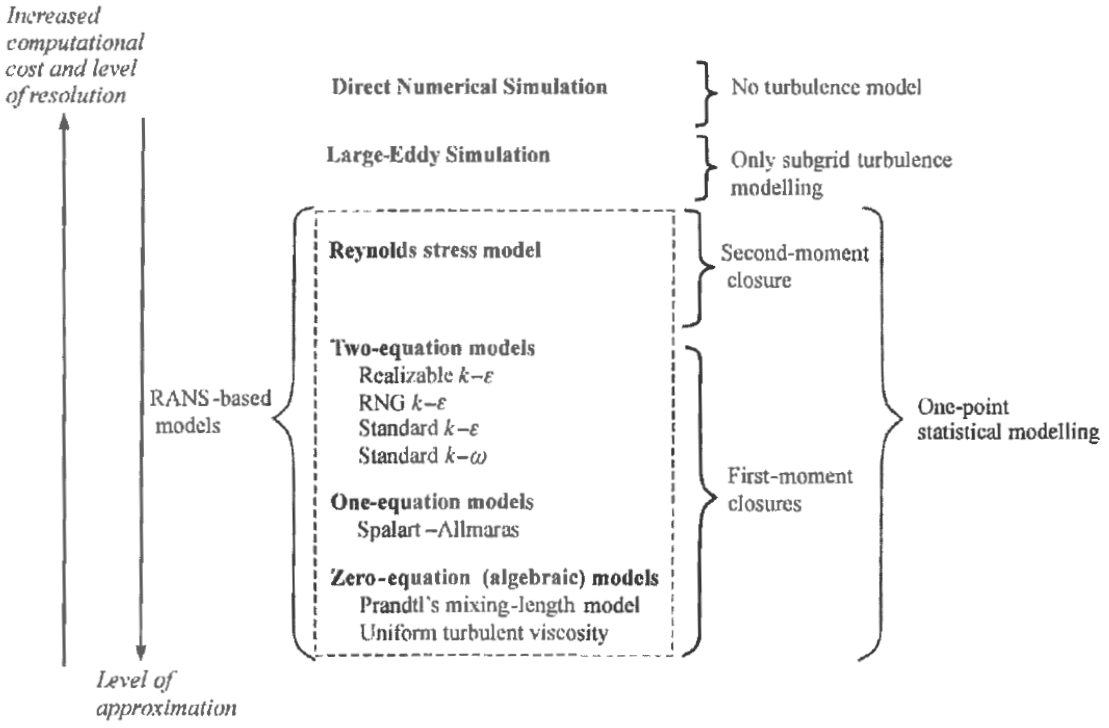

Figure 2.6 Schematic overview of turbulence modelling [Andersson, 2012]

In CFD one of the most popular models is the Standard k-ε turbulence model due to a good balance in generality and economy for CFD problems. The model is validated for a wide range of applications in order to calculate thin shear layer and recirculating flows, which explains the popularity of the model. The k-ε model is a so called two-equation model, is RANS-based and uses five closure coefficients ($C_\mu, C_{\varepsilon 1}, C_{\varepsilon 2}, \sigma_k$ and σ_ε) in order to close the two equations for the turbulent kinetic energy k and the energy dissipation ε. These coefficients are assumed to be universal. However, for specific flows with for example swirling and separating flow these coefficients can vary depending on the type of flow.

A variation on the Standard k-ε model is the Realizable k-ε model. The model provides improved simulations for swirling flows and flow separations, which enables to handle round jets. The model is improved by considering the closure coefficient C_μ not as a constant but a variable. This means that C_μ is a function of the local state of the flow to ensure that the normal stresses are positive under all flow conditions. Analysing the components of the normal components of the Reynolds stress tensor that follows from the Boussinesq approximation, it becomes clear that the normal stress can become negative for a *constant* closure coefficient C_μ in case the strain becomes too large:

$$\langle u_i u_i \rangle = \sum_i \langle u_i^2 \rangle = \frac{2}{3}k - 2\nu_T \frac{\partial \langle U_i \rangle}{\partial x_j} \qquad (2.3)$$

where

$$\nu_t = C_\mu \frac{\nabla U \sqrt{k}}{\varepsilon} \qquad (2.4)$$

However, a negative normal stress is not possible by definition, since the normal stresses are defined as the sum of squares. The Realizable k-ε model uses a *variable* C_μ so this will never occur.

2.3.1.2 Near wall treatment

Near the walls the gradients regarding velocity and turbulence properties are much higher compared to the core region of the flow. This means that the discretization procedures, which are used in the core flow, are not suitable for solving the near wall flow. [Bredberg, 2000] explains that the standard method to calculate the turbulence in a near wall region is to apply a very fine mesh close to the wall, to resolve the flow. From an engineering point of view this is not desirable because it is causing high computational costs. To avoid this problem, functions for the near-wall region are introduced to reduce the computational time considerably.

In general there are two types of implementations in a finite volume code regarding wall functions. The first type is to add a source term in the momentum equations and the second type is to modify the turbulent viscosity in cells next to the wall. The applied functions in OpenFOAM are from the second type which is described in more detail in section 4.2.3.

2.3.2 Software

Several software packages are considered to create a numerical model. OpenFOAM is found to be the most suitable choice for this study. The advantages of OpenFOAM are explained below. For a broader overview of the considered software packages is referred to Appendix C.

OpenFOAM is a free and open source CFD code and is primary designed for problems in continuum mechanics. [Liu & García, 2008] used OpenFOAM as well for three-dimensional numerical model with free water surface and mesh deformation for local sediment scour where the model FOAMSCOUR is developed.

There are several advantages using OpenFOAM in this research. The advantage lies in a combination of the fact that OpenFOAM is applicable for non-hydrostatic (CFD) models, it is an open source software and there is both online support and support from Deltares and TU Delft.

The advantage of the fact that OpenFOAM is open source is that the software is for free contrary to e.g. FLUENT and the source code is accessible for the user. This implies that OpenFOAM can be adapted on each level of the computation for a specific situation. For example, one can think about both the numerical issues like numerical schemes, numerical solvers and the meshing but also the physical properties, turbulence models and boundary conditions. All those aspects of the software can be adapted or even developed from scratch. However, developing software requires at least basic knowledge of C++, since this is the basic language of OpenFOAM.

In OpenFOAM a wide variety of solvers, numerical schemes, boundary conditions and CFD models and mesh generation tools are already implemented and can be applied relatively easy once you are familiar with the software. The CFD models vary from RANS to LES and offer the opportunity to work with multiphase models (e.g. air and water). The access to the source code also enables the user to understand the possibilities and the limitations of specific tools in OpenFOAM. Beside this OpenFOAM gives the opportunity for post processing with other software like Matlab or Python. This enables the user to establish an interaction between different types of software.

Matlab is used to implement the morphological relations in the model. By disconnecting the hydrodynamics and the morphological calculations the programming of the numerical model itself can be simplified.

Within TU Delft Faculty Electrical Engineering, Mathematics and Computer Science and also online, several tutorials are available to get familiar with the CFD package. The only limitation in the use of OpenFOAM lies in the amount of time available to introduce to the software, C++ programming knowledge of the user and the absence of an interface which can discourage the user to apply the software. Also it is important to be aware that OpenFOAM only operates on Linux systems.

Nevertheless, it can be concluded that OpenFOAM offers a great variability in the use for a specific situation and enables the user to modify and adapt the model in a way which fits in the topic and the objective of the research.

2.4 Morphological relations

A mesh deformation technique is applied in this study to model the local scour due to bow thrusters by using a boundary adjustment technique. The morphological relations which are found in this study and which can be related to local scour due to high flow velocities only concern boundary adjustment techniques. The sediment transport theory is explained in Appendix A.7. Multiphase models are not considered for this study. The advantage of multiphase models is that no empirical relations are required. However, for multi-phase modelling regarding scour it is required to develop a suitable solver in the CFD software. This way of modelling is expected to be beyond the time frame and engineering scope of a MSc Thesis regarding local scour problems.

2.4.1 Erosion rate

Boundary adjustment techniques are used to calculate the bed level change based on local sedimentation and erosion (entrainment), instead of the gradient in sediment transport. The flow simulations provide the shear stress near the bed. In case the critical shear stress is reached the morphology plays a role and the bed changes.

2.4.1.1 Erosion mechanism – permeability and dilatancy

In general several expressions for the calculation of the erosion, e.g. the one from Van Rijn, are validated for bed loads due to relative low flow velocities (about 1 m/s). In general those formulas overestimate the erosion for higher flow velocities. In the particular case of this research regarding scour due to bow thrusters, the velocities can reach values of about 8 m/s, depending on the type of propulsion system of the vessel. The formulation of [Van Rhee, 2010] for the erosion is valid for both the lower and the higher velocity regime since the influence of the permeability and dilatancy is taken into account. This is achieved by modifying the critical Shields parameter. A comparison between the erosion rate calculated by Van Rijn and by Van Rhee is depicted in Figure 2.7.

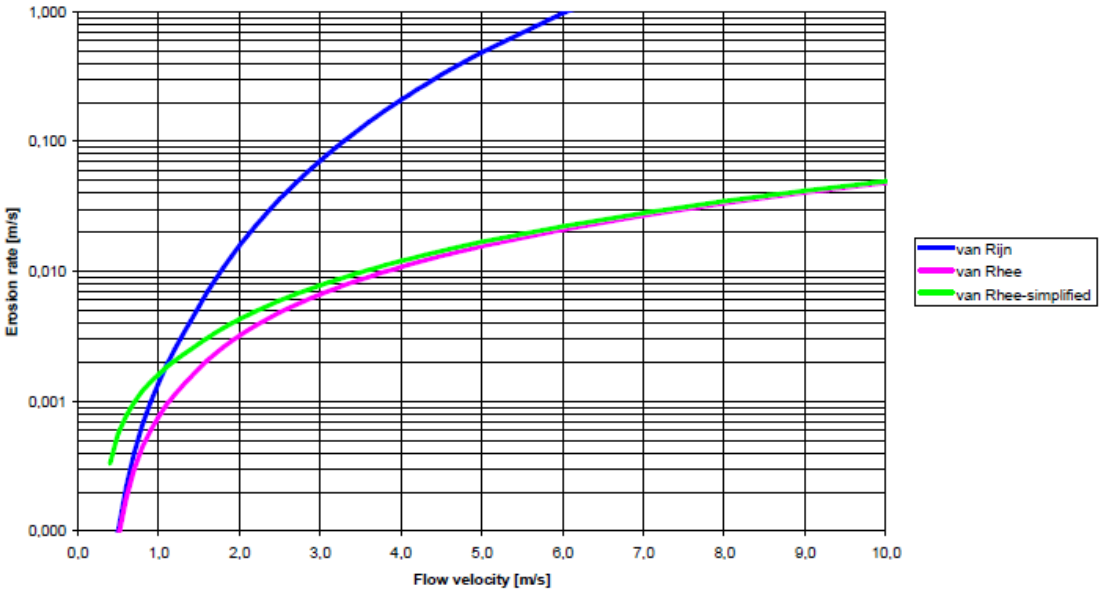

Figure 2.7[1] Comparison of erosion rate according to Van Rijn and Van Rhee [Bisschop et al., 2010]

The expansion (or dilatation) of the volume will proceed till a certain value of the porosity. In other words, when the sediment is exposed to high shear velocities, the particles can only be picked up when the top layers are in a state of sufficiently low porosity n_l. The dilatation of the soil volume will force the water to flow into the pores between the particles which cause a hydraulic gradient which hinders the erosion.

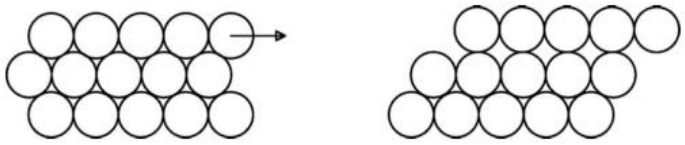

Figure 2.8 Increase in pore volume due to shear [Van Rhee, 2010]

Another advantage of formulation of Van Rijn is that the effects on sediment transport on a sloping surface are taken into account.

[Mastbergen & Van Den Berg, 2003] made use of the same approach as described above, i.e. the effects of an hydraulic gradient due to dilatancy on a sloping face are taken into account. [Mastbergen & Van Den Berg, 2003] validated their findings; however, the authors stated that the very high flow velocity regime is beyond the scope of the research.

2.4.1.2 Validation - [Van Rhee, 2010]

Van Rhee validated the expression for the erosion rate for the (very) high flow velocity regime using two types of research.

---

[1] The green line in the figure representing 'van Rhee-simplified' can be ignored, since this expression is not used in this research. This relation is derived from the formula of Van Rhee by [Bisschop et al., 2010] and is only valid for the very high velocity regime of the flow.

(1) The research in the Delft Hydraulics Erosion flume which are carried out by the Dutch dredging industry by WL|Delft Hydraulics, which involved erosion of a sand bed in a closed flume. In fact the flow velocities in the flume were also low; however, clay was added in five experiments to reduce the permeability. The condition under which the influence of permeability becomes significant is derived by Van Rhee.

$$\frac{v_e}{k_l} > 3 \qquad (2.5)$$

Where v_e is the erosion velocity of the downward moving bed and k_l is the permeability. So in fact eq. (2.5) defines whether the flow is in the high-velocity regime. In this experiment in the Delft Hydraulics Erosion flume the ratio between erosion velocity and permeability varied from 5 – 60.

(2) For the other part of the validation [Van Rhee, 2010] used data from [Roberts et al., 1998]. These authors performed experiments in a flume to determine the effects of particle size and bulk density of the bed on the erosion of quartz particles. The reason for this validation is mainly to validate a larger data set for a larger range of particle sizes.

2.4.1.3 Applied theory[2] - [Van Rhee, 2010]

[Van Rhee, 2010] gives an expression for the velocity v_{sed} of the moving bed due to erosion or sedimentation. This expression is based on the near bed concentration c_b and the concentration of sediment in the settled bed. Equating the volume of particles moving through the interface to the volume of particles stored in the bed leads to the velocity of the upward moving bed and can be written as:

$$v_{sed} = \frac{S - E}{\rho_s(1 - n_0 - c_b)} \qquad (2.6)$$

Where S is the settling flux [kg/m²/s], E is the entrainment rate or pick-up flux [kg/m²/s], ρ_s is the density of particles [kg/m³], n_0 is the porosity of the settled bed [-], and c_b is the near-bed volumetric concentration [m³/m³]. The settling flux is given by:

$$S = \rho_s w_s c_b \qquad (2.7)$$

Where w_s is the settling velocity of the particles in [m/s]. The settling of the sediments is described here since it is taken into account in the approach of [Van Rhee, 2010], however in this thesis the effects of settling sediment are neglected.

The entrainment rate will be bigger than zero when the bed shear stress exceeds a certain threshold value, which is expressed by the critical Shields parameter $\Psi_{s,cr}$, where $\Psi_{s,cr}$ is a function of the particle size d, and its value is found with the Shields curve. The relation between sediment pickup and the Shields parameter is known as a pick-up function, which is physically derived by Van Rijn (1984) and reads as follows:

---

[2] The equations mentioned in this subsection and which are implemented directly in the numerical model, are indicated with a * in the equation numbering, e.g. (2.9)*.

$$\Phi_p = \frac{E}{\rho_s\sqrt{\Delta g d}} = 0.00033 D_*^{0.3}\left(\frac{\Psi_s - \Psi_{s,cr}}{\Psi_{s,cr}}\right)^{1.5} \quad (2.8)$$

where D_* is defined as a dimensionless particle diameter.

$$D_* = D_{50}\cdot\sqrt[3]{\frac{\Delta g}{\nu^2}} \quad (2.9)^*$$

The expression from Van Rijn is validated for relative low flow velocities. Van Rhee proposed and validated a method for the pick-up rate due to higher velocities including the stability of particles on a sloping surface with an hydraulic gradient. By using a modified critical Shields parameter $\Psi^1_{s,cr}$ the stability criterion in eq. (2.10) is proposed for high velocities, by applying an extra force acting on the particles due to an inward directed hydraulic gradient.

$$\Psi^1_{s,cr} = \Psi_{s,cr}\left(\frac{\sin(\phi-\beta)}{\sin\phi} + \frac{v_e}{k_l}\cdot\frac{n_l - n_0}{1-n_l}\frac{A_1}{\Delta}\right) \quad (2.10)^*$$

In this expression v_e is the erosion velocity (i.e. velocity of the downward moving bed) perpendicular to the bed, k_l is the permeability of sediment bed at minimum compaction eq. (2.11), n_l is the bed porosity in loose conditions, estimated as maximum porosity n_{max}, n_0 is the bed porosity prior to erosion, A_1 is a coefficient for which $A_1 = 3/4$ for single particle mode and $A_1 \approx 1.7$ for a continuum mode, and Δ is the relative sediment density $= (\rho_s - \rho)/\rho$. In the single particle mode the particle itself is analysed, and in the continuum mode the stability of a small block of soil is considered.

$$k_l = C_k\frac{g}{\nu}D_{15}^2\frac{n_l^3}{(1-n_l)^2} \quad (2.11)^*$$

Where $C_k = \frac{1}{160}$ is a constant.

[Mastbergen & Van Den Berg, 2003] also used the factor $(n_l - n_0)/(1-n_l)$ to take the effects of the increasing porosity into account. In this research it is stated that $(n_l - n_0)/(1-n_l)$ represents the porosity increase of the sand bed from undisturbed to loose conditions.

It is difficult to determine the value for n_l. Van Rhee suggested the following to estimate n_l: *"We therefore took the maximal porosity* $\mathrm{n_{max}}$ *(which can be determined from geotechnical tests) as the best estimate of* $\mathrm{n_l}$*. This is not unreasonable since the porosity will have to be increased above the critical density to bring the sediment bed into such a fluid state that it can be picked up by the flow."*

The critical parameter is calculated according to [Shields, 1936]. A smooth fit to the Shields curve was according to [Van Rhee, 2010] given by Brownlie (1981):

$$\Psi_{s,cr} = 0.22\boldsymbol{R}_p^{-0.6} + 0.06\exp(-17.77\boldsymbol{R}_p^{-0.6}) \quad (2.12)^*$$

Where $\boldsymbol{R}_p$ is the Reynolds number for the particles, here defined as

$$\boldsymbol{R}_p = \frac{D_{50}\sqrt{\Delta g D_{50}}}{\nu} \quad \textbf{(2.13)*}$$

The modified critical Shields parameter is used in eq. (2.8) to obtain the modified pick-up function for high flow velocities, which results in eq. (2.14).

$$\Phi_p^1 = 0.00033 D_*^{0.3} \left(\frac{\Psi_s - \Psi_{s.cr}^1}{\Psi_{s,cr}^1} \right)^{1.5} \quad \textbf{(2.14)*}$$

The following expression for the erosion velocity of the bed caused by extreme high flow velocities is derived.

$$\frac{1}{1 - n_0 - c_b} \left(\Phi_p^1 \sqrt{g \Delta D_{50}} - c_b w_s \right) - v_e = 0 \quad \textbf{(2.15)}$$

This expression is implicit and needs to be solved numerically, since the modified critical Shields parameter Φ_p^1 is function of $\Psi_{s,cr}^1$, and $\Psi_{s,cr}^1$ is function of the erosion velocity v_e. In case deposition of the sediment particles is neglected, by assuming that the near bed sediment concentration is zero, eq. (2.15) can be simplified to eq. (2.16).

$$\frac{1}{1 - n_0} \cdot \Phi_p^1 \sqrt{g \Delta D_{50}} - v_e = 0 \quad \textbf{(2.16)*}$$

2.4.2 Stability parameters

The stability parameters are mainly assessed with help of [Hoan, 2008] and summarised in appendix A.4.

A transport formulation of stones or sand should be available in order to calculate the (amount of) sediment transport or bed damage level. This amount of damage and/or sediment transport is function of different variables involved. [Hoan, 2008] made an overview of the dominant governing variables regarding stones which is presented in Table 2.1.

Table 2.1 Dominant governing variables [Hoan, 2008]

Governing variables	Expression	Dimension
Bed shear stress	$\tau = \rho u_*^2$	[N/m^2]
Velocity	u_x, u_y, u_z	[m/s]
Turbulence	$k, \sigma(u_x), \sigma(u_y), \sigma(u_z)$	[m^2/s^2]
Specific submerged density of stone	$\Delta = (\rho_s - \rho)/\rho$	[-]
Grain size diameter	d	[m]

The ratio between load and strength is used in many formulations to determine the threshold of movement of the particle. In here the load is often the bed shear stress induced by the flow velocity of the water and the strength is mainly function of the stone

size. One of the classical formulations is the one of [Shields, 1936] for uniform flow. This approach is used and adapted later on by different researches of which an overview is presented in Appendix A.4.

The Shields parameter is dependent on the load, which is the bed shear stress, and the strength, which is the submerged weight of the particle. The bed shear stress is in reality often not the only load, since in many practical applications turbulence also plays an important role. The Shields parameter is given by:

$$\Psi_s = \frac{\tau_b}{\rho \Delta g d} = \frac{u_*^2}{\Delta g d} \qquad (2.17)$$

in which d is the stone diameter and $u_* = \sqrt{\tau_b/\rho}$.

Researchers like [Hoan, 2008] and [Hofland, 2005] studied the influence of turbulence on the stability parameter, since the expression of [Shields, 1936] is only valid for uniform flow. Characteristic for the expressions of van Hoan and Hofland is that RANS data is used to determine the bed load. This data is the mean flow velocity u and the turbulent kinetic energy k, which is averaged over the water column. The height of this column depends on the turbulent mixing length. The applied length scale in the case of Hoan and Hofland is the Bakhmetev mixing length L_m. The turbulence in RANS models only represents the second order moments of the velocity components. This implies that velocities on a higher level above the bed can determine the higher order moments of the velocity fluctuations near the bed, which represents the extreme forces on the particles.

2.5 Experimental data

For the validation of the velocity field near the bed the physical scale model of [Schmidt, 1998] is used and briefly explained in next subsection. In addition, the scour is validated with the full scale scour measurements in the Port of Rotterdam along the Parkkade (section 2.5.2).

2.5.1 Physical scale model: flow velocity field

Several researchers like [Van Der Laan, 2005], [Nielsen, 2005] and [Schmidt, 1998] performed physical model research in order to investigate the diffusion or spreading of velocity field due to bow thrusters of vessels moored near a vertical quay. [Van Der Laan, 2005] and [Nielsen, 2005] performed only measurements for a single keel clearance contrary to [Schmidt, 1998]. The research of Schmidt is used to validate the numerical model since the main purpose of the research was to investigate the velocity field as function of the distance from the keel to the bed (keel clearance) and the distance from the outflow opening of the thruster and quay (quay clearance). Six different keel clearances and three different quay clearances are studied. Additional to the research regarding the velocity field, a research regarding scour due to bow thrusters is carried out.

The physical modelling is carried out by placing two different scale models of vessels in a water basin with different keel and quay clearances and the vessels are equipped with two different four bladed propellers (scale 1:45 and 1:18). The flow velocity between the quay and the scale model is measured using a 2-Dimensional-Laser-Doppler-Anemometer (2D-LDA). This resulted in pictures like Figure 2.9.

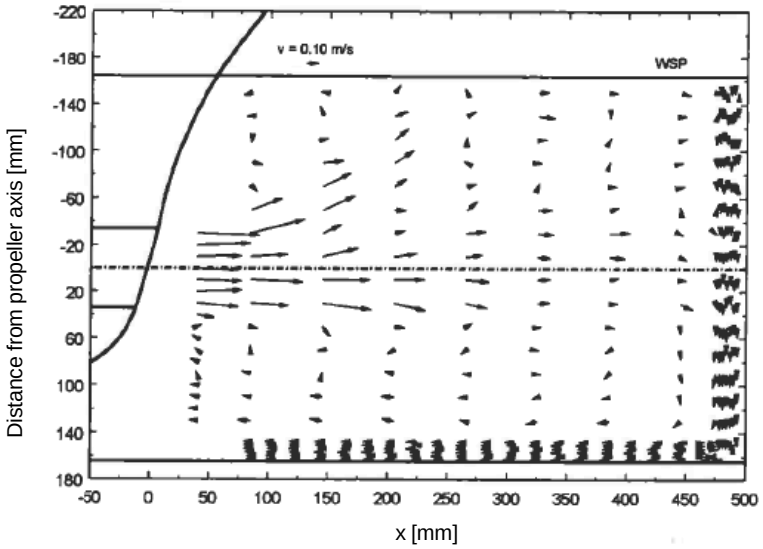

Figure 2.9 Velocity field between vessel and a vertical wall [Schmidt, 1998]

The results of the velocity measurements can be used to validate the velocity field of a numerical model. The data is useful because the velocities near the bed are measured at several locations along the bed. A part of the results and the dimensions of the scale model of Schmidt are presented in Appendix B.2.

2.5.2 Full scale tests: scour due to inland vessels near vertical quay wall

In April 2013 the Port of Rotterdam performed full scale tests in front of the quay wall of the Parkkade (along the New Meuse River next to the Parkhaven) to measure scour holes due to bow thrusters and main propeller.

Two different inland vessels, MTS Noordzee and MTS Jade, departed several times from a vertical quay wall. After each departure the bathymetry near the quay was measured with a survey boat of the Port of Rotterdam, using a multi-beam echo sounder.

These experiments are performed using both bow thrusters and main propeller (a Contra Rotating Propeller in case of MTS Jade), on different locations along the quay wall and with different applied power. MTS Jade is equipped with two azimuthal main propellers, which means that the propellers can be turned around over 360 degrees. The main propeller of the Jade is used perpendicular to the quay wall during berthing. The results are processed by the Port of Rotterdam and reported by [Blokland, 2013].

A summary of the main results regarding MTS Noordzee is presented in this chapter in order to validate the numerical model. The measurements of MTS Jade are not presented, since the numerical model is based on the dimensions and applied power of

MTS Noordzee only, because the maximum amount of departures on the same location is six, contrary to MTS Jade where a maximum of four departures are studied.

Also the governing soil parameters and the position of the vessel is presented in this chapter. For more background information regarding amongst others the location and specifications of the inland vessel is referred to appendix B.1 and [Blokland, 2013].

2.5.2.1 Soil survey

In general the soil consists of a top layer of clay of about 75 cm, with underneath a sandy layer which also contains silt, clay layers and peat. On several locations along the quay wall the soil composition is determined by taking soil samples. The properties of the sample which are closest to the bow thruster of the vessel MTS Noordzee are presented in Appendix B.1. The main properties at this location, which are important for the modelling of the scour, are presented in Table 2.2.

Table 2.2 Soil properties near bow thruster of MTS Noordzee

Governing variable	Expression	Value	Dimension
Grain diameter where 50% of the grain mass has a smaller diameter	D_{50}	235	[μm]
Grain diameter where 15% of the grain mass has a smaller diameter	D_{15}	125	[μm]
Minimum porosity of clay	$n_{clay,min}$	57.7	[%]
Maximum porosity of clay	$n_{clay,max}$	74.0	[%]
Average porosity of clay	$n_{clay,average}$	65.9	[%]
Minimum porosity of sand	$n_{sand,min}$	40.8	[%]
Maximum porosity of sand	$n_{sand,max}$	46.4	[%]
Average porosity of sand	$n_{sand,average}$	42.4	[%]
Cohesion	c	5	[kPa]

The grain size diameters are measured below the lowest point of the scour hole in the sandy layer (i.e. below NAP -10.00m). Beside this also results regarding the cohesion of the top layer with clay are known, following from a triaxial test. The results are also presented in Appendix B.1

2.5.2.2 Position of the vessel

The properties of the position of the moored vessels are presented in Table 2.3. During the departure the distance between the vessel and the quay is observed visual. The observed distances are plotted in Figure 2.10. For the departure with the use of one bow thruster the distance is observed by two observers (wn.1 and wn.2). For the departure with the use of two bow thrusters there is only one observation. Considering only the first 100 seconds one can approximate that the average velocity during departure is about 0.15 m/s.

Table 2.3 properties of the moored vessels

Parameter	Unit	MTS Noordzee	MTS Jade
Water level relative to NAP	[m]	-0.55	-0.45
Bed level relative to NAP	[m]	-7.70	-8.00
Draught	[m]	4.10	3.85
Keel clearance	[m]	3.05	3.70
Maximum power per thruster	[kW]	320	405
Diameter of thruster duct D_0	[m]	0.91	0.91
Dist. thruster - quay	[m]	3.25	5.19
Dist. thruster axis - keel	[m]	0.66	0.66
Dist. thruster axis - bed (h_{pb})	[m]	3.71	4.36

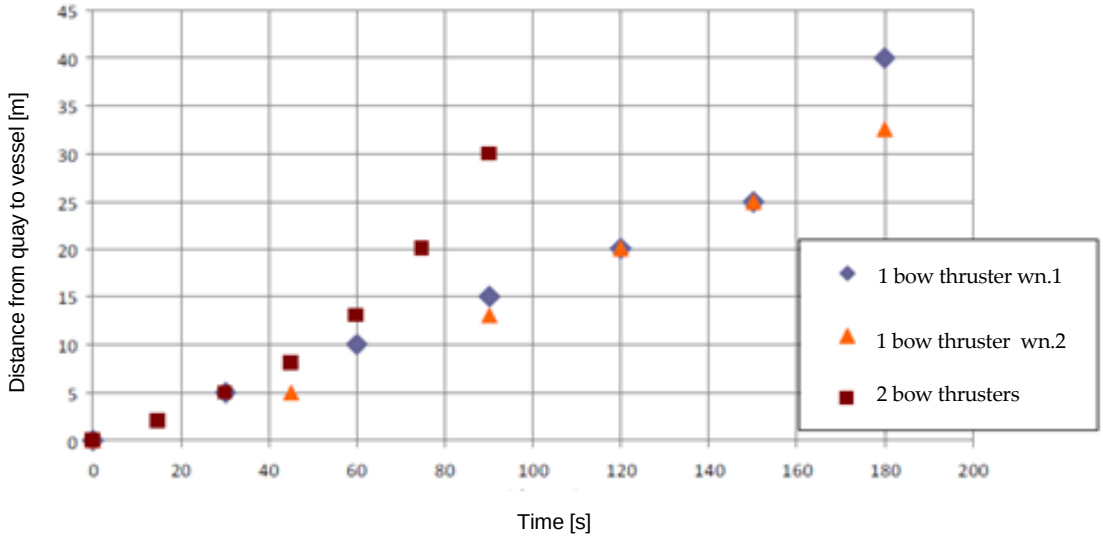

Figure 2.10 Distance between vessel (MTS Noordzee) and quay

2.5.2.3 *Summary results test with MTS Noordzee*

The measured scour depth of the first two departures of MTS Noordzee is:

- 1st departure: 60 cm
- 2nd departure: 20 cm, total 80 cm
- Totally for 6 departures: 175-185 cm

The increase of the scour depth per departure is unknown for the 3th till the 6th departure due to measurement errors. The average increase of the scour hole for the last four departures is 26 cm.

A cross section of the scour hole perpendicular to the quay wall is depicted in Figure 2.11. Note that the red dotted line is the original bed level before the tests are performed.

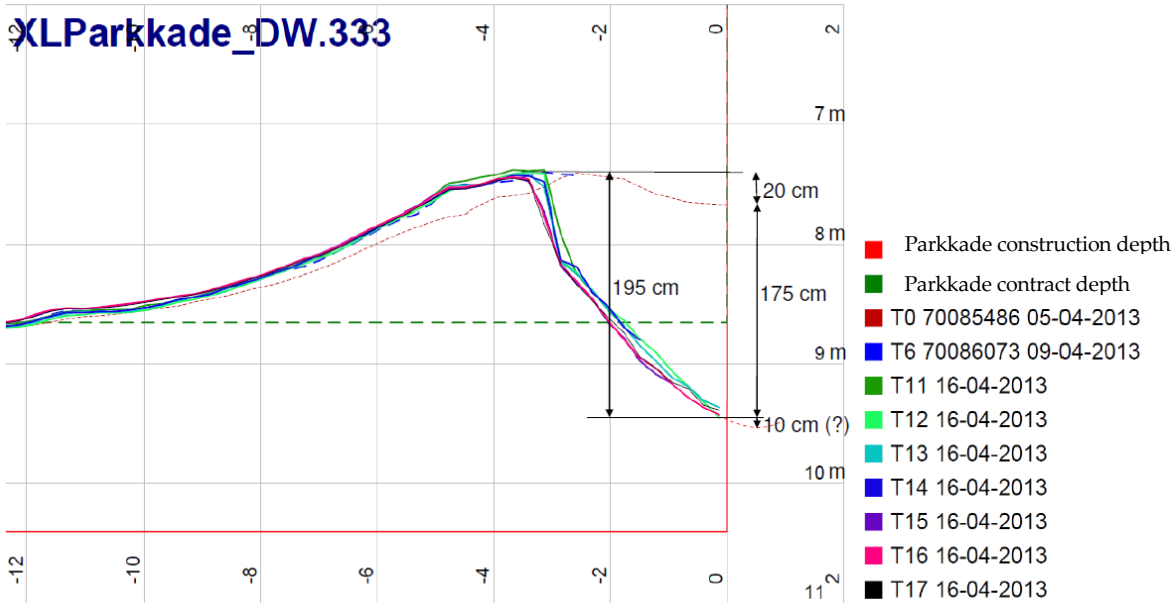

Figure 2.11 Bed level measurement near quay wall after six departures of MTS Noordzee

2.6 Conclusions applied theory and literature

In this study several choices are made regarding the use of the theory which is studied. The main division is (1) the hydraulic modelling part, (2) the erosion of the bed near the quay wall and (3) the software.

2.6.1 Hydraulic modelling

For the hydraulic modelling, first of all, it is important to determine the efflux velocity of the thruster. This is done by assuming a cylindrical outflow, which is equal to the diameter of propeller duct, and using the expression of Blaauw and Van der Kaa (1978) for the efflux velocity V_0, which is a function of amongst others the power of the bow thruster. Other expressions are available, but they are in general not a function of the power of the thruster. This is not practical for the use in this case, since the power is the only available property of the bow thrusters of the vessels used in the full scale test in the Port of Rotterdam.

To solve the flow the Realizable k-ε model will be used, which is a RANS method. The reason to use RANS instead of LES is that the computational time is much lower. The Realizable k-ε model is applied since in this model the normal stresses are positive under all flow conditions. Because of this the model gives improved simulation for swirling flows and flow separations, which enables to handle round jets.

For the validation of the near bed velocities the analytical formulation according the Dutch method and the physical model from [Schmidt, 1998] are used.

2.6.2 Erosion modelling

The local scour can be modelled by calculating the erosion velocity (i.e. the velocity of the moving bed perpendicular to the bed) on each cell centre near the bed, based on the flow properties on the cell face. For this case the formulation of [Van Rhee, 2010] described in subsection 2.4.1. might be useful. This is mainly because this equation performs well for both high and low bed shear stresses. An important modification, compared to other formulations, is that the effect of dilatancy is taken into account, which prevents that the erosion velocity increases too much with increasing bed shear stresses. Moreover, the effect on sediment transport on a sloping surface with a hydraulic gradient is taken into account. The predicted erosion rates by Van Rhee agree well with experiments.

2.6.3 Software

OpenFOAM will be applied to model the hydrodynamics, for the following reasons: (1) OpenFOAM is an open source software package, which means it is for free and it gives the user a wide variability of implementing the model for a specific situation due to access to the source code. (2) The software performs well for local (relative small scale) problems where non-hydrostatic effects play an important role. (3) There is sufficient online support available and beside this also support from Deltares and the TU Delft.

3 Numerical Model with Non-erodible Bed

In this chapter the modelling of the flow velocity field is described for a non-erodible bed, using a simplified model for the thruster induced water jet. Values for the velocity gradient ∇U and turbulent kinematic viscosity ν_t are used to calculate the bed shear stress resulting in the erosion rate. This chapter aims to obtain realistic flow velocities near the fixed bed.

Section 3.1 describes the geometry of the different models. Two cases are developed which will be assessed in order validate the hydrodynamic model. The first case consists of real size models, based on the dimensions of full scale experiments of the inland vessel MTS Noordzee (see section 2.5). In Case 1 the bottom velocities from the numerical model are compared with the results from the empirical equation (2.2). Case 2 is based on the physical tests of [Schmidt, 1998] where flow velocities are measured for a scale model of a vessel. In Case 2 the near bed velocities from the numerical model are compared with the results of the physical model by [Schmidt, 1998].

Section 3.2 and 3.3 describes the hydrodynamics and the solver of the numerical model respectively. In section 3.4 the obtained results and the validation of the model is presented, based on the physical scale model of [Schmidt, 1998] and the Dutch method to determine the maximum bed velocity as described in section 2.2.2.

In the last sections the conclusions regarding the validation of the numerical model are presented.

3.1 Geometry of the case studies

3.1.1 Case 1: Full scale numerical model

The first case consists of seven subcases where a simplified geometry of a vessel near a quay is modelled, assuming the vessel as a rectangular block. The variation in those subcases is based on different combinations of keel clearance (distance from keel to the bed) and quay clearance (distance from quay wall to outflow opening of the bow thruster). The dimensions of the numerical domain are based on the cross section of the Parkkade (see also section 2.5) as depicted in Figure 3.1. Case 1.7 is an additional case which is elaborated in order to study the velocity profile over the height next to the quay wall, for a larger variation in quay clearances. This case is only studied for the steady state situation and is not taken into account for the comparison of the near bed velocities, but only to study the velocity profile over depth. The centre line of the bow thruster is taken at 0.65 m from the keel of the vessel for all cases. The geometries of the seven subcases are summarized in Table 3.1 and depicted in Figure 3.2.

Table 3.1 Geometry of case 1.1 to 1.6

Case	Quay clearance [m]	Keel clearance [m]	Water depth [m]
1.1	2.5	4.0	8.0
1.2	2.5	2.0	8.0
1.3	2.5	1.0	8.0
1.4	5.0	4.0	8.0
1.5	5.0	2.0	8.0
1.6	5.0	1.0	8.0
1.7	3.75 - 13	3.0	7.0

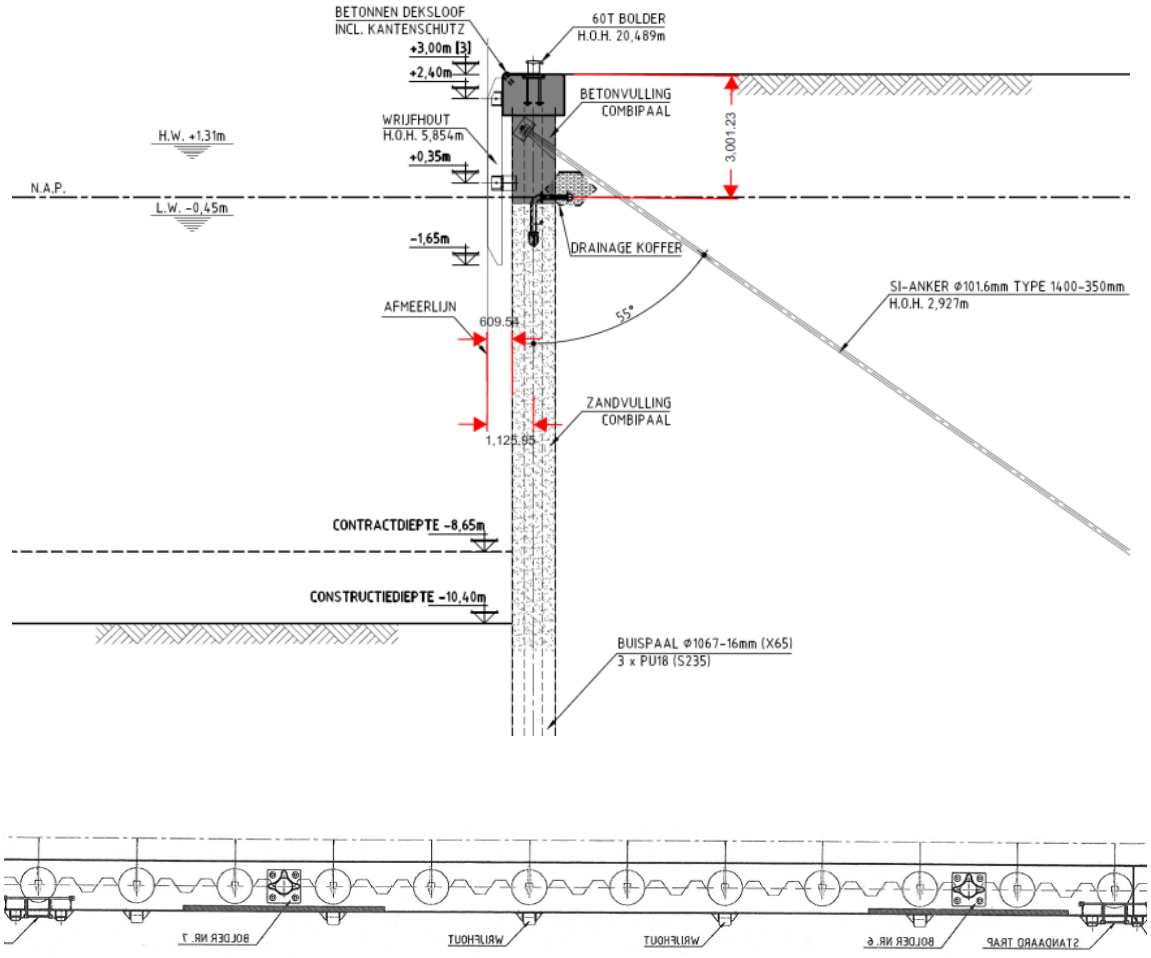

Figure 3.1 Cross section and top view of the quay "Parkkade" in Rotterdam

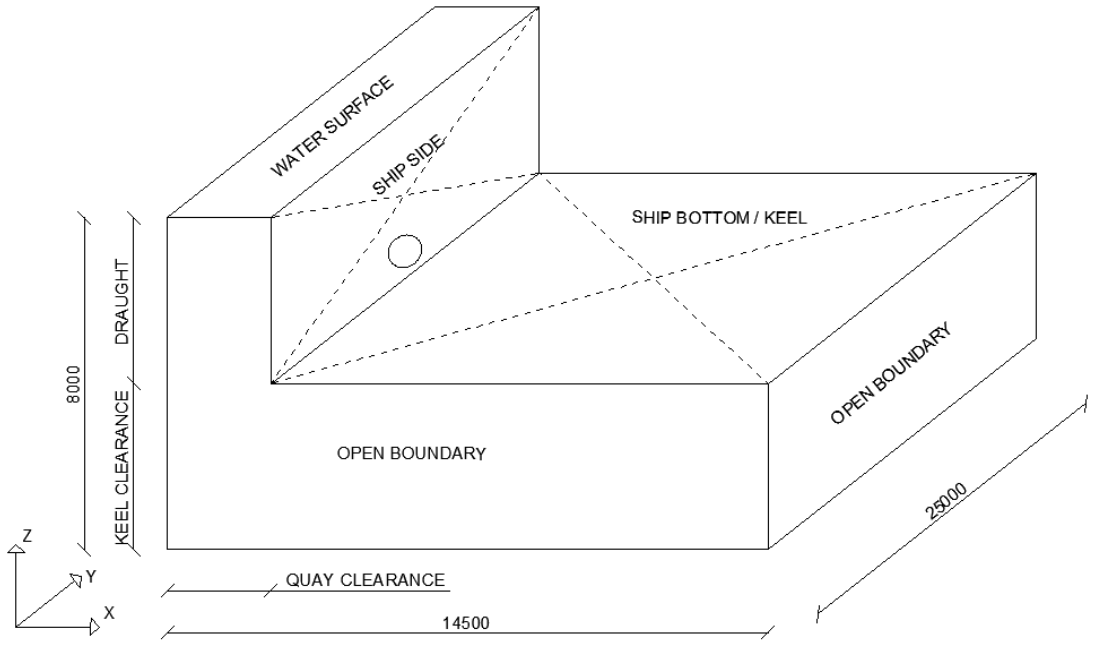

Figure 3.2 Model geometry for case 1-6 [mm].

3.1.2 Case 2: Physical model of Schmidt

In Case 2 the 1:45 scale model of Schmidt is modelled based on Figure 3.3 and an example of the geometry of case 2.1 is shown in Figure 3.4. In Figure 3.3 h_p is the distance from the bed to the centre of the bow thruster, L is the quay clearance and D_0 is the diameter of the bow thruster. An overview of the geometry of the subcases is presented in Table 3.2.

Table 3.2 Geometry of the different cases based on Figure 3.3

Case	D_0 [cm]	h_p [cm]	L [cm]
2.1	6.80	11.30	27.00
2.2	6.80	16.40	27.00
2.3	6.80	23.80	27.00
2.4	6.80	14.80	27.00
2.5	6.80	14.80	37.00
2.6	6.80	14.80	49.50
2.7	6.80	16.40	37.00

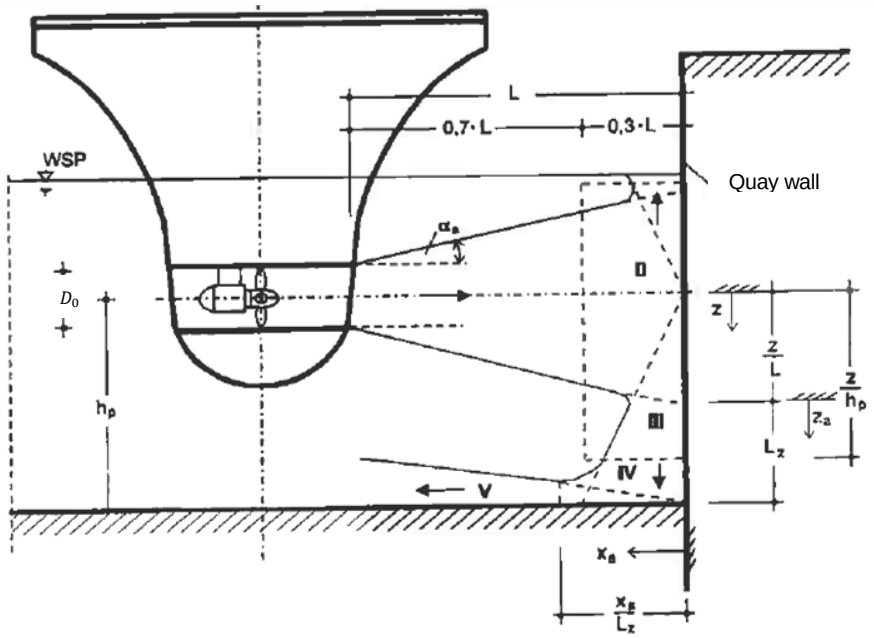

Figure 3.3 Propeller jet distribution near a vertical quay wall [Schmidt, 1998]

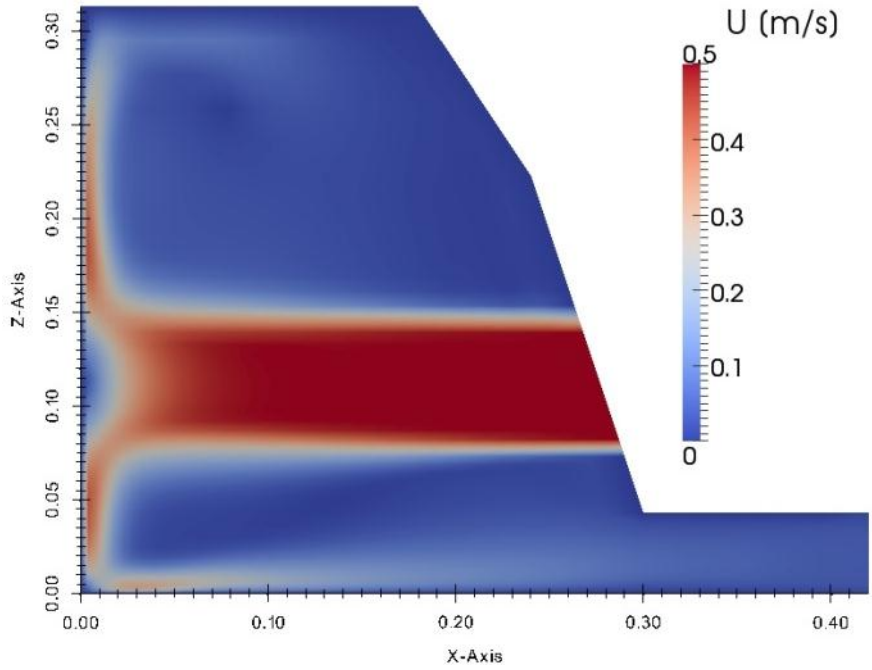

Figure 3.4 Geometry of cross section case 2.1 at the centre of the bow thruster at t=60s [m]

3.2 Hydrodynamics

For the calculation of the hydrodynamics the Realizable k-ε model is used.

The jet velocity is modelled separately from the case models. It is modelled as a cylinder with an inlet and outlet. The flow properties near the outlet of the cylinder are mapped on the specific location in the case model where the thruster is located. The diameter of the cylinder is equal to the propeller duct of the bow thruster. Within OpenFOAM an option to impose a local circular boundary condition on the domain was not found.

There are two types of cylinders compared *for case 2*, to calibrate the model:

- Cylinder without zero velocity core (applied for case 1 and case 2);
- Cylinder with a zero velocity core (to simulate the axis of the propeller, where the velocity is zero). In fact this is just a reduction of the outflow velocity averaged over the full circular surface of the propeller in order to obtain reliable bed velocities. This is only applied for case 2 since the outflow velocity is *not* determined with eq. (3.1). A physical shortcoming in this way is that the conservation of momentum is not taken into account. This is also not possible, since no clear outflow velocity profile near the thruster in the physical model is presented.

Note that the difference regarding the thrusters between the two cases is that the velocity of the full scale test (case 1) is calculated by eq. (3.1)and the velocity of the physical test (case 2) is obtained from [Schmidt, 1998] and reduced by a zero velocity core.

$$V_0 = \zeta \cdot 1.17 \left(\frac{P_0}{\rho D_0^2} \right)^{\frac{1}{3}} \qquad (3.1)$$

ζ is a factor for energy loss in the channel system of the thurster. For the channel system of the MTS Noordzee the value of ζ can be estimated with 0.9 [Meijer & Verhey, 1993]. The input values for equation (3.1) are based on the full scale test dimensions of MTS Noordzee described in section 2.5.2. This results for a maximum applied power of 320 kW in an efflux velocity of 7.7 m/s for ζ=0.9 and 8.5 m/s for ζ=1. In the numerical model an efflux velocity of 8 m/s is applied.

The outflow velocity for case 2 according to [Schmidt, 1998] is obtained from the attachments with the measurements of the scale models by measuring the vector length of the flow field. This flow velocities are about 0.5 m/s.

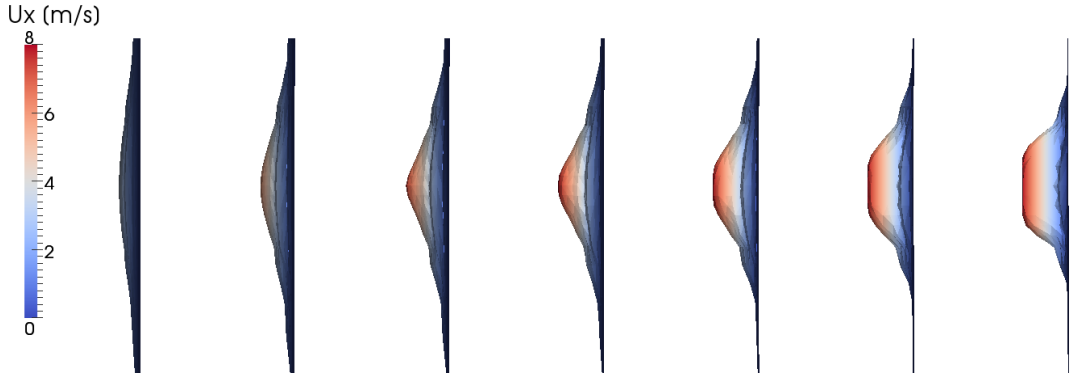

Figure 3.5 Velocity profile of the jet along x-axis in the numerical model

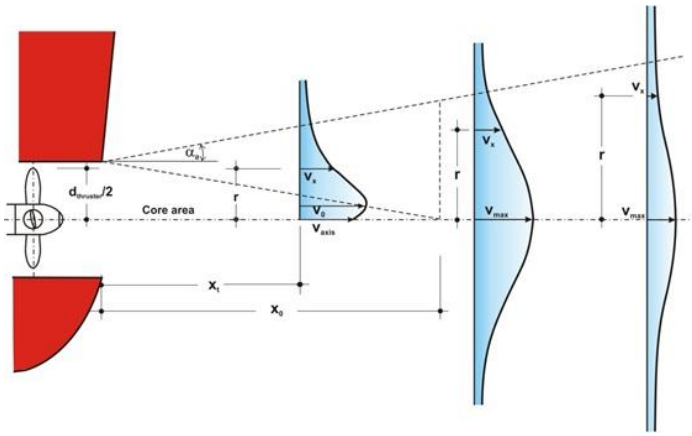

Figure 3.6 Velocity distribution induced by a bow thruster

The behaviour of the velocity profile of the jet in the numerical model depicted in Figure 3.5 is from qualitative point of view similar as described in the theory in section 2.2.1. There is a radial spreading of the velocity profile, however this spreading is much smaller than in reality. The propeller is causing this radial spreading; however in the numerical model the influence of the propeller is neglected. The consequences of this are elaborated in section 3.5.2.

3.3 Flow solver - Pressure Implicit with Splitting of Operators

The numerical model is modelled in OpenFOAM, using the solver pisoFoam, which is a transient solver for incompressible flow. This means that the behaviour of the flow in time is simulated, in contrary to a steady-state approach where only the final equilibrium stage of the flow is simulated. PISO stands for Pressure Implicit with Splitting of Operators and is a pressure-velocity calculation procedure developed originally for the non-iterative computation of unsteady compressible flows [Versteeg, 1995]. No wall functions are applied since only the near bed velocity is examined a few centimetres above the bottom.

3.4 Results and validation of velocity field

3.4.1 Results case 1.1 – case 1.6

For Case 1 (full scale model) the maximum bed velocities are determined with the numerical model in OpenFOAM using a transient solver for incompressible flow, to get insight in the development of the hydrodynamics in time.

In Figure 3.7 the velocity field of Case 1.2 is presented at the cross section near the thruster in order to get an impression of the results in general.

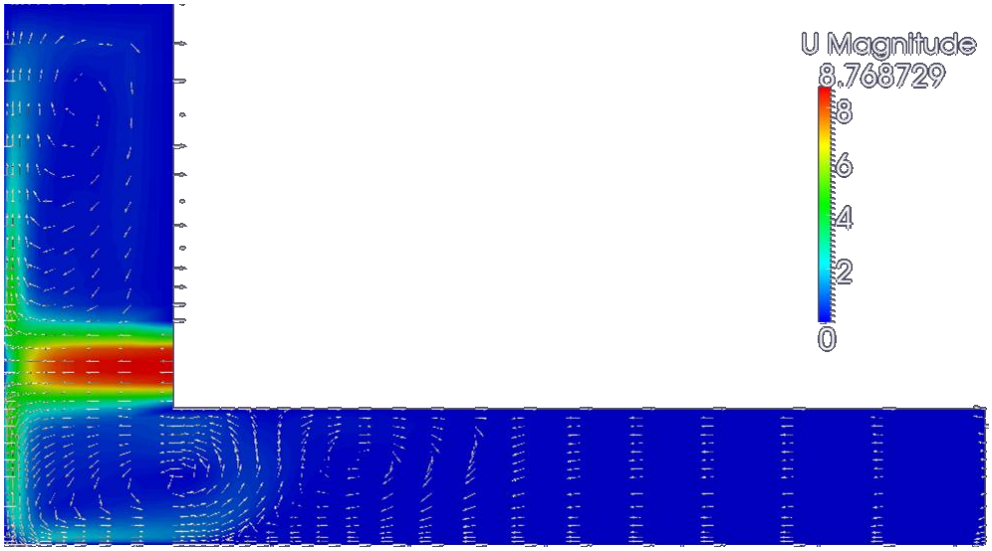

Figure 3.7 Fully developed velocity field [m/s] of Case 1.2

Analyzing the velocity field in time shows that the there are two kind of maximum bed velocities. First (Figure 3.9), in the developing stage of the velocity field the velocities are highest when the deflected jet hits the bottom at about 1 second after the start of the simulation (depending on the keel- and quay clearance). Second, (Figure 3.8) when the velocity field is fully developed the maximum bed velocity does not vary in time anymore and the velocities are in all cases slightly lower than in the developing phase.

For validation of Case1 the Dutch method is used. The Dutch method (and also the German methods) calculates the maximum bed velocity for the fully developed situation (t=infinite).

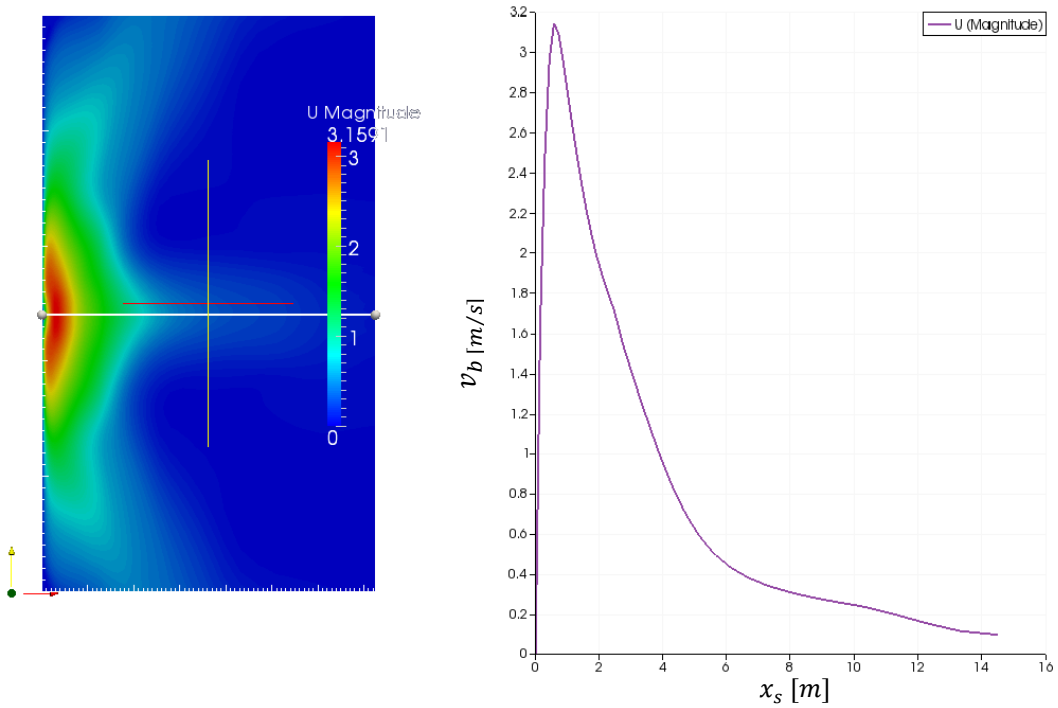

Figure 3.8 Near bed velocity field of Case 1.3, fully developed (left) and bed velocity [m/s] plotted over line Y=12m as function from distance to quay wall (right)

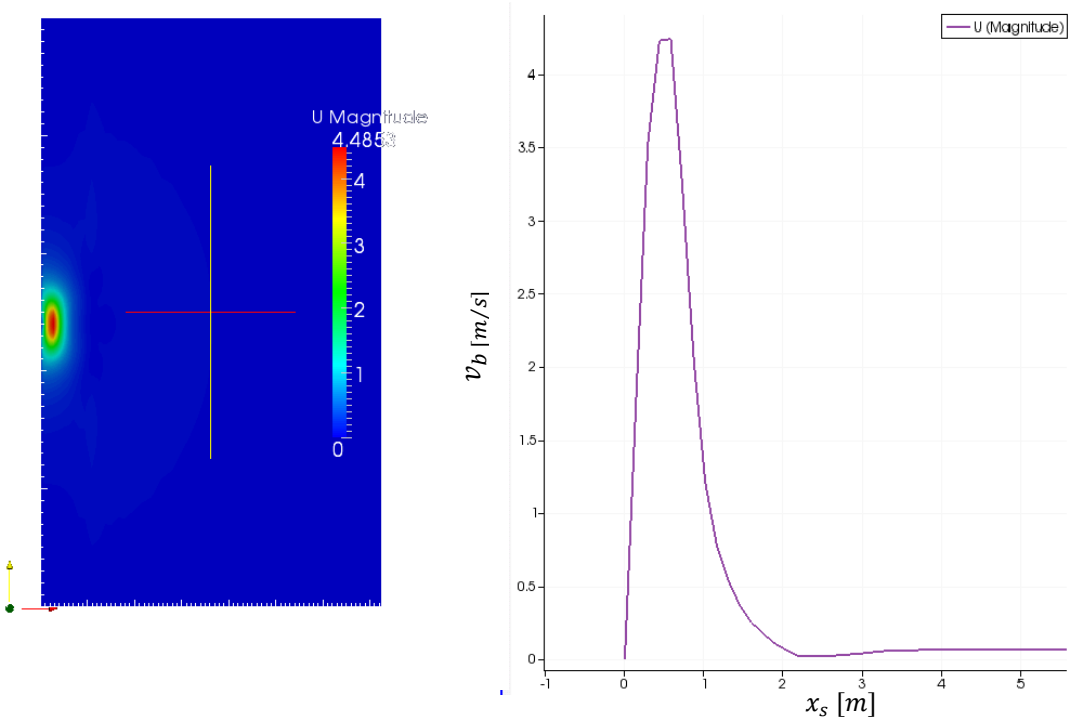

Figure 3.9 Near bed velocity field Case 1.3 when jet hits the bed at t≈1s (left) and velocity plotted over line Y=12 m as function from distance to quay wall (right)

Table 3.3 Maximum bed velocities of numerical model compared with analytical results according to the Dutch method

Output Dutch Method		Case1.1	Case1.2	Case1.3	Case1.4	Case1.5	Case1.6
L	[m]	2.5	2.5	2.5	5	5	5
h_p	[m]	4.65	2.65	1.65	4.65	2.65	1.65
D_0	[m]	0.85	0.85	0.85	0.85	0.85	0.85
L/h_p	[-]	0.54	0.94	1.52	1.08	1.89	3.03
$V_{b,max}$	[m/s]	1.53	2.68	4.31	1.53	2.60	3.00
Output numerical model							
$V_{b,max,t=1}$	[m/s]	1.3	2.6	4.4	1.2	1.8	3.2
$V_{b,max,t=inf}$	[m/s]	1.1	2.2	3.2	1	1.6	2.4

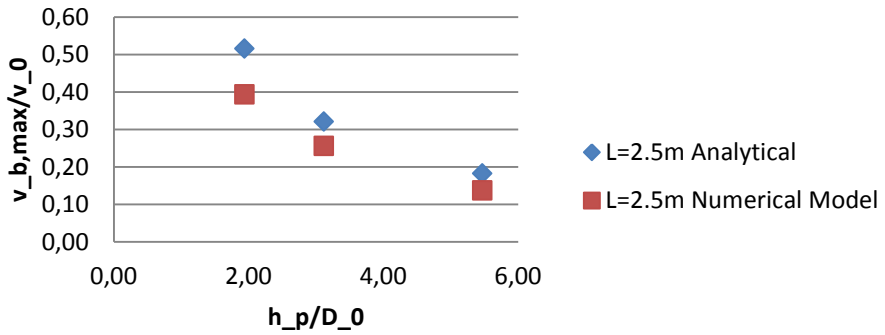

Figure 3.10 Maximum bed velocities of numerical model compared with analytical results according to the Dutch method for L/D_0=2.75 (L=2.5m)

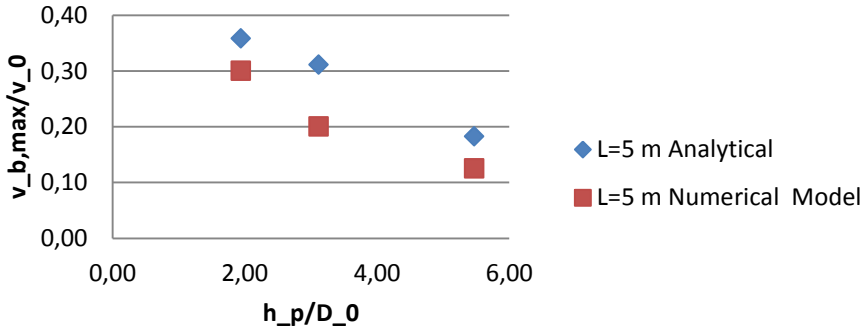

Figure 3.11 Maximum bed velocities of numerical model compared with analytical results according to the Dutch method for L/D_0=5.5 (L=5m)

3.4.2 Velocity distribution over depth – case 1.7

An additional simulation in addition to previous cases is performed to give insight in the velocity profile over depth (Figure 3.12). The distance from propeller axis to the bed is h_p=3.65m. The depicted velocity profile is determined at a distance x_s=0.5m from the quay wall, in the center line of the thruster jet.

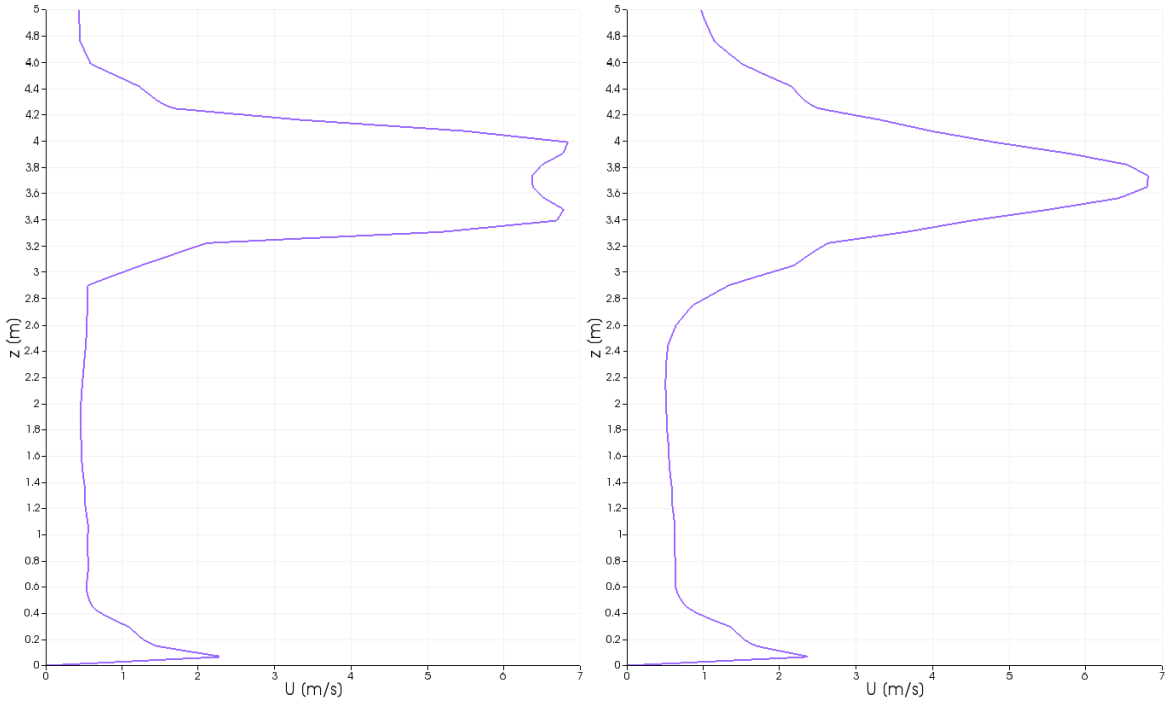

A: L=3.25m B: L=7m

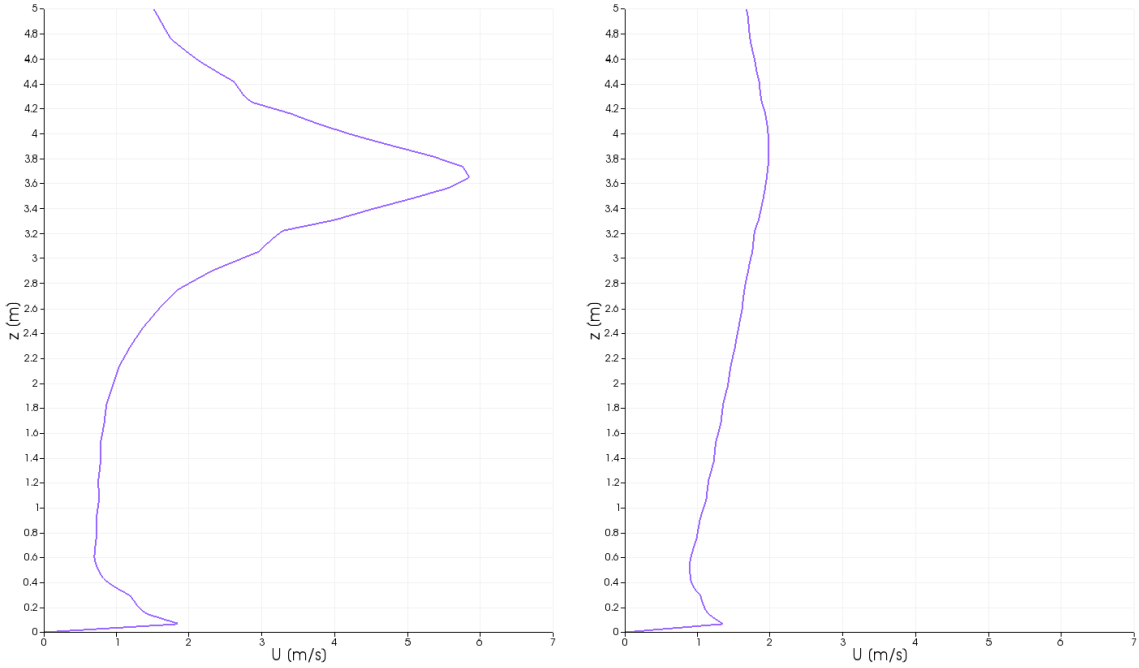

C: L= 10m D: L= 13m

Figure 3.12 Velocity profile over depth with h_p 3.65 m

3.4.3 Results case 2

To get more insight in the velocity field a small scale numerical model is compared with the physical scale model of [Schmidt, 1998]. A selection of the different options, which Schmidt investigated, is analysed and modelled with OpenFOAM.

This section presents a comparison of the maximum bed velocities only. In Appendix D a detailed comparison of the near bed velocity profiles is depicted, for the different cases as explained in subsection 3.1.2, Table 3.2. Because the efflux velocity of the thruster is never exactly the same for both the physical and the numerical model, the velocities are presented as dimensionless parameters obtained by dividing the bed velocity, v_b by the efflux velocity V_0.The maximum bed velocities are plotted as function of the dimensionless quay clearance, L/D_0, (Figure 3.13) and the dimensionless keel clearance, h_p/D_0 (Figure 3.14).

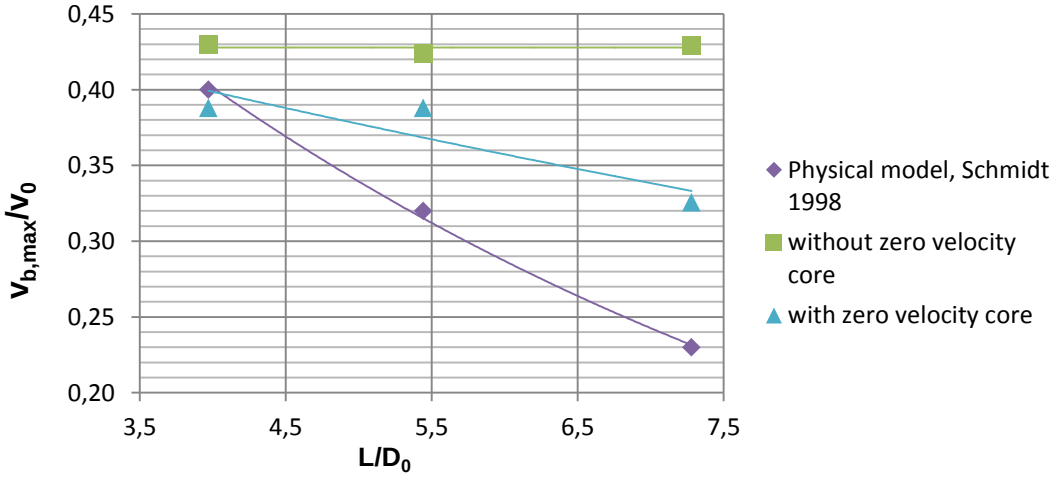

Figure 3.13 Correlation dimensionless bed velocity and dimensionless quay clearance in the physical and the numerical model - h_p/D_0=2.18

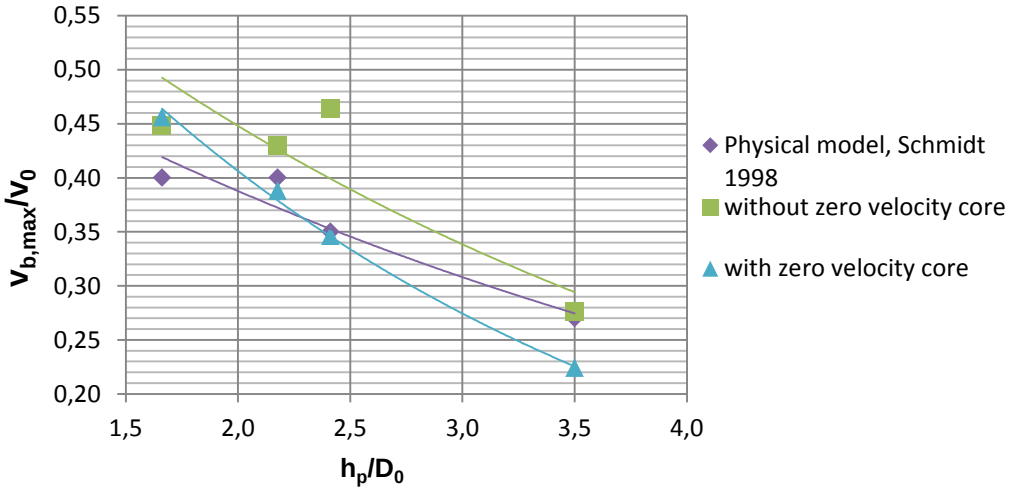

Figure 3.14 Correlation dimensionless bed velocity and dimensionless keel clearance in physical and numerical model - $L/D_0 = 3.97$

3.5 Conclusions regarding velocity field

Two types of numerical models are developed in order to simulate and validate the velocity field induced by a bow thruster. The first case concerns full scale models in which the maximum near bed velocity is examined. The second case is a numerical model which simulates the physical experiments of [Schmidt, 1998]. In this case the behaviour of the full velocity field in the physical experiments can be compared with the behaviour of the velocity field in the vicinity of the bow thruster in the numerical model.

3.5.1 Case 1: Full scale numerical model

Fore case 1.1 to 1.3 the quay clearance is 2.5 m and the bed velocities of the numerical model are in the same order of magnitude as calculated with the Dutch method. When the quay clearance is 5.0m the differences are larger. Qualitatively it can be concluded that for larger quay and keel clearances the bed velocity of the numerical model is less reliable due to the lack of radial spreading, which becomes more clear analysing case 2.

3.5.2 Case 2: Physical model of Schmidt

For relative small quay- and keel clearances the numerical model approaches the physical model of Schmidt rather accurate. The bigger the keel clearance the less accurate the numerical model is. For the keel clearance this trend is not so clear: for h_p/D_0=1 the calculation is larger than the physical model of Schmidt and for h_p/D_0=3.5 the calculation is smaller than Schmidt. By studying the velocity fields the reason for this difference becomes clear. In the physical model the jet is diverging with a certain angle α_s (Figure 3.15). In the numerical model this angle is much smaller. Because of this in the physical model the flow velocity in the horizontal jet decreases faster, which results in a lower flow velocity at the point where the jet hits the quay wall and consequently also at the point where the jet hits the bed. This is why the velocities near the bed in the physical model are lower.

In the numerical model the jet is not diverging due to a combination of (1) the lack of swirling flow, since the thruster is modelled as a local cylindrical velocity boundary condition with flow parallel to the centre axis and (2) a relative coarse mesh.

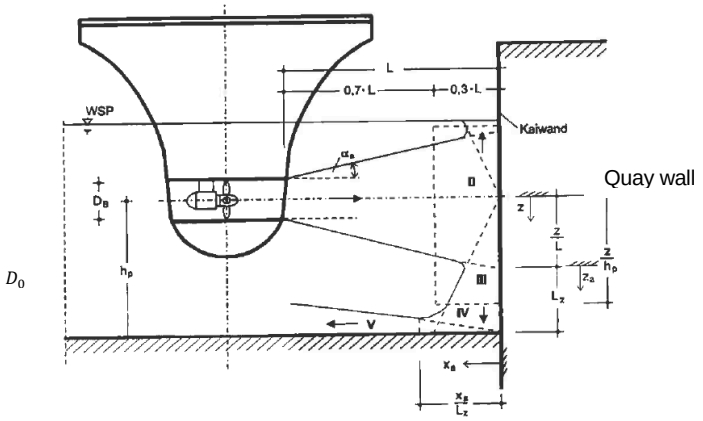

Figure 3.15 Schematization of the velocity field near a vertical quay wall

4 Numerical Model with Erodible Bed

4.1 Introduction to structure of numerical model

The numerical model, calculating the bow thruster induced scour, is divided into two main parts, which are summarized in Figure 4.1. (1) The velocity field is calculated with the CFD software OpenFOAM. The near bed properties of the fluid that follows from this computations are exported from OpenFOAM and imported in Matlab. (2) With Matlab the shear forces, erosion rate and finally the bed level update is calculated in each centre of the cell face. On its turn the new xyz-coordinates of the updated bed level are imported in OpenFOAM and the same procedure is repeated till the increase of the scour hole per departure is less than 10 cm.

Every time the loop in Figure 4.1 is repeated the mesh is changing to simulate the movement of the vessel. This means that in every time step the distance between the outflow opening of the thruster and the quay wall is increasing. In the following departure the vessel is moved again next to the quay wall to start a new departure.

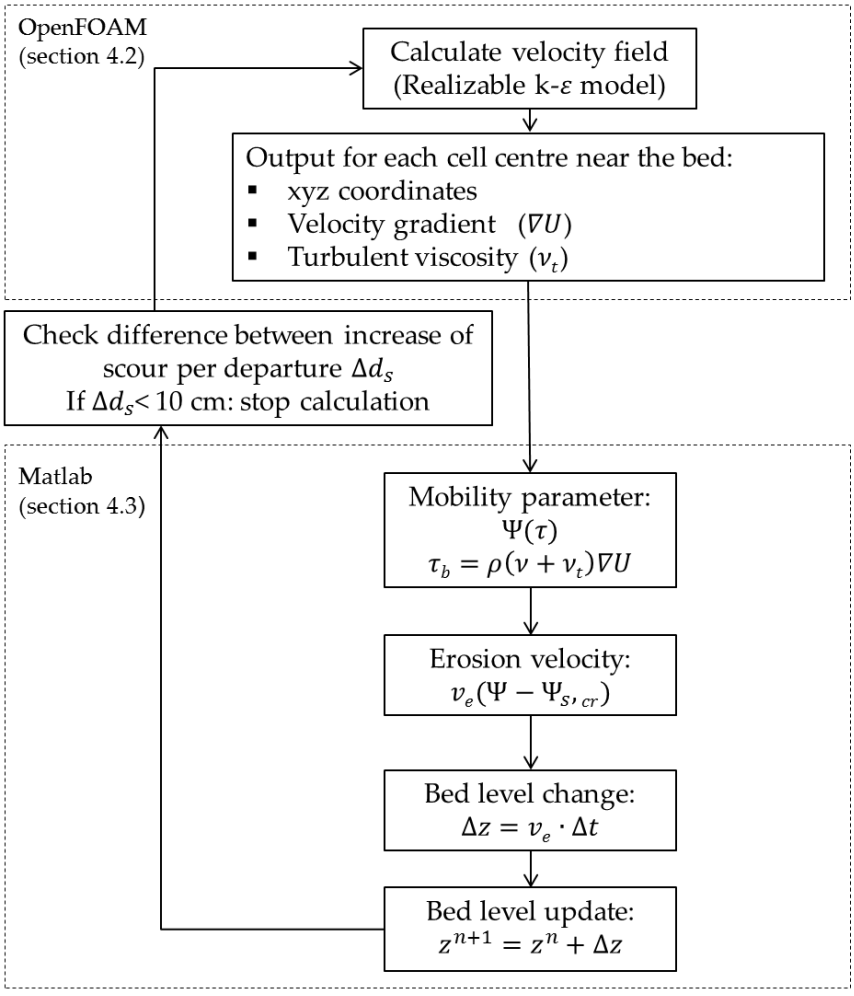

Figure 4.1 Schematic overview of the calculation steps in scour model

In section 4.2 aspects regarding the hydrodynamic model in OpenFOAM are described, considering mesh generation, the flow solver and the boundary conditions. After that, section 4.3 describes how the empirical relation, to calculate the erosion, is implemented in the numerical model. In section 4.4 the applied parameters regarding soil properties and ship dimensions are given, which leads to the results as elaborated and discussed in section 4.5. Finally a summary of the assumptions in the model are elaborated in section 4.6.

4.2 Hydrodynamic model (OpenFOAM)

4.2.1 Flow solver - Semi-Implicit Method for Pressure-Linked Equations

The steady state solver simpleFoam is used, in contrast to chapter 3 where the transient solver pisoFoam is used. The transient character of the model is applied two times in case a transient solver is used. I.e. in the transient flow solver in OpenFOAM and the bed level update calculation every time step of the iteration in Matlab (Figure 4.1). This would not be a problem if the time steps are synchronized. However for this approach it is not efficient to model.

In reality the bow thruster needs about 10 seconds before it reaches its maximum power. However, one of the assumptions in the model is that an exact modelling of the flow field during the 10 seconds of increasing power is not essential in the prediction of the scour. This means that the outflow velocity V_0 is not reached immediately after activation of the bow thruster. The effect of a sudden high impact of the jet at the sea bed does not occur in reality in contrast to what happens in case of applying the transient solver, which is used for the velocities in the numerical model without non-erodible bed as described in chapter 3.

The name of the solver is 'simpleFoam', where SIMPLE stands for Semi-Implicit Method for Pressure-Linked equations. A general description of this algorithm is given based on [Versteeg, 1995]. The algorithm is a guess-and-correct procedure for the pressure calculation on a staggered grid arrangement. To initiate the calculation process a pressure field is guessed to obtain the velocity components. The velocity components are on its turn used to recalculate the pressure field.

4.2.2 Mesh generation

The dimensions of the mesh are based on the full scale test of MTS Noordzee as described in Table 2.3. The footprint of the x-y domain is 18.25x14 m^2 and is depicted in Figure 4.2. Where in this figure in blue and red a cross section of the velocity field in the water body near the outflow opening of the bow thruster is depicted and in grey the quay wall and the eroded bed.

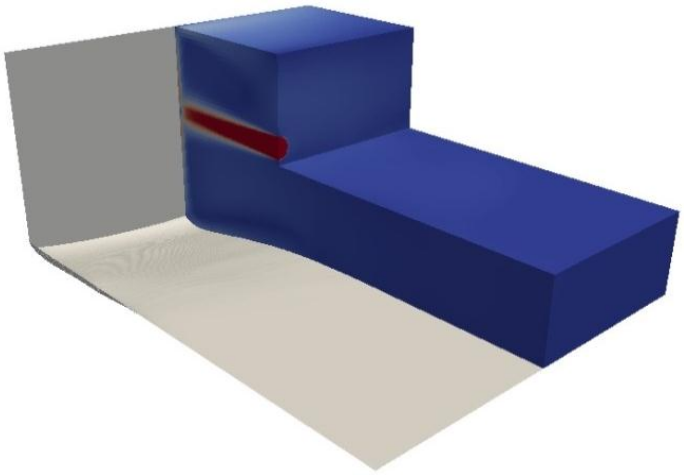

Figure 4.2 Overview of the 3D computational domain

4.2.2.1 Overall grid size

The domain consists of cubic cells, which are refined in certain regions. The mesh is refined near the bed, near the inflow opening of the jet and near the location where the jet hits the quay wall. Two different grid sizes are compared. In the first case the biggest grid cells are 15x15x15 cm^3 and in the second case 30x30x30 cm^3. The results show that the coarser grid sizes performs even better (see Figure 4.5 and Figure 4.6). I.e., a more regular decrease of the scour increment in time, compared with the model with a fine mesh. Beside this the calculation time is reduced by reducing the number of cells with a factor 2^3.

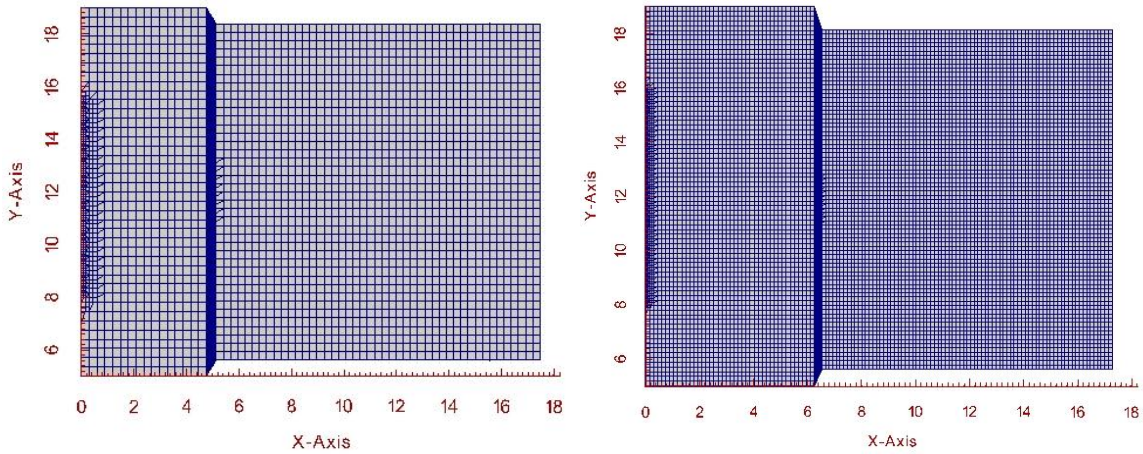

Figure 4.3 xy-plane of the computational domain (left: coarse mesh, right: fine mesh)

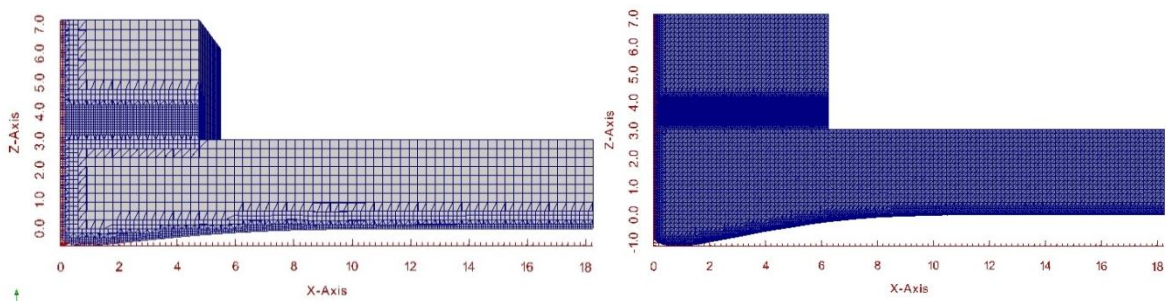

Figure 4.4 xz-plane of the computational domain (left: coarse mesh, right: fine mesh)

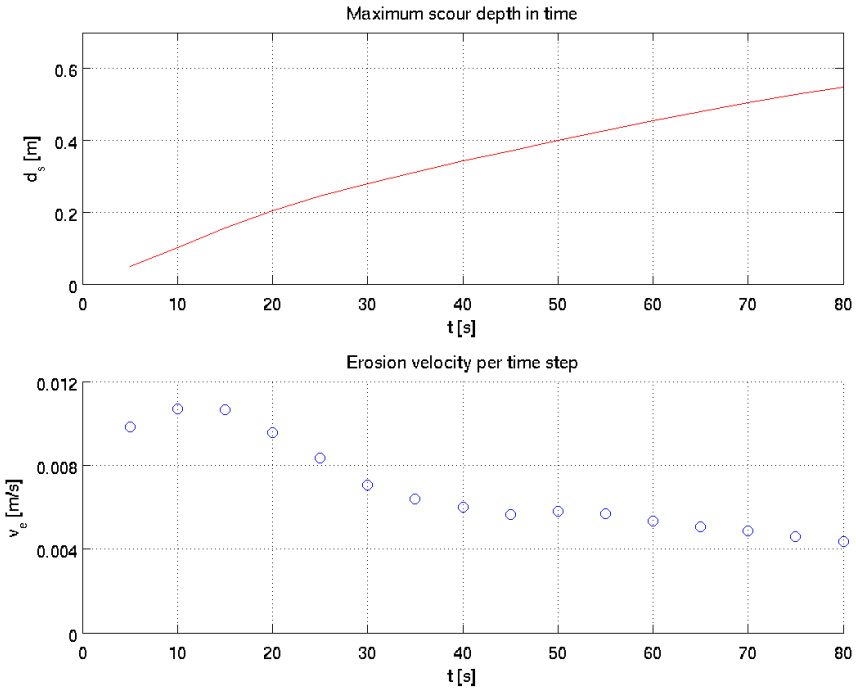

Figure 4.5 Coarse mesh - 1 departure

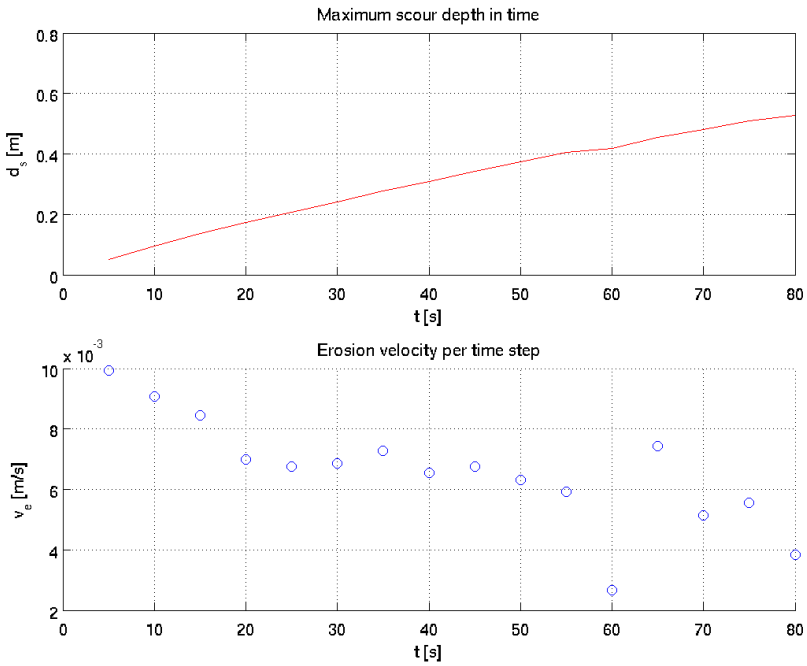

Figure 4.6 Fine mesh – 1 departure

4.2.2.2 Cell refinement

The refinement of the cells, especially near walls, influences the use of the wall function. Near the bed the mesh can be refined in order to obtain proper y^+ values by adding layers near the bed which are sufficient small for standard wall functions. According to [Andersson, 2012] sufficient small is in general $30<y^+<100$[3] and for high Reynolds numbers the upper limit may increase up to 300-500. The coarse grid described in the previous section is applied in the current model. For the refinement of the cells near the quay wall and the bed two options are considered:

1. Cell splitting near the bed (Figure 4.7): The cells are split two times near the bed. In this case the cells are not refined so far to obtain sufficient small y^+ values. However, the results regarding the maximum scour depth are similar to the full scale test in Rotterdam. Also the model behaves as expected regarding erosion velocity, which is decreasing (see Figure 4.9) during the departure(s). Further on the model is stable and does not lead to numerical errors or errors in the mesh refinement. One should notice that in this case the wall functions are not applied due to relative coarse cells near the bed;
2. Add cell layers near walls (Figure 4.8): By adding layers near walls it is possible to generate sufficient small y^+ values in order to fulfil the requirements for applying wall functions. This leads to results regarding final scour depth which are in the same order of magnitude, as the model with coarse cells near the walls. However, the model is less stable due to imperfections in the settings of the mesh generator. This causes locally high peaks in wall distances, and so in the turbulent kinematic viscosity and velocity gradients. The results regarding maximum scour depth and the increase in scour are much less continuous (see Figure 4.10). This can be solved by improving the mesh generation. Due to a limited time frame of this research the model is not further optimized in order to obtain a better physical representation of the hydrodynamics.

[3] y^+ is the relative wall distance. See section 4.2.3 for more detailed explanation.

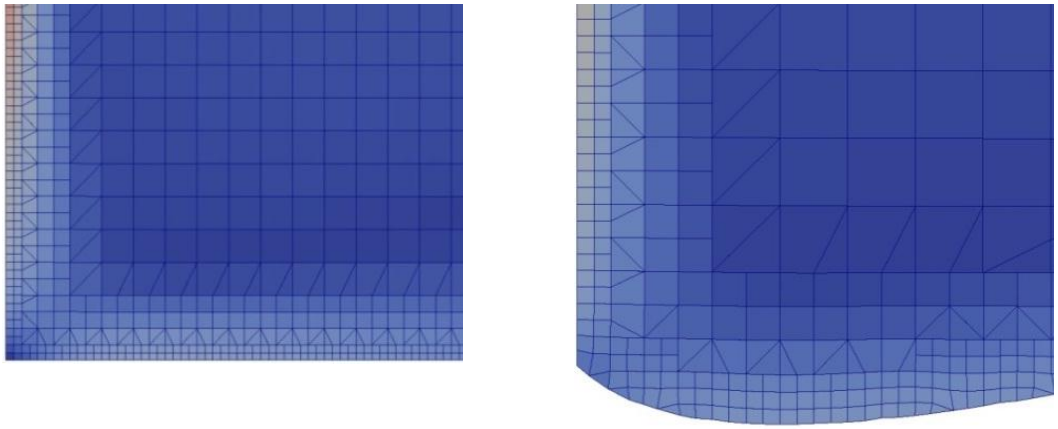

Figure 4.7 Mesh near quay wall and bed generated by cell splitting (model 1). Left: mesh at first time step. Right: Mesh after scour development

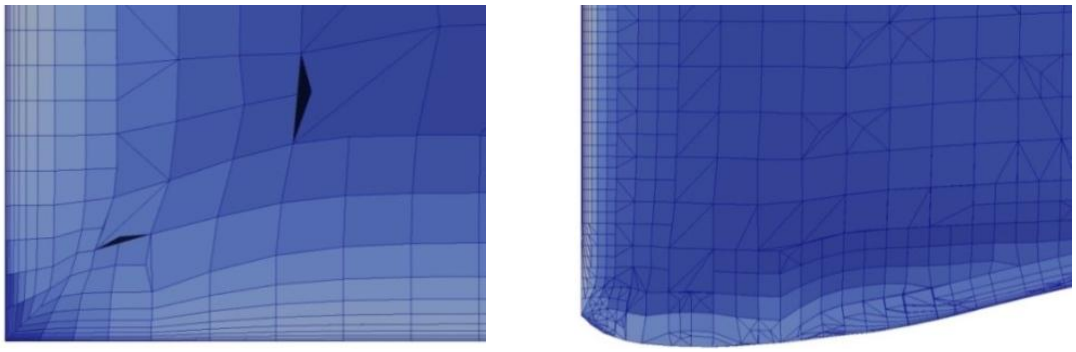

Figure 4.8 Mesh near quay wall and bed generated by adding layers (model 2). Left: mesh at first time step. Right: mesh after scour development.

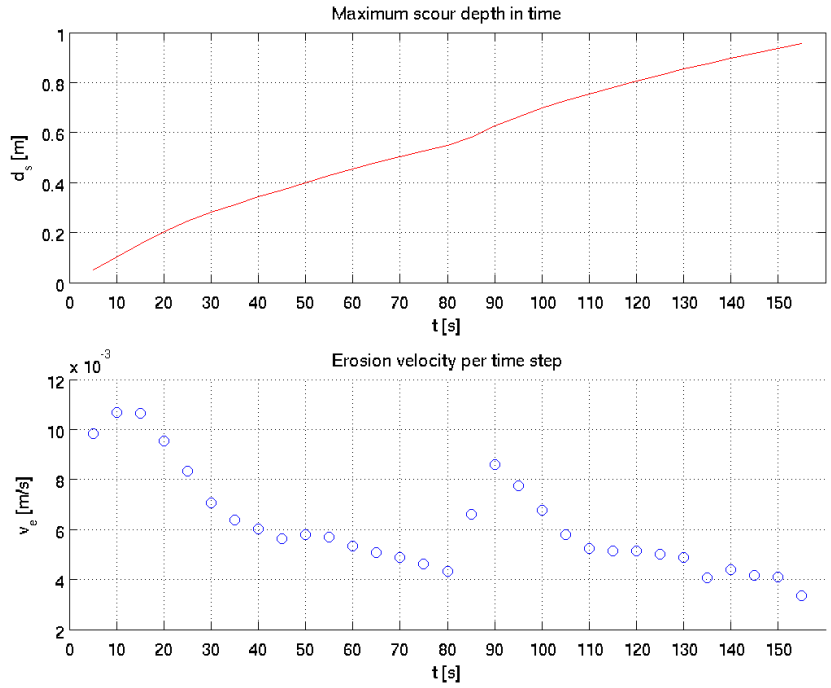

Figure 4.9 Model 1: without wall functions - 2 departures

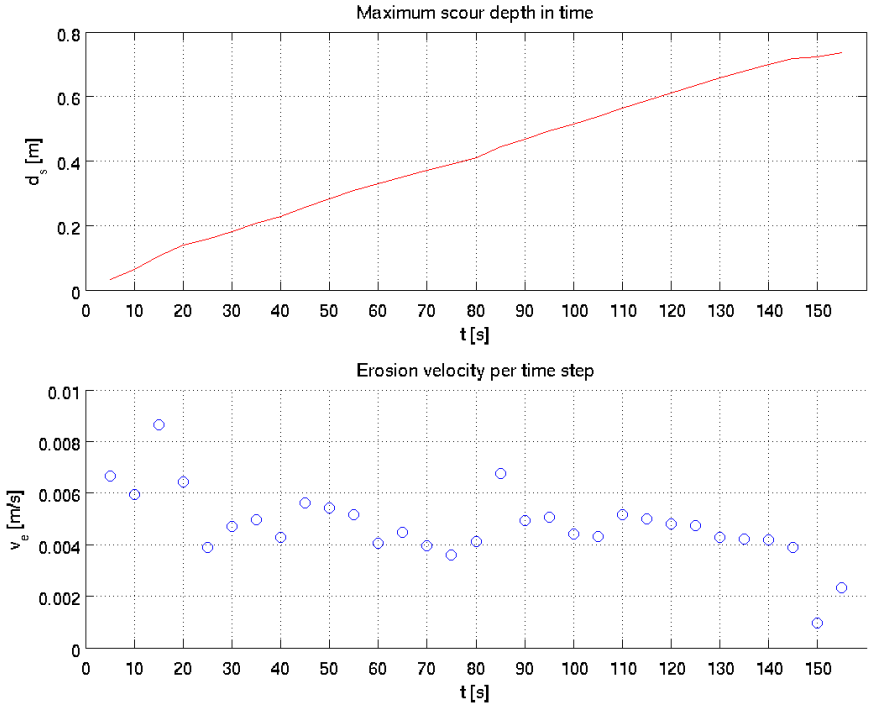

Figure 4.10 Model 2: With wall functions - 2 departures

4.2.2.3 Moving vessel

The movement of the vessel is modeled based on an average speed of the vessel of 0.15 m/s during departure from the quay wall. This speed is derived from Figure 2.10 in section 2.5.2.2 where the distance between quay and vessel is plotted in time for the inland vessel MTS Noordzee. The movement of the vessel is discretized with the same time step ($\Delta t = 5$ seconds) as applied for the time step for the calculation of the bed level change. In fact each time step the mesh is regenerated with an adapted position of the vessel relative to the quay and the bed level coordinates from the previous time step. For an average speed of 0.15m/s and a time step of 5 seconds this means a displacement of the vessel of 0.75m per time step in x-direction. In Figure 4.11 this is shown, where in blue and red a slice of the numerical domain for the flow velocities near the thruster is depicted, and in grey the quay wall and the eroded bed.

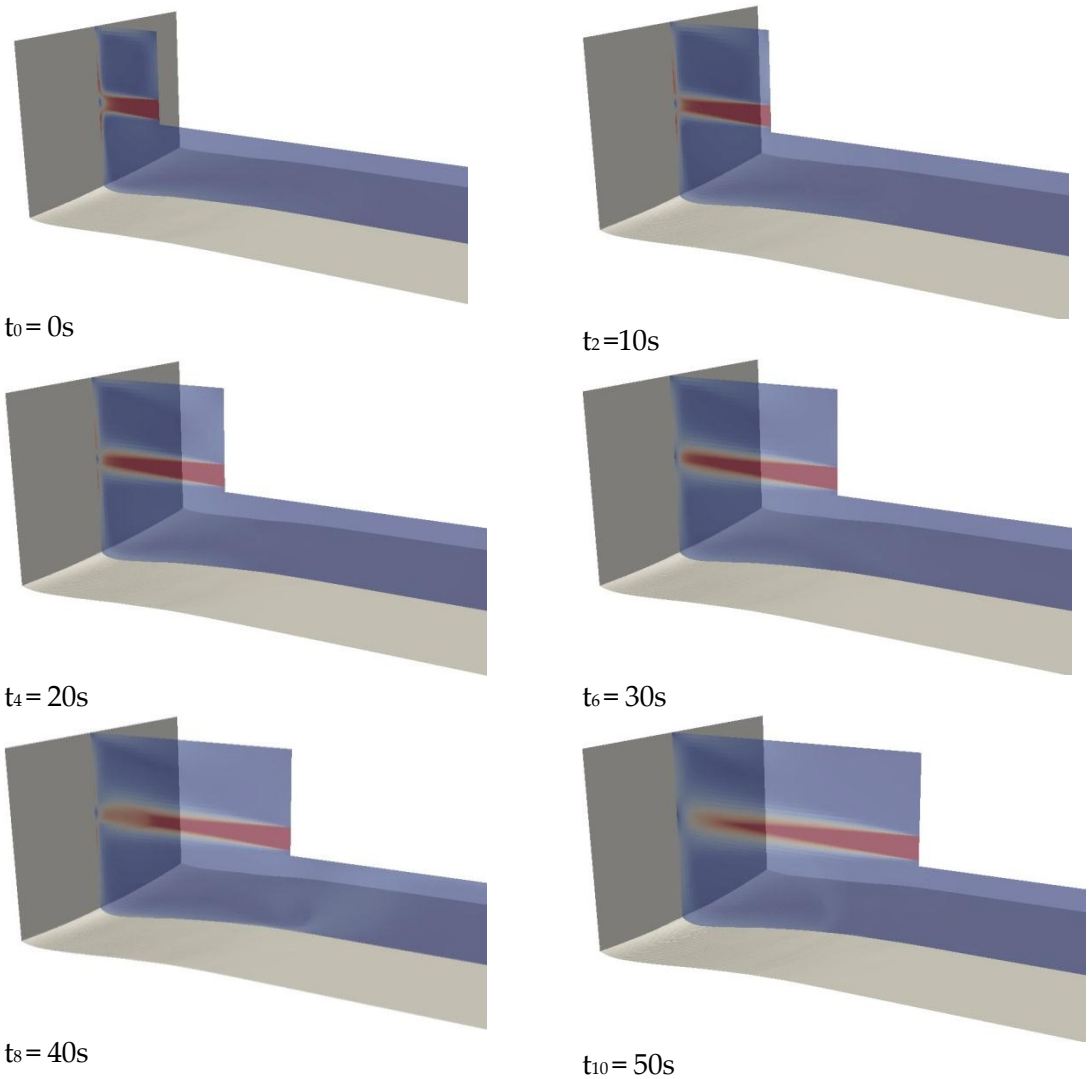

Figure 4.11 Position of the modeled vessel during 2nd departure.

4.2.3 Boundary conditions

For the following parameters the boundary conditions are specified in OpenFOAM:

- Turbulent kinematic viscosity (ν_t)
- Energy dissipation rate (ε)
- Turbulent kinetic energy (k)
- Pressure (p)
- Velocity (U)

There are six boundaries in the model which are named as follows:

- quayWall
- seaBed
- shipBottom (i.e. the flat keel of the modelled vessel)
- shipSide (i.e. the side of the vessel closest to the quay wall)
- openBoundaries
- waterSurface

Per boundary the boundary conditions for each parameter are specified and explained below.

4.2.3.1 Turbulent kinematic viscosity

The wall function applied in OpenFOAM is nutkWallFunction for incompressible fluids. This boundary condition provides a turbulent kinematic viscosity condition based on turbulence kinetic energy. Equation (4.1) and (4.2) are used in this model.

$$y^+ = \frac{u^* y}{\nu} = C_\mu \frac{y\sqrt{k}}{\nu} \qquad (4.1)$$

Where y^+ is a dimensionless wall distance, y the wall distance, k the turbulent kinetic energy and ν the kinematic viscosity of the fluid.

$$\nu_T = \nu \frac{y^+ \kappa}{\ln(E y^+) - 1} \qquad (4.2)$$

Where ν_T is the turbulent kinematic viscosity, κ the Von Kármán constant and E is an integration constant that depends on the roughness of the wall which numerical value is 9.8 for smooth walls. Equation (4.2) is an approximation of the turbulent viscosity assuming that in the logarithmic layer $\nu_t \gg \nu$.

The following is important to realize regarding the turbulent kinematic viscosity:

- The turbulence viscosity is not a property from the fluid but from the flow, in contrary to the kinematic viscosity. The turbulence viscosity models the transfer of momentum caused by turbulent eddies, which is called the Boussinesq eddy viscosity assumption;
- The turbulent kinematic viscosity near walls depends on the dimensionless wall distance y^+. This means the mesh near the bed should be modelled carefully in

order to obtain reliable properties of the flow near the bed. It is important that y^+ values are between 30 and 100.

4.2.3.2 Energy dissipation

Two different kind of boundary conditions are specified. The first one is a Dirichlet boundary condition specified as a fixed value of 0.000765 for the boundaries 'openBoundaries' and 'waterSurface'.

The second is the epsilon wall function which is applied for the remaining boundaries, since all of them can be considered as a wall. The source code for the wall function contains two equations, one for the turbulence dissipation field (ε) and one for the turbulence generation field (G)

$$\varepsilon = C_\mu \frac{k}{\kappa y} \tag{4.3}$$

$$G = C_\mu (\nu_T + \nu) \frac{\sqrt{k}}{\kappa y} \nabla \mathrm{U} \tag{4.4}$$

This boundary condition calculates ε and G and inserts the near wall values directly into the epsilon equation from the turbulence model to act as a constraint.

4.2.3.3 Turbulent kinetic energy

Two different kinds of boundary conditions are specified. The first one is a Dirichlet boundary condition specified as fixedValue of 0.00325 for the boundaries 'openBoundaries' and 'waterSurface'.

The second is the turbulent wall function. This wall function provides a condition for the turbulence k for the case of high Reynolds number flow using wall functions.

4.2.3.4 Pressure

Except for the openBoundaries all boundary conditions are set to be zeroGradient. This is a Neumann boundary condition which sets the derivative of the pressure at the boundary equal to zero.

For the openBoundaries a mixed inlet and outlet boundary condition is imposed. For the pressure this boundary condition is specified as 'outletInlet' which means that normally a Dirichlet boundary condition is imposed but it becomes a homogeneous Neumann boundary condition when the flow reverses.

4.2.3.5 Velocity

Except for the openBoundaries all boundary conditions are set to be fixedValue. This is a Dirichlet boundary condition which sets the value for the velocity at the boundary equal to zero.

For the openBoundaries a mixed inlet and outlet boundary condition is imposed. For the velocity this boundary condition is specified as 'inletOutlet' which means that normally a Dirichlet boundary condition imposed but it becomes an outflow boundary condition when the flow reverses.

4.3 Erosion model (Matlab)

An *erosion rate* or an *erosion velocity* (i.e. the velocity of the downward moving bed perpendicular to bed) is calculated in order to determine the displacement of the bed cells. This method is described in section 4.3.1. The expression for the erosion velocity is implicit and needs to be solved numerically. The applied numerical method is described in section 4.3.2. In order to calculate the erosion velocity, the *mobility parameter* is required which is formulated in section 4.3.3.

4.3.1 Mesh deformation due to erosion

The erosion velocity is determined with the function of [Van Rhee, 2010] as described in section 2.4.1.

The erosion velocity v_e is calculated numerically using the bisection method[4]. The advantage of the bisection method is that it is always converging and relative simple to implement in the model. A disadvantage is that the bisection method converges slowly compared to e.g. Newton Raphson. However, in this case the additional computation time is insignificant, since the most time consuming part of the total calculation is the hydrodynamic model in OpenFOAM. The calculation of the erosion velocities is in the order of percentages of the total computation time.

With the obtained erosion velocity the bed level change is calculated by multiplying the erosion velocity with a time step Δt of 5 seconds. When the time step is increased to e.g. 10 seconds, irregularities in the bed mesh will appear inducing unstable simulations. When the time step is chosen smaller the computational time increases considerably. The updated bed level z^{n+1} in z-direction can be calculated with eq. (4.5).

$$z^{n+1} = z^n - \Delta z = z^n - v_e \cdot \Delta t \qquad (4.5)$$

The equation above is only valid for the initial time step, since the bed is horizontal in this time step. However, during scour development the bed is placed under an angle. This is important to realize since the erosion velocity is defined perpendicular on the bed. To calculate the erosion velocity, and so the displacement of the cell centres perpendicular to the bed, the unit normal vector $\widehat{\boldsymbol{N}}$ on each cell face is multiplied by the erosion velocity in order to obtain the displacement of the cell centres $\Delta\widehat{\boldsymbol{U}}$ in x, y and z direction.

$$\Delta\widehat{\boldsymbol{U}} = \Delta t \cdot v_e \cdot \widehat{\boldsymbol{N}} \qquad (4.6)$$

Where

$$\Delta\widehat{\boldsymbol{U}} = \begin{bmatrix} \Delta x \\ \Delta y \\ \Delta z \end{bmatrix}$$

and

[4] See section 4.3.2 for a description of the bisection method

$$\widehat{\boldsymbol{N}} = \begin{bmatrix} u \\ v \\ w \end{bmatrix}$$

where by definition

$$\sqrt{u^2 + v^2 + w^2} = 1$$

The updated bed level coordinates $\widehat{\boldsymbol{U}}^{n+1}$ are calculated by adding the change in bed level $\Delta\widehat{\boldsymbol{U}}$ to the original bed level coordinates $\widehat{\boldsymbol{U}}^{n}$ of the previous time step

$$\widehat{\boldsymbol{U}}^{n+1} = \widehat{\boldsymbol{U}}^{n} - \Delta\widehat{\boldsymbol{U}} \qquad (4.7)$$

The bed level angle β in eq. (2.10), where the modified Shields parameter is calculated, is determined with the z-component w of the unit normal vector.

$$\beta = \cos^{-1}(w) \qquad (4.8)$$

4.3.2 Bisection method

The erosion velocity is calculated for each cell centre on the bed. Since Van Rhee's expression for the erosion velocity is implicit it needs to be solved numerically. The numerical method applied in this case is the bisection method, which is described with according to [Vuik et al., 2007].

> *"Suppose f is a continuous function defined on the interval* $[a, b]$ *in which the product of* $f(a)$ *and* $f(b)$ *is negative. According to the intermediate value theorem*[5] *a number* p *exists in* (a, b) *where* $f(p) = 0$*. It is assumed there is just one* p *like that. In the method the interval is bisected in each step where* p *lies. Starting the method with* $a_1 = a$ *and* $b_1 = b$ *and take for* p_1 *the average of* a_1 *and* b_1*:*
>
> $$p_1 = \frac{1}{2}(a_1 + b_1) \qquad (4.9)$$
>
> *In case* $f(p_1) = 0$ *the calculation can be stopped, otherwise* $f(p_1)$ *has the same sign as* $f(a_1)$ *or* $f(b_1)$*. If* $f(p_1)f(a_1) > 0$ *than take* $a_2 = p_1$ *and* $b_2 = b_1$*, else* $a_2 = a_1$ *and* $b_2 = p_1$*. After that the same procedure is repeated for the interval* $[a_2, b_2]$*. Since the bisection method is an iterative method a stop criteria is required. The stop criteria is defined in this case as"*
>
> $$|f(p_n)| < \varepsilon \qquad (4.10)$$

Where $\varepsilon = 1 \cdot 10^{-6}\ m/s$.

[5] "*Intermediate value theorem: Assume* $f \in C[a, b]$*. Let* $f(a) \neq f(b)$ *and let* F *be a number between* $f(a)$ *and* $f(b)$*, then there exists a number* $c \in (a, b)$ *such that* $f'(c) = 0$*."*

4.3.3 Mobility parameter

To determine de mobility parameter two options are considered:

1. Method similar to [Hoan, 2008] or [Hofland, 2005] as described in Appendix A.4, which using the flow velocity and kinetic turbulence energy averaged over a certain length scale relative to the bed;
2. General method in which the bed shear stress is determined based on the flow properties near the bed, which can be used to calculate Shields mobility parameter according to equation (4.11)

$$\Psi_s = \frac{\tau_b}{\rho \Delta g d} \qquad \textbf{(4.11)}$$

Characteristic for the first method is that non-local properties of the flow are used, in contrast to the second method where the region close to the bed is examined. In the current model the second approach is applied.

Hofland argued why the use of non-local parameters can be justified (and is even necessary) by looking at the definition of the turbulent kinetic energy k. Namely, knowing that k obtained from the k-ε model only represents the second order moments of the velocity components it is possible to justify the use of the non-local parameters for k and u.

However, using the method according to [Hofland, 2005] for this specific case is doubtful. The main problem is the use of the length scale over which the flow velocity u and turbulent kinetic energy k is averaged. In the case of Hofland the length scale (L_H) of the turbulence is in the order of the water depth, which is definitely not the case for a horizontal jet over the bed. Hofland used a flume with turbulent flow, with lower flow velocities and a logarithmic average velocity profile over depth. The deflected jet due to a bow thruster near the bed is far from logarithmic and approaches more or less block shaped velocity profile. This means that the choice of a proper mixing length without further detailed research would be rather arbitrary for this study.

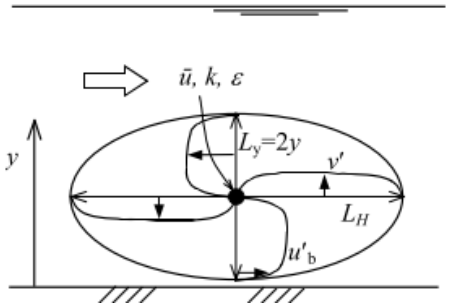

Figure 4.12 Model of large scale eddy that causes damage [Hofland, 2005]

In the expression of Van Rhee Ψ_s is determined with equation (4.12) in which the turbulent kinematic viscosity ν_t represents the influence of turbulence on the bed shear stress.

$$\Psi_s = \frac{\tau_b}{\rho \Delta g D_{50}} = \frac{\rho(\nu + \nu_T)\nabla U}{\rho \Delta g D_{50}} = \frac{(\nu + \nu_T)\nabla U}{\Delta g D_{50}} \quad (4.12)$$

The values for the turbulent viscosity ν_t and the velocity gradient ∇U follow from the numerical model in OpenFOAM on each cell face near the bed. The other parameters are constants which are described in the next section.

4.4 Applied parameters

The parameters in Table 4.1 are used in the erosion model in Matlab in order to obtain results which are similar to the measured scour depth in the Port of Rotterdam. In Table 4.2 the main dimensions regarding the vessel in OpenFOAM are given. Those values are also used in each run for the sensitivity analysis, unless noticed otherwise.

The parameters in Table 4.1 and Table 4.2 indicated with a star * will vary in the sensitivity analysis.

Table 4.1 Fixed parameters in the numerical model in Matlab

Variable	Expression	Value	Dimension
Gravitational acceleration	g	9.81	[m/s^2]
Density of sand particles	ρ_s	2650	[kg/m^3]
Density of salt water	ρ	1025	[kg/m^3]
Grain size diameter*	D_{50}*	225	[µm]
Grain size diameter*	D_{15} *	90	[µm]
Kinematic viscosity of water (T=10°C)	ν	1.307*10^{-6}	[m^2/s]
Porosity prior to erosion*	n_0 *	40	[%]
Porosity of the loose soil condition*	n_1 *	44	[%]
Coefficient in expression for permeability	C_k	1/160	[-]
Coefficient for for single particle mode	A_1	¾	[-]
Near bed sediment concentration	c_b	0	[m^3/m^3]
Friction angle of sand	φ	30	[°]
Time step in quasi-steady state model	Δt	5	[s]

The standard grain size diameters as mentioned in Table 4.1 are based on the soil parameters from the full scale test in the Port of Rotterdam (section 2.5.2).The common values for natural sands of the porosities are given by [Mastbergen & Van Den Berg, 2003]. The value for n_0 suggested by those authors, is in the same order of magnitude with the soil survey regarding the sand parameters in the Port of Rotterdam.

The near bed sediment concentration c_b is assumed to be zero. This means that settlement of the sediment particles is neglected.

Table 4.2 Dimensions regarding vessel in computational domain in OpenFOAM

Variable	Expression	Value	Dimensions
Distance from thruster axis to bed	h_p	3.65	[m]
Keel clearance	K	3.00	[m]
Diameter of thruster duct	D_0	0.91	[m]
Efflux velocity *	V_0 *	8.00	[m/s]
Water depth	h	7.15	[m]
Minimum distance between vessel and quay	L_{min}	3.25	[m]
Maximum distance between vessel and quay	L_{max}	14.5	[m]
Horizontal displacement of vessel per time step	ΔL	0.75	[m]

4.5 Results

This section presents the results regarding the scour development applying the parameters as mentioned in Table 4.1 and Table 4.2. Figure 4.13 gives an overview of the numerical domain during the 6th departure of the vessel for the case of MTS Noordzee. The directions of the velocities show the behaviour of the hydrodynamics. It is clearly visible that the jet hits the wall and the deflected jet is causing the largest erosion near the toe of the quay wall. Note that the arrows in the figure only indicate the flow direction, and not the magnitude of the flow velocity U. The magnitude of the flow is indicated by colours. Also the scour depth is indicated by the grey shaded area.

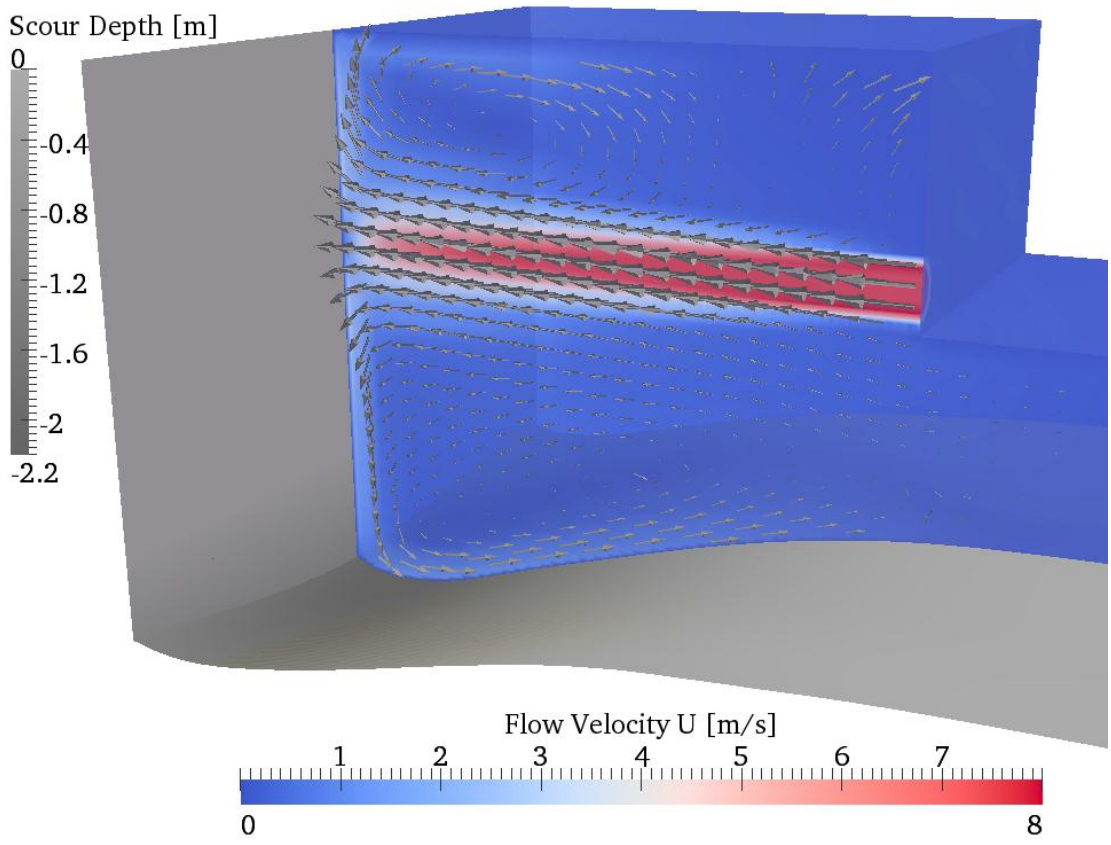

Figure 4.13 Computational domain during 6th departure of the vessel

4.5.1 Dimensions of scour hole in horizontal plane

The dimensions of the scour hole in the horizontal xy-plane are depicted in Figure 4.14. It is remarkable that in y-direction the scour hole is larger compared to the dimensions of the scour hole in x-direction. The width of the scour hole (in cross-direction) is about 9 meters (Figure 4.14 and Figure 4.17). Also the measurements from the full scale test with MTS Noordzee results in a relative small width of the scour hole of 4 meter. It is important to note that in case a low flow velocity near the bed occurs nothing happens with the sediment until a critical erosion velocity is reached. This is especially the case for cohesive materials. This can result in a difference in width of the scour hole between measurements and numerical model, since further away from the quay wall the near bed velocities near the wall are relative low.

In addition the bed angle of the slope is different. In the full scale tests the slope is about 2:3 and in the numerical model about 1:3. The difference in slope angle can be due to the fact that the top layer of the soil along the Parkkade consists of clay. This could be also the reason for the difference in dimensions between measurements and numerical model. Another reason for the difference in slope is that in the numerical model the sedimentation is neglected; however in the measurements in Figure 4.17 it is visible that there is a relative small amount of sedimentation in the direction perpendicular to the quay wall (but no sedimentation in longitudinal direction).

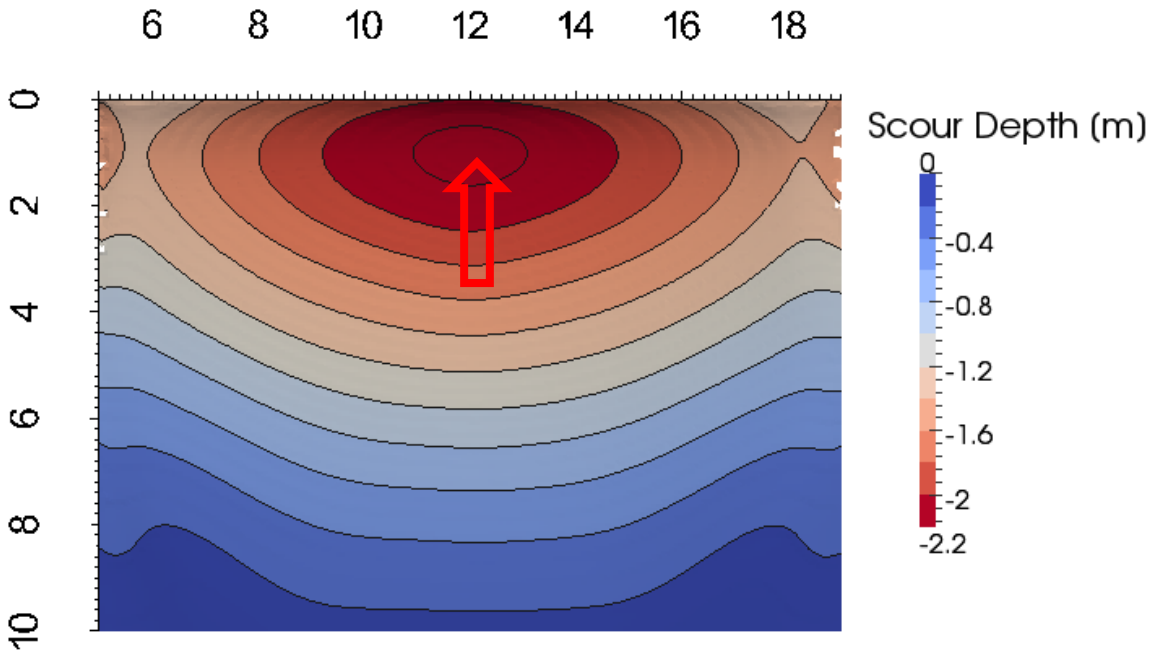

Figure 4.14 Bed profile of numerical simulation (xy-plane) after six departures of the vessel with dimensions in [m]

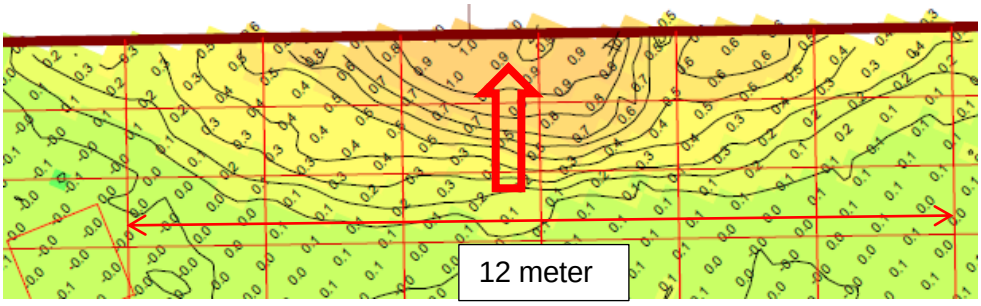

Figure 4.15 Measurements scour depth along Parkkade – 2 departures Jade – Compact Jet Bow Thruster

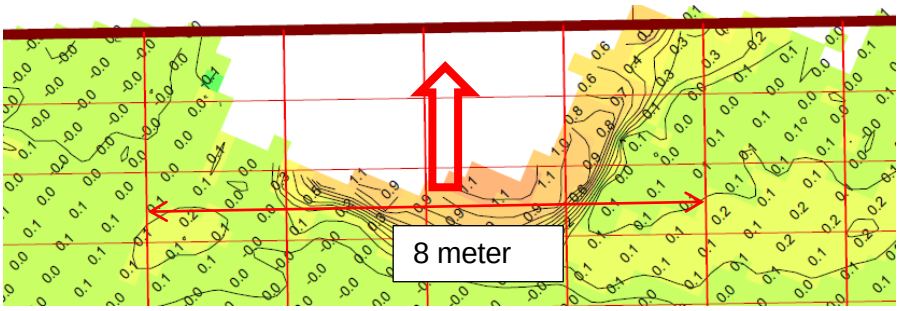

Figure 4.16 Measurements scour depth along Parkkade – 6 departures MTS Noordzee

Note regarding Figure 4.15 and Figure 4.16:

The location of the bow thruster in the figures below are indicated with a red arrow.

The thick red line corresponds to the front of the concrete upper structure of the quay wall. The front of the concrete upper structure lies 0.75 m in front of the center line of the steel combi-wall (existing of piles and sheet piles underneath the concrete upper structure, see Figure 3.1). The front of the concrete upper structure lies 0.54 m in front of the front of the sheet piles and 0.95 m in front of the back side of the sheet piles. The mean position of the front surface of the quay wall below water is estimated about 0.6m behind the thick red line.

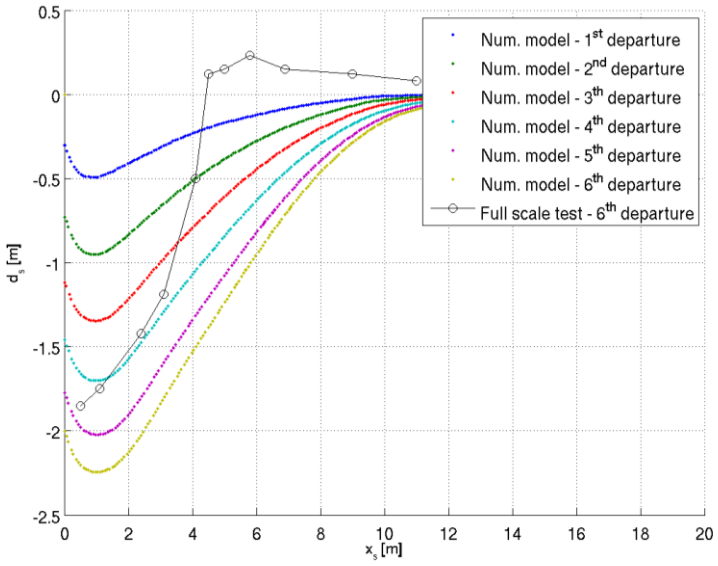

Figure 4.17 Cross section of the scour hole in the numerical model compared with full scale tests

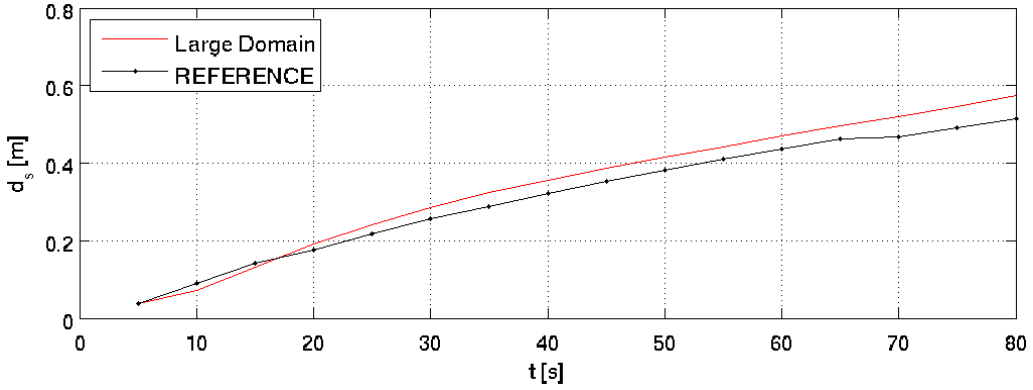

Figure 4.18 Influence of the domain boundaries on maximum scour depth

In Figure 4.14 it seems like a second scour hole will develop on the boundaries of the domain. This is in reality not the case, but is caused by the boundaries of the numerical domain. In order to study the influence of the boundaries an additional simulation for a single departure is performed with a large domain in longitudinal direction. Figure 4.18 compares the maximum scour depth for the first departure with the small domain (REFERENCE case, i.e. first departure of the simulation with 6 departures elaborated in this chapter) and the large domain. This shows that the effect of the boundaries on the maximum scour depth is relative small.

4.5.2 Maximum scour depth

The model behaves as expected regarding the decrease of erosion in time. In Figure 4.20 it is visible that during the departure the erosion velocity is decreasing. The erosion velocity is different on each cell face, so in the figure the erosion velocity of the deepest point of the scour hole is calculated. Each peak of the erosion velocity in Figure 4.20 indicates the start of a departure of the vessel. In the sequent departures the maximum erosion velocity per departure is always lower than the maximum erosion velocity in the departure before. Due to the increase of the scour depth in time the flow velocity near the bed is lower and because of this also the erosion. This results in a decreasing increase of the scour depth (Δd_s), after each sequent departure of the vessel. This is depicted in Figure 4.21.

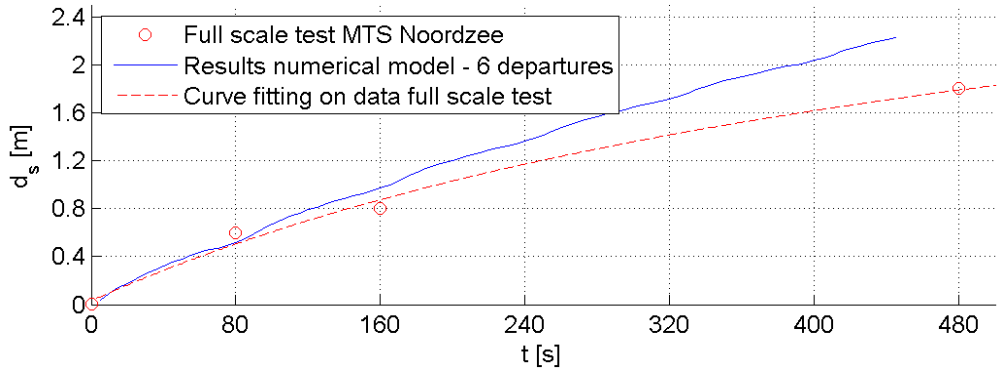

Figure 4.19 Maximum scour depth in time – 6 departures

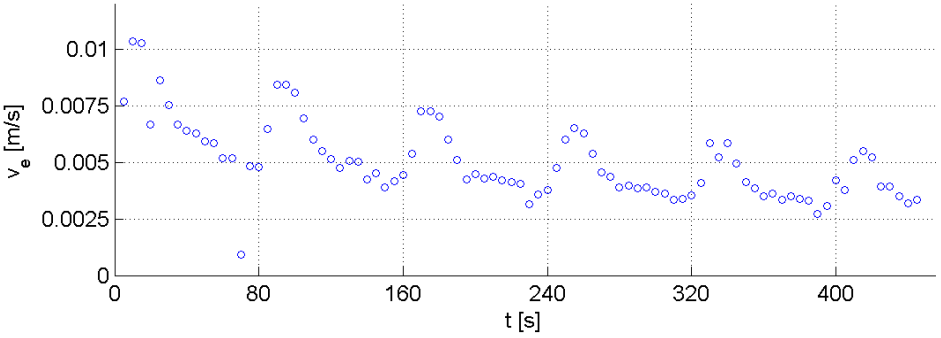

Figure 4.20 Erosion velocity at the maximum depth of the scour hole during 6 departures

However, the increase of the scour depth in the model is conservative compared to the measurements. The more departures the larger is the deviation between measured and calculated scour depth. It seems like this is because the soil near the Parkkade consists of clay and fine sand with clay layers. However, the measurements of the scour depth near the Parkkade show no correlation between erosion depth and clayey or sandy characteristics of the soil. Probably the upper part of the clay is very low consolidated and therefor has a low strength. Contrary to this, the scour in the numerical model is described with an empirical relation for sand. It is difficult to attribute the difference in behavior regarding the increase in scour depth to the amount of fine sediments and clay near the Parkkade in the Port of Rotterdam, or to the hydrodynamics in the numerical model.

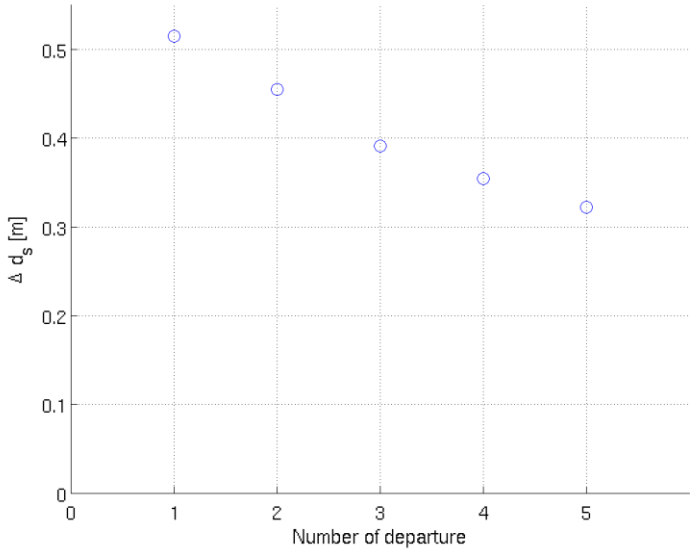

Figure 4.21 Difference in scour depth per departure

In the introduction part of this chapter (Figure 4.1) the equilibrium depth is defined in case the difference in erosion between two sequent departures $\Delta d_s < 10\ cm$. After five departures this is not yet the case. Due to calculation time the simulation is stopped during the sixth departure of the vessel, since the difference in scour depth between the fourth and the fifth departure is still 32 cm (Figure 4.21).

4.5.3 Increase of maximum quay clearance

The maximum distance between ship and quay in the numerical model is 14.5m, since the computational domain is limited in x-direction. In order to study the influence on the maximum scour depth in this model the distance between keel and ship is increased for a single departure up to 21.5m. The maximum scour depth and the erosion velocity are depicted in Figure 4.22 and Figure 4.23. The increase in maximum scour depth from t=80s up to t=150s is rather big. Since the radial spreading of the propeller jet in the model is underestimated, the near bed velocities are overestimated for a large quay clearance, which makes it difficult to define a maximum distance between ship and quay. Hence the choice of this distance is rather arbitrary. However, this does not influence the results from the sensitivity analysis.

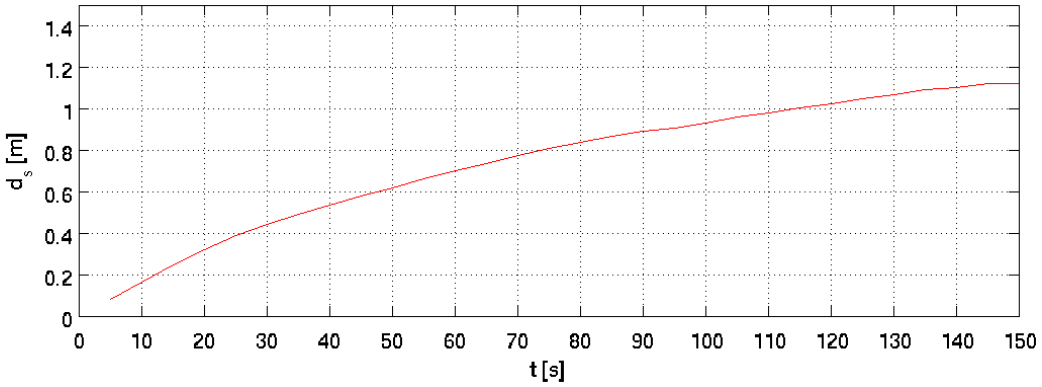

Figure 4.22 Maximum scour depth during 1 departure with increased maximum quay clearance

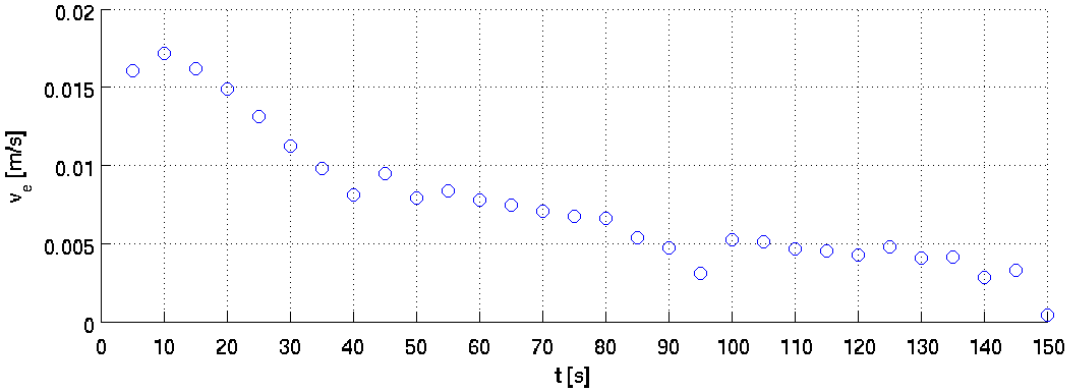

Figure 4.23 Erosion velocity during 1 depature with increased maximum quay clearance

4.6 Conclusions regarding assumptions in the numerical model

Several assumptions are made in the numerical model. The assumptions from the model are elaborated and divided in the hydrodynamics and modelling of erosion. A comparison between applied parameters of the numerical model and the real parameters during the full scale test along the Parkkade is presented in the last subsection.

4.6.1 Hydrodynamics

Regarding the hydrodynamics the following remarks and assumptions are made:

- The numerical model is quasi-transient. The hydrodynamic model in OpenFOAM is steady state and the erosion is calculated based on the steady state conditions for a time step of five seconds.

- Wall functions are not taken into account in the model for the numerical model. This is a limitation in the sense that the influence of turbulence and (high) velocity gradients near the wall is not modelled proper. However, this does not lead to unrealistic results regarding the scour depth. This can be explained, since the maximum load on the bed is also determined by flow properties in the water column above the location of erosion according to [Hoan, 2008] and [Hofland, 2005]. By applying a relative coarse mesh near the bed this averaging is a side effect of the lack in the model regarding the mesh generation. Although this is rather speculative and from physical point of view not desirable, it does not affect the sensitivity analysis for soil parameters regarding the erosion.

- The influence of the propeller on radial spreading of the jet is not taken into account. The radial spreading of the jet is underestimated. This implies that the decrease of the flow velocity along the jet axis is also underestimated, which implies that the decrease of the maximum bed velocity for increasing distance L between ship and quay is also underestimated.

- In reality the bow thruster needs about 10 seconds before it reaches its maximum power. In the model this problem is tackled by the steady state approach of the hydrodynamics, to avoid a peak in the near-bed velocity when the jet hits the bottom in the first few seconds of the simulation. Beside this the applied power is assumed to be constant in time in the numerical model however during the first 10 seconds of the departure this is not the case.

- The efflux velocity V_0 of the thruster is in all cases 8 m/s.

- The influence of the shape of the ship is not studied. The shape of MTS Noordzee is assumed to be a rectangular cross section in the numerical model. The ship length is assumed to be infinite.

- The simulation of 1 departure is stopped when the distance between quay and ship is 14.5m.

- It should be noticed that for a thruster with a channel system it is not clear how much influence the propeller has on the propagation and spreading of the jet. In the thruster with the channel systems the jet is making an angle of 90 degrees after passing the propeller and is then flowing through a few meters long channel. This will reduce the influence of the vorticity created by the rotating propeller.

4.6.2 Erosion

Regarding the erosion and the soil the following remarks are made:

- The model is valid for non-cohesive soil, in this case sand. However, the top layer of the soil located in the Port of Rotterdam where the full scale tests are elaborated consists of clay. This might influence the validation of the model.

- Settling of the sediment is not taken into account. This can be justified, since the measurements shows that there is hardly any sedimentation near the location of the local scour. According to [Blokland, 2013] this is can (partly) be a result of advection of the sediment due to the river flow, in the case of the port of Rotterdam. The sediment is stirred up and will settle upstream.

- Sand slides are not considered in the model.

4.6.3 Comparison parameters full scale test and numerical model

In Table 4.3 the numerical values in the numerical model and the full scale tests are compared. The soil parameters along the Parkkade are indicated with a range of numerical values. E.g. for grain size diameter D_{50} the minimum value which is measured is 178 μm and the maximum measured value is 246 μm.

Table 4.3 Comparison between parameters from the full scale test (reality) and the numerical model

Variable	Expr.	Value		Dimension
		Numerical model	Full scale test	
Grain size diameter	D_{50}	225	178 - 246	[μm]
Grain size diameter	D_{15}	90	69 - 155	[μm]
Gradation 1	D_{60}/D_{10}	-	1.6 - 2.6	[-]
Gradation 2	D_{50}/D_{15}	2.5	1.8 - 2.6	[-]
Porosity prior to erosion	n_0	40	40.8 - 46.3	[%]
Porosity of the loose soil condition	n_1	44	unknown	[%]
Friction angle of sand	φ	30	30 - 40	[°]
Cohesion	c	-	1 - 6	[kPa]
Distance from thruster axis to bed	h_p	3.65	3.65	[m]
Keel clearance	K	3.00	3.00	[m]
Diameter of thruster duct	D_0	0.91	0.91	[m]
Efflux velocity [6]	V_0	8.00	≈7.7 - 8.5	[m/s]
Water depth	h	7.15	7.15	[m]
Minimum distance between vessel and quay	L_{min}	3.25	3.25	[m]

[6] This is not a measured value, but the estimated value based on an the maximum applied power of 320 kW estimated with equation (2.1)

5 Sensitivity Analysis

In this chapter the sensitivity of the model to several input parameters is presented, which might influence the development of the scour in time. The soil parameters regarding grain size diameter and porosity are investigated and, in addition, the sensitivity to the applied power. A short summary of the results and conclusions are presented in section 5.4. Each run for a particular combination of input parameters contains two departures of the vessel. It is expected that this amount of departures provides enough information to analyse the sensitivity of the model.

Note: The applied (standard) parameters in the sensitivity analysis are described in section 4.4, Table 4.1. However, the fixed values for the grain size diameter in the sensitivity analysis are different from the values in Table 4.1. Unless noticed otherwise $D_{15} = 125\ \mu m$ and $D_{50} = 235\ \mu m$ for the runs in the sensitivity analysis.

5.1 Grain size diameter

The erosion velocity is a function of two different grain diameters, D_{15} and D_{50}. The influence of D_{50} is expected to be relative low since it is in the root for both the equation of the modified Shields parameter and the expression for the erosion velocity. For D_{15} this is not the case. The permeability is a function of D_{15}^2 which might result in a higher sensitivity for D_{15}. For clarity an overview of the governing equations regarding the erosion velocity is given below.

Expression for erosion velocity: $\frac{1}{1-n_0}\left(\Phi_p^1\sqrt{g\Delta \boldsymbol{D_{50}}}\right) - v_e = 0$

Modified dimensionless pick-up rate: $\Phi_p^1 = 0.00033 D_*^{0.3}\left(\frac{\Psi_s - \Psi_{s.cr}^1}{\Psi_{s,cr}^1}\right)^{1.5}$

Dimensionless particle diameter: $D_* = \boldsymbol{D_{50}} \cdot \sqrt[3]{\frac{\Delta g}{\nu^2}}$

Modified Shields parameter: $\Psi_{s,cr}^1 = \Psi_{s,cr}\left(\frac{\sin(\phi-\beta)}{\sin\phi} + \frac{v_e}{k_l}\cdot\frac{n_l - n_0}{1-n_l}\frac{A_1}{\Delta}\right)$

Permeability of sediment: $k_l = C_k \frac{g}{\nu}\boldsymbol{D_{15}^2}\frac{n_l^3}{(1-n_l)^2}$

To quantify the influence of the grain diameters several combinations of grain size diameters are used in the numerical model.

5.1.1 Description of applied diameters

The separate influence of the change of D_{50} and D_{15} is investigated by keeping D_{15} constant in the first eight runs and keeping D_{50} constant in the last five runs. The constant values $D_{50} = 235$ μm and $D_{15} = 125$ μm are based on the local soil conditions in the Port of Rotterdam located nearest to MTS Noordzee. The variation in the grain size diameters in the sensitivity analysis is based on the different results of the soil survey

along the quay Parkkade in the Port of Rotterdam. In addition two simulations are carried out for relative coarse sand and three simulations (D11-D13) with a constant grading, but different grain sizes. The values for the grain size diameters are presented in Table 5.1.

Table 5.1 Variation of grain size diameters for different runs

	Run	D_{50} [μm]	D_{15} [μm]	D_{50}/D_{15} [-]
D_{15} constant	D1	150	125	1.2
	D2	200	125	1.6
	D3	225	125	1.8
	D4	**235**	**125**	**1.9**
	D5	245	125	2.0
	D6	300	125	2.4
	D6A	600	125	4.8
	D6B	1200	125	9.6
D_{50} constant	D7	235	50	4.7
	D8	235	80	2.9
	D9	235	100	2.4
	D4	235	125	1.9
	D10	235	140	1.7
D_{50}/D_{15} constant	D11	150	80	1.9
	D12	200	107	1.9
	D4	235	125	1.9
	D13	300	160	1.9

Note: Run D1, D7, D8 and D11 contain very fine sand particles. In reality those values only occur in the transition zone between clay and sand regarding particle size. However the empirical relation is validated for sand. Run D4 is the reference case in the entire sensitivity analysis.

5.1.2 Discussion of Results

The maximum depth of the scour hole d_s is plotted in time, for two departures. Each departure in the model takes 80 seconds in the real time. The graphs for the scour development in time, resulting from the different runs in the simulation, are divided in plots for:

- Scour depth in time with a constant value $D_{15} = 125\,\mu m$, for fine sand ($150\,\mu m < D_{50} < 300\,\mu m$) (Figure 5.1);
- Scour depth in time with a constant value $D_{15} = 125\,\mu m$, for coarse sand ($600\,\mu m < D_{50} < 1200\,\mu m$) (Figure 5.2);
- Scour depth with a constant value $D_{50} = 235\,\mu m$, for fine sand with varying D_{15}. ($50\,\mu m < D_{15} < 140\,\mu m$) (Figure 5.3.).
- Scour depth with a constant grading $D_{50}/D_{15} = 1.9$, for fine sand $150\,\mu m < D_{50} < 300\,\mu m$ (Figure 5.4).

An overview of the maximum scour depth after two departures as function of the grain size diameter D_{15} and D_{50} are respectively depicted in Figure 5.6 and Figure 5.5.

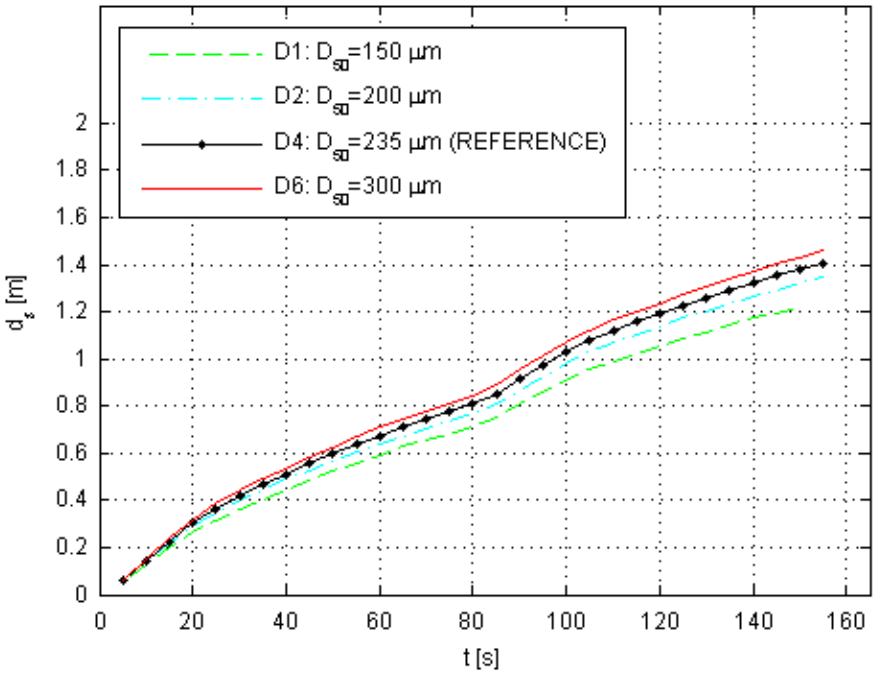

Figure 5.1 Scour depth in time for fine sand– D_{15} is constant - 2 departures

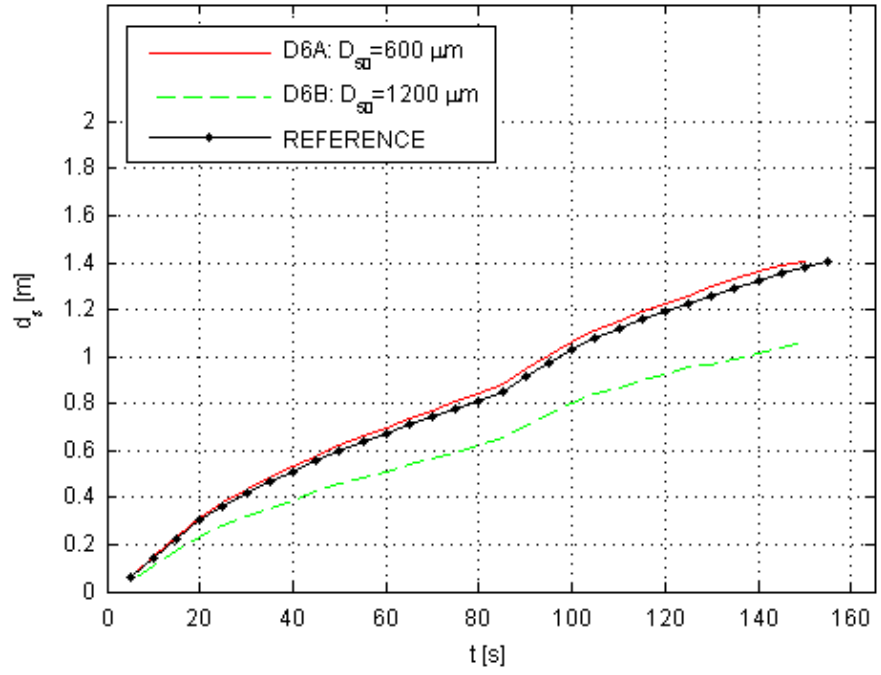

Figure 5.2 Scour depth in time for coarse sand – $D_{15} = 125\ \mu m$ is constant - 2 departures

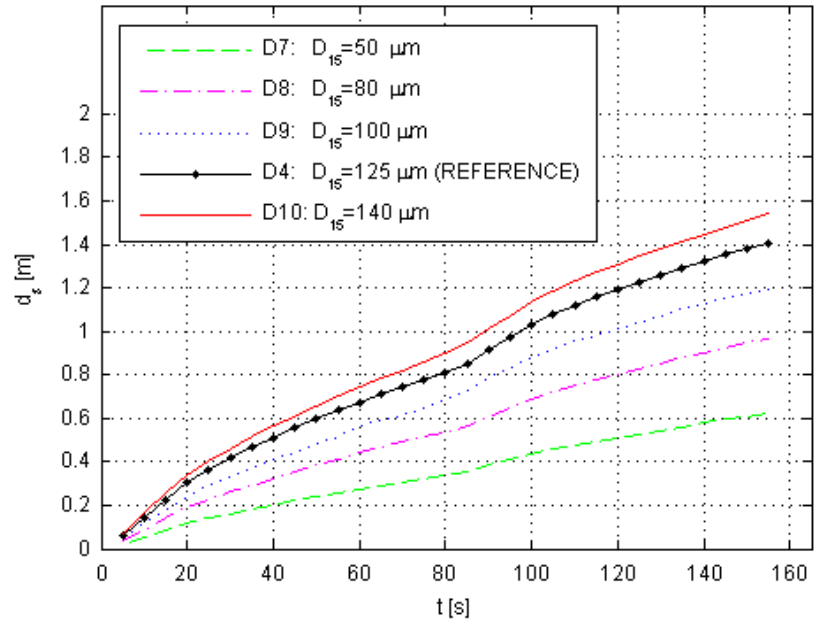

Figure 5.3 Scour depth in time for fine sand - $D_{50} = 235\ \mu m$ is constant – 2 departures

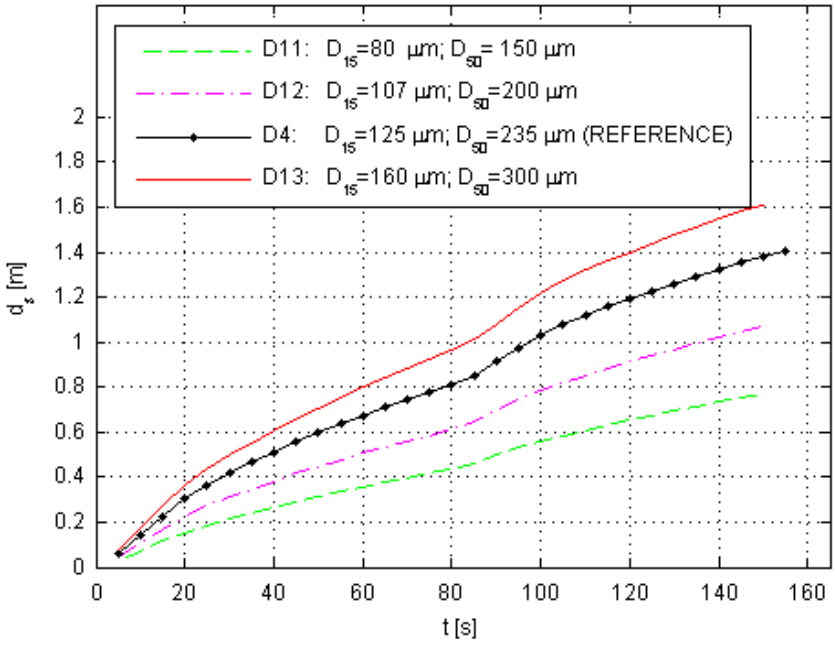

Figure 5.4 Scour depth for relative fine sand during 2 departures– constant grading $D_{50}/D_{15} = 1.9$

5.1.2.1 Influence of grain size diameter

As expected the model is sensitive for variations in the parameter D_{15}. Comparing run D7 ($D_{15} = 50\mu m$) and run D10 ($D_{15} = 140\mu m$) the difference in maximum scour depth is almost 1 meter. A decreasing grain size diameter in general results in lower erosion velocities. This seems counterintuitive, since one could expect that larger particles are more difficult to be picked up by the flow due to its weight. However there is a physical explanation why this is not always the case. In case the soil contains a relative large amount of fine sand, the pores between the bigger grains are filled with smaller particles. This is increasing resistance for the water to flow between the pores to bring the soil in a

state of sufficient porosity in order to erode. This implies a higher hydraulic gradient and an increase of the effect of hindered erosion, which results in lower erosion velocities and less scour.

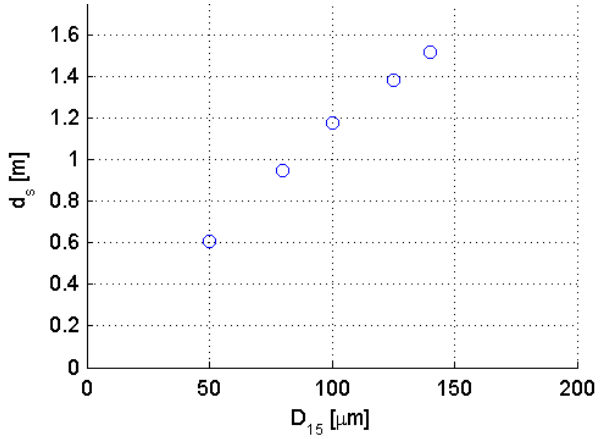

Figure 5.5 Maximum scour depth as function of grain size D_{15} after 2 departures

In Figure 5.6 the same effect is observable for the grain size parameter $D_{50} \leq 300\mu m$, but the effect is much smaller. The difference in maximum scour depth for run D1 ($D_{50} = 150\ \mu m$) and run D6 ($D_{50} = 300\ \mu m$) is just 23 cm. In case the particles becomes larger, the mass is also bigger, which causes more gravitational resistance against erosion due to the weight of the particles, which results in lower bed erosion. For $225\ \mu m < D_{50} < 600\ \mu m$ the maximum scour depth is more or less constant. In case $D_{50} > 600\ \mu m$ the maximum scour depth is decreasing again due to the increasing weight of the particles.

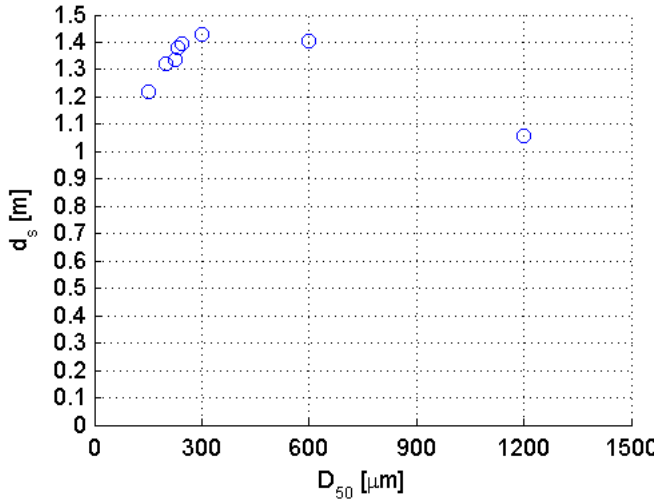

Figure 5.6 Maximum scour depth as function of grain size D_{50} after 2 departures

5.1.2.2 Influence of grain size distribution on maximum scour depth

Analytical solutions for both constant and variable soil gradings are plotted as function of D_{50} in Figure 5.7, in order to study the sensitivity of the grain size distribution on the rate of erosion. To study the effect on the resulting maximum scour depth several numerical simulations has been carried out with constant grain size, in the range of relative fine sand (Figure 5.8).

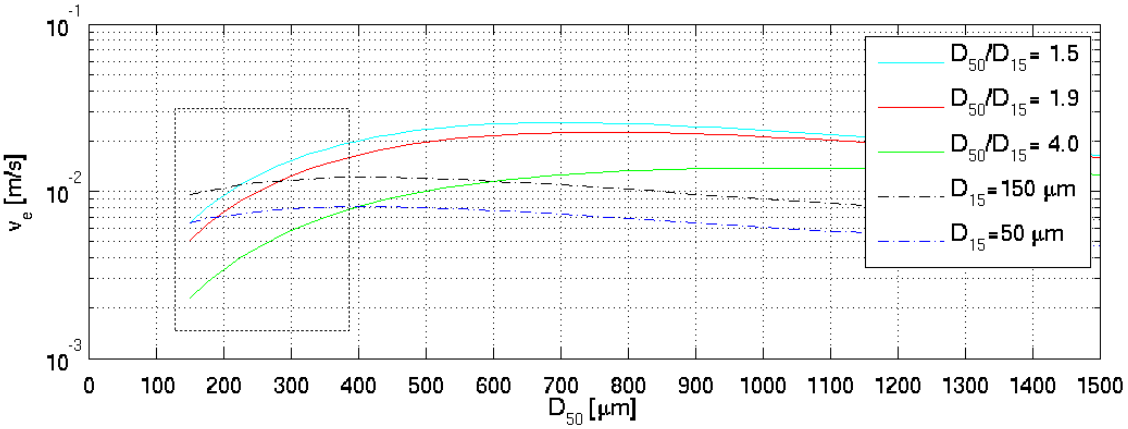

Figure 5.7 Analytical solution for the erosion velocity according to [Van Rhee 2010] for different constant and variable grading's – dashed square indicates range in grain size diameters of simulations in Figure 5.8

In both the analytical solution and the numerical model the same trends regarding erosion velocity are visible. Namely, in case the grain size distribution is constant, with increasing grain size diameter D_{50}, the erosion is more sensitive compared to the analytical solution of the erosion velocity with a constant D_{15} (i.e. variable grading). This is not surprising, since the previous sections show that the erosion velocity is mainly governed by the amount of fine sediments. In case the gradation remains constant, and D_{50} is increasing, the amount of fine sediment D_{15} have to increase as well by definition of the grading D_{50}/D_{15}.

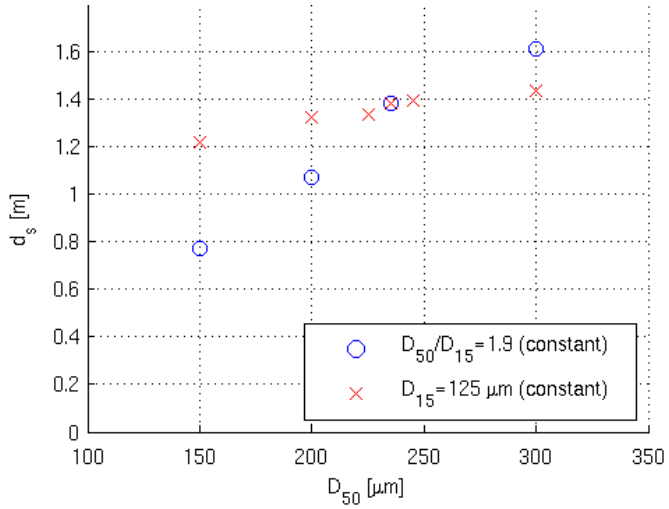

Figure 5.8 Comparison for maximum scour depth between soil with constant grading $D_{50}/D_{15} = 1.9$ and a constant $D_{15} = 125\ \mu m$

The dimensionless maximum erosion depths of all simulations in the sensitivity analysis regarding grain size diameter are plotted as function of the grain size distribution in Figure 5.9. This shows the correlation between scour depth and the grading of the soil. In case the grading becomes very high, i.e. a large amount of fine particles in the soil, the maximum erosion depth is increasing considerably.

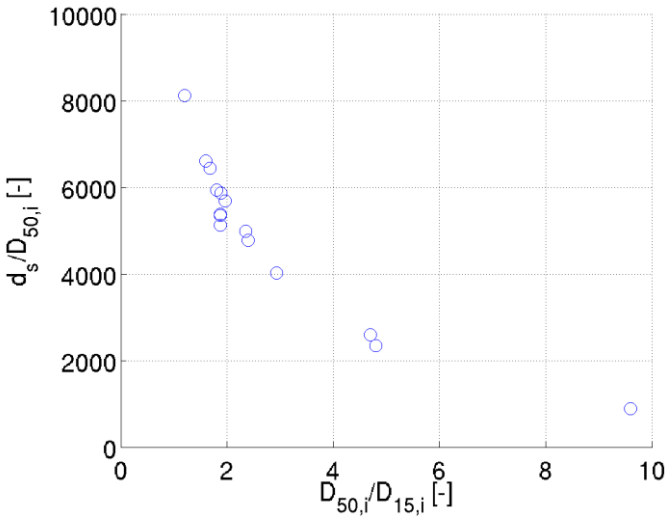

Figure 5.9 Correlation between maximum scour depth after two departures and grading of the soil – i indicates the number of the simulation, where i=1,2,…n

Note: The dimensionless scour depth is defined as the absolute scour depth after two departures, divided by the median grain size diameter D_{50} of the *particular* simulation.

5.1.2.3 Comparison with [Shields, 1936]

The critical Shields parameter and the erosion velocity (equivalent to the maximum scour depth) are compared in Figure 5.10. This is done by means of an analytical computation, where only the grain size diameter is variable. It is visible that the erosion velocity is inversely proportional to the critical Shields parameter. One can conclude that where the critical Shields parameter is the smallest, the erosion velocity and following from this the maximum scour depth is maximal.

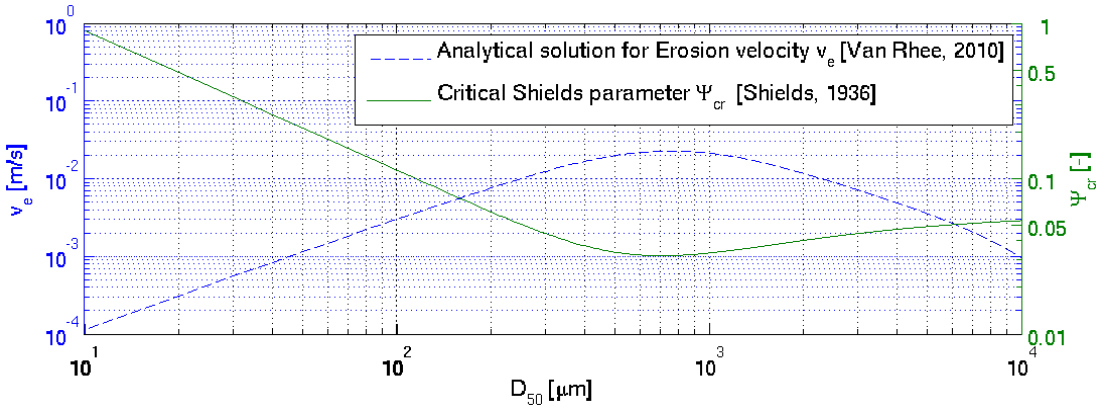

Figure 5.10 Critical Shields parameter compared with the analytical solution for the erosion velocity of [Van Rhee, 2010] as function of grain size diameter

Above it is assumed that the trend of erosion velocity from the analytical expression as function of grain size diameter is equivalent to the trend of the maximum scour depth from the numerical model. This assumption is verified below by comparing the results from the numerical model and the analytical solution.

Both erosion velocity and maximum scour depth show the same trend considering the grain size diameter. The maximum scour depth, following from the numerical model, as function of the grain size diameter is plotted in Figure 5.11 and compared with the erosion velocity which is calculated analytical for a fixed bed load, and identical soil parameters as the numerical model.

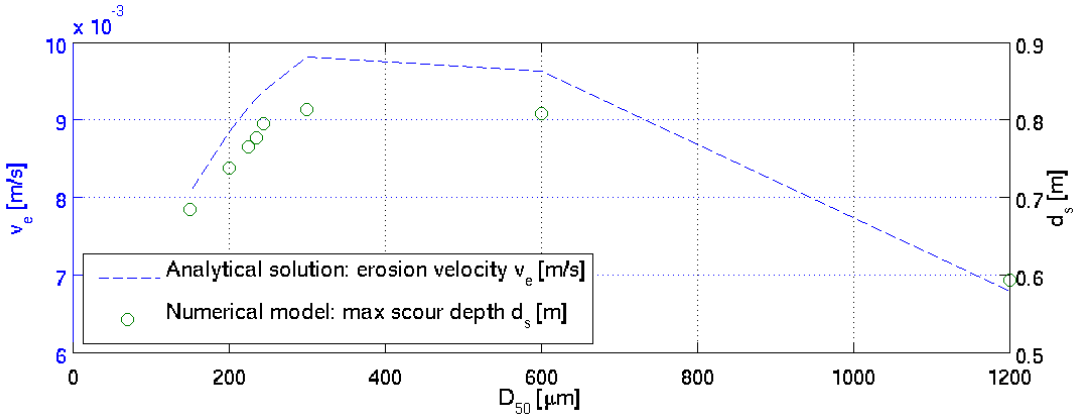

Figure 5.11 Comparison of erosion depth and erosion velocity as function of grain size diameter

5.2 Porosity

The porosity of the soil is an important parameter in the contribution to the scour since it influences the load on the bed due to the hydraulic gradient, which hinders the erosion. The porosity prior to erosion n_0 is quite often known, but the porosity of the loose soil conditions n_l after dilatation of the soil is more difficult to determine.

5.2.1 Description of applied parameters

The correlation between the porosity of the soil and the scour depth is studied for different types of ratios between n_0 and n_l, since the two different porosities are used in several expressions in order to calculate the erosion velocity. The first ratio r_1 which is considered is $r_1 = n_0/n_l$. This ratio gives information regarding the relative difference between the two porosities. The second ratio $r_2 = (n_l - n_0)/(1 - n_l)$ represents the influence of the porosity in the modified Shields parameter on the erosion velocity, neglecting the influence of the porosity on the permeability. The third ratio r_3 is derived in eq. (5.1). In this ratio the influence of porosity is considered involving the influence of the porosity on the permeability of the sediment. r_3 is in fact a measure for the resistance against, or hindering of, erosion. For clarity of the derivation of eq. (5.1) the expressions related to the erosion velocity which are applied in the model and described in section 2.4.1 are repeated below.

Note: In the applied formulation permeability is a function of porosity. However in reality a high porosity does not always imply a high permeability. E.g. clay has in general a high porosity, but due to the flow resistance the permeability is low. In fact the permeability depends on the size of the pores between the grains, through which the water flows. This diameter determines the wall resistance and so the permeability. So, the amount of voids in the soil sample, which is expressed by the porosity, is not related directly to the permeability.

Expression for erosion velocity: $\frac{1}{1-\boldsymbol{n_0}}\left(\Phi_p^1\sqrt{g\Delta D_{50}}\right) - v_e = 0$

Modified dimensionless pick-up rate: $\Phi_p^1 = 0.00033 D_*^{0.3}\left(\frac{\Psi_s - \Psi_{s.cr}^1}{\Psi_{s,cr}^1}\right)^{1.5}$

Modified Shields parameter: $\Psi_{s,cr}^1 = \Psi_{s,cr}\left(\frac{\sin(\phi-\beta)}{\sin\phi} + \frac{v_e}{k_l}\cdot\frac{\boldsymbol{n_l - n_0}}{\boldsymbol{1-n_l}}\frac{A_1}{\Delta}\right)$

Permeability of sediment: $k_l = C_k\frac{g}{\nu}D_{15}^2\frac{\boldsymbol{n_l^3}}{\boldsymbol{(1-n_l)^2}}$

$$\Psi_{s,cr}^1 = f\left(k_l^{-1}\cdot\frac{n_l - n_0}{1-n_l}\right) = f\left(\left[\frac{n_l^3}{(1-n_l)^2}\right]^{-1}\cdot\frac{n_l - n_0}{1-n_l}\right) = f\left(\frac{(n_l - n_0)(1-n_l)}{n_l^3}\right) \quad \textbf{(5.1)}$$

The parameters for each run of the sensitivity analysis regarding porosity are given in Table 5.2.

The first five runs (run n1-n5) are based on an increase of the *absolute difference* between the bed porosity prior to erosion n_0 and the porosity of the loose soil n_l, where the

erosion prior to erosion remains constant and the porosity of the loose soil is increased each run. Physically this means that the porosity of the soil itself is not investigated, but the influence of the amount of dilatation of the soil during the erosion process.

The last five runs (run n6-n10) are based on a *relative difference*. The porosity prior to erosion n_0 is increasing, and the porosity of loose sand n_l is 10% higher than the porosity prior to erosion. In this case the ratio between both values for the porosity remains constant; however the porosity of the soil is different in each run. Physically this means that the porosity of the soil itself is investigated and not the influence of the dilatation of the soil itself.

Table 5.2 Porosity parameters each run

	Run	$\boldsymbol{n_0}$ [%]	$\boldsymbol{n_l}$ [%]	$\frac{\boldsymbol{n_0}}{\boldsymbol{n_l}}$	$\frac{\boldsymbol{n_l - n_0}}{\boldsymbol{1 - n_l}}$	$\frac{\boldsymbol{(n_l - n_0)(1 - n_l)}}{\boldsymbol{n_l^3}}$
Absolute difference	n1	40	44	0.91	0.07	0.26
	n2	40	46	0.87	0.11	0.33
	n3	40	48	0.83	0.15	0.38
	n4	40	50	0.80	0.20	0.40
	n5	40	52	0.77	0.25	0.41
Relative difference	n6	41	45.1	0.91	0.07	0.25
	n7	43	47.3	0.91	0.08	0.21
	n8	45	49.5	0.91	0.09	0.19
	n9	47	51.7	0.91	0.10	0.16
	n10	50	55	0.91	0.11	0.14

5.2.2 *Discussion of results*

The maximum depth of the scour hole d_s is plotted in time, for two departures. Each departure in the model takes 80 seconds in the real time. In Figure 5.12 the scour depth for the five runs regarding the absolute difference between n_0 and n_l are depicted (n1-n5). In Figure 5.14 the scour depth for five runs regarding the relative difference between n_0 and n_l are depicted (n6-n10). The effect of the difference between an increase of the relative and absolute difference of the porosities is better visible in Figure 5.13 and Figure 5.15. Here the maximum scour depth after two departures is plotted as function of $r_2 = (n_l - n_0)/(1 - n_l)$ as an indication for the porosity properties of the soil.

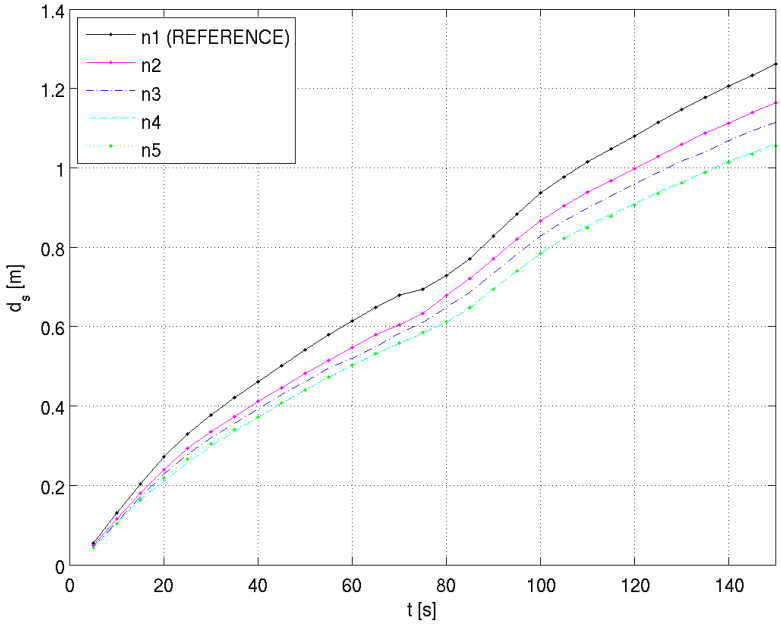

Figure 5.12 Run n1-n5: Maximum scour depth in time – Absolute difference n_0 and n_1– 2 departures

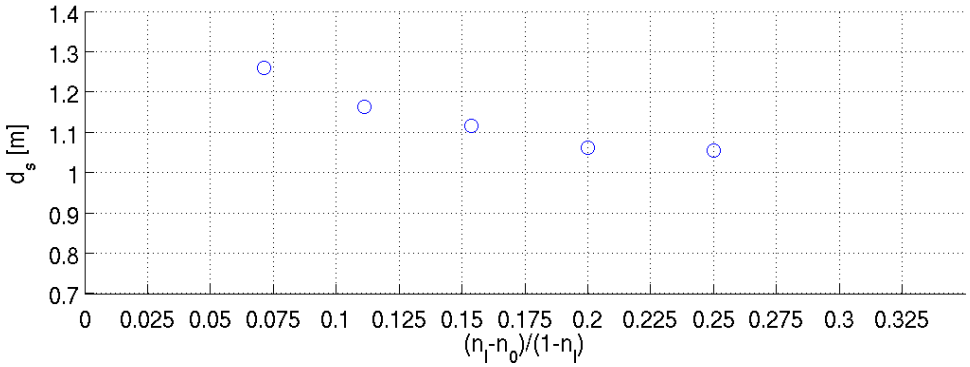

Figure 5.13 Run n1-n5: Maximum scour depth after 2 departures - Absolute difference n_0 and n_l

The model is not very sensitive for increasing the absolute difference between the porosities n_0 and n_l, i.e. the influence of the dilatation on the hindered erosion. Figure 5.13 shows that an increasing difference between the porosities n_0 and n_l results in less scour with a difference between run n1 and n5 of 23 cm. This can be explained by looking at the increase of resistance against erosion due to difference in porosity. As mentioned before in section 2.4.1 the layers of sand are picked up by the flow as soon the

soil is in a state of sufficient porosity. This porosity is represented by n_l. As soon the difference between n_0 and n_l becomes bigger, the flow of water in the soil, between the pores, is causing a hydraulic gradient which hinders the erosion, which implies a lower scour depth. Moreover, it is visible that when the difference in porosity is increasing, the influence of the hindered erosion becomes less. Run n4 and n5 results in almost the same scour depth.

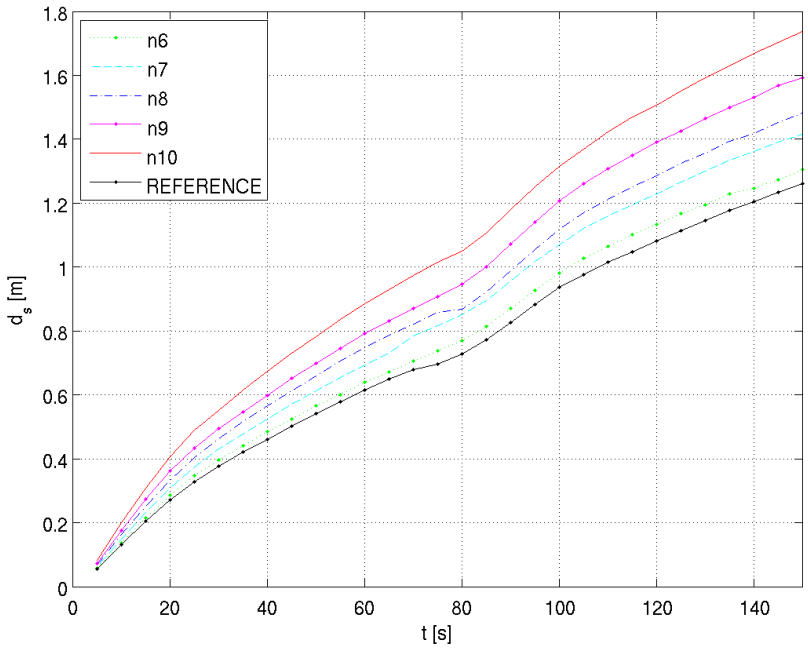

Figure 5.14 Run n6-n10: Maximum scour depth in time – Relative difference n_0 and n_l – 2 departures

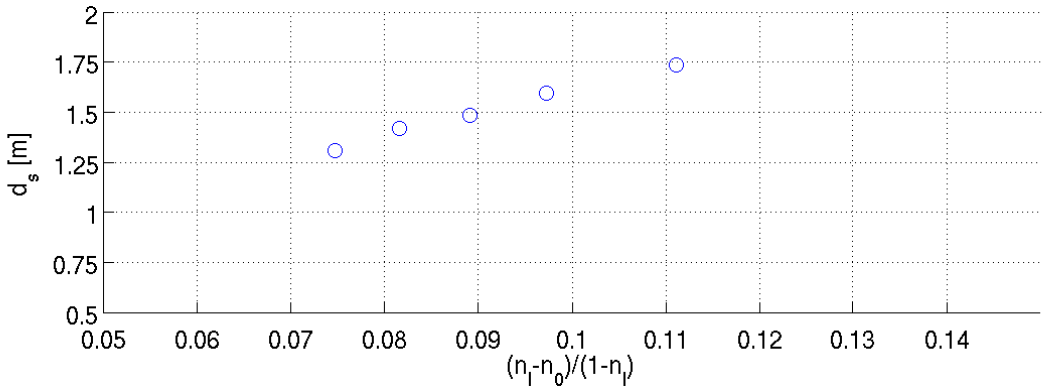

Figure 5.15 Run n6-n10: Maximum scour depth after two departures - Relative difference n_0 and n_l

For the last five runs (run n6-n10), where the increase of the relative difference between n_0 and n_l is studied, the model is more sensitive. The difference in maximum scour depth after two departures in run n6 and n10 is 45 cm. A higher porosity results also in an increase of the maximum scour depth (see also Figure 5.16). This can be explained since a higher porosity implies that the soil is looser. When the soil is looser the water will flow easier between the pores and the layers of grain particles will be picked up faster by the flow.

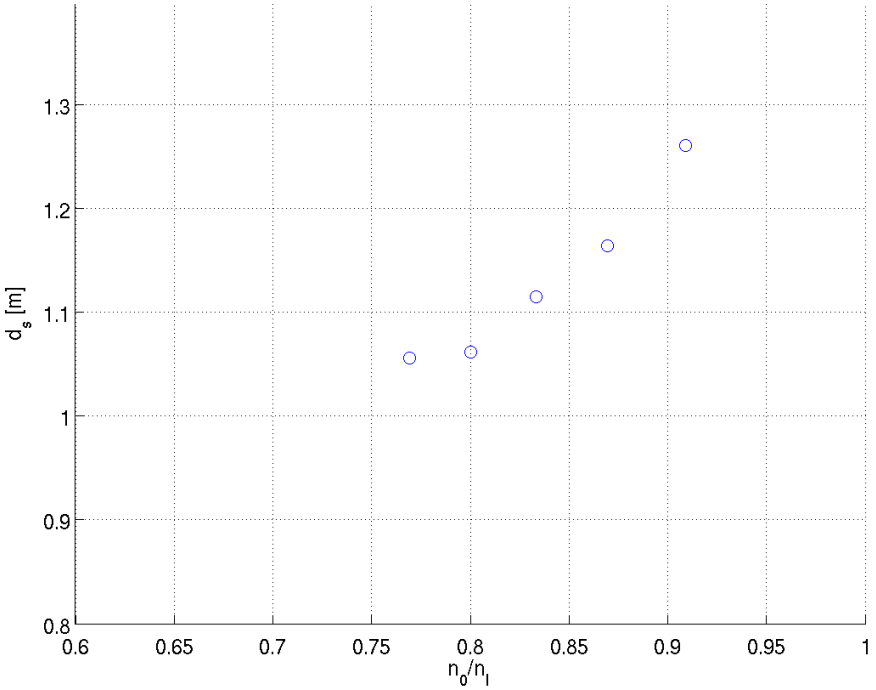

Figure 5.16 Maximum scour depth as function of $r_1 = n_0/n_l$

A valid comparison between all runs regarding the maximum scour depth as function of the porosity can only be made by looking at $r_3 = (n_l - n_0)(1 - n_l)/n_l^3$ which is derived in eq. (5.1) and plotted for the maximum scour depth after two departures in Figure 5.17 for run n1 to n10.

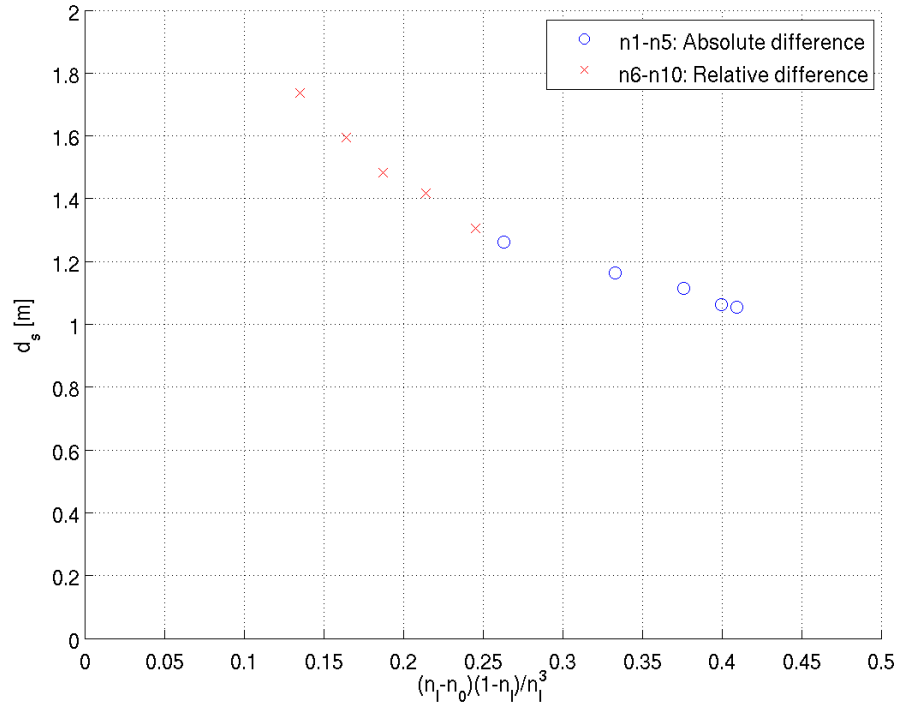

Figure 5.17 Maximum scour depth after two departures for all runs as function of $r_3 = (n_l - n_0)(1 - n_l)/n_l^3$

5.3 Applied power

The applied power of the vessel is not directly an input parameter of the numerical model. However the applied power of a bow thruster is related to the efflux velocity and the diameter of the propeller duct.

5.3.1 Description of applied parameters

In this section the scour as function of the applied power of the bow thruster is studied since in practice skippers rarely use the maximum amount of power during berthing and departing. Till this far only an efflux velocity of the thruster of 8 m/s is applied in the model. In addition this chapter two extra calculations are carried out for an efflux velocity of 4 m/s and 6 m/s which is respectively equivalent to 11% and 35% of the maximum power (320kW), of the bow thruster of MTS Noordzee.

During the full scale test in the Port of Rotterdam the maximum power is applied. In the model however, an outflow velocity of 8 m/s is used, which is equivalent to 85% of the maximum power of MTS Noordzee. The sensitivity analysis shows this does not influence the results significantly, since the outflow velocity V_0 is proportional to the cube root of the applied power $P_0^{1/3}$ (Figure 5.20).

Table 5.3 Applied power[7] for different runs

Run	P_0 [kW]	D_0 [m]	V_0 [m/s]
P1	34	0.91	4.0
P2	114	0.91	6.0
D4	272-320	0.91	8.0

5.3.2 Discussion of results

Figure 5.18 shows that in case the efflux velocity V_0 is reduced with 50% (equivalent to a reduction of the power of 89%), the scour depth is reducing with 67 % from 1.41m to 0.46m. The relation between outflow velocity and the scour depth seems to be linear looking at Figure 5.19. This is not the case for the relation between maximum scour and applied power of the vessel. The relation is characterized by a decreasing increase of the scour for increasing applied power. This can be explained by the non-linear relation between applied power and efflux velocity.

The linear relation between efflux velocity and scour in Figure 5.19 does not indicate this is valid in general. When the keel clearance is lower, the near bed velocities will increase and with this also the influence of the hindered erosion due to an increasing hydraulic gradient on the soil.

[7] The applied power varies depending on the type of coefficient which is used in eq.(3.1)

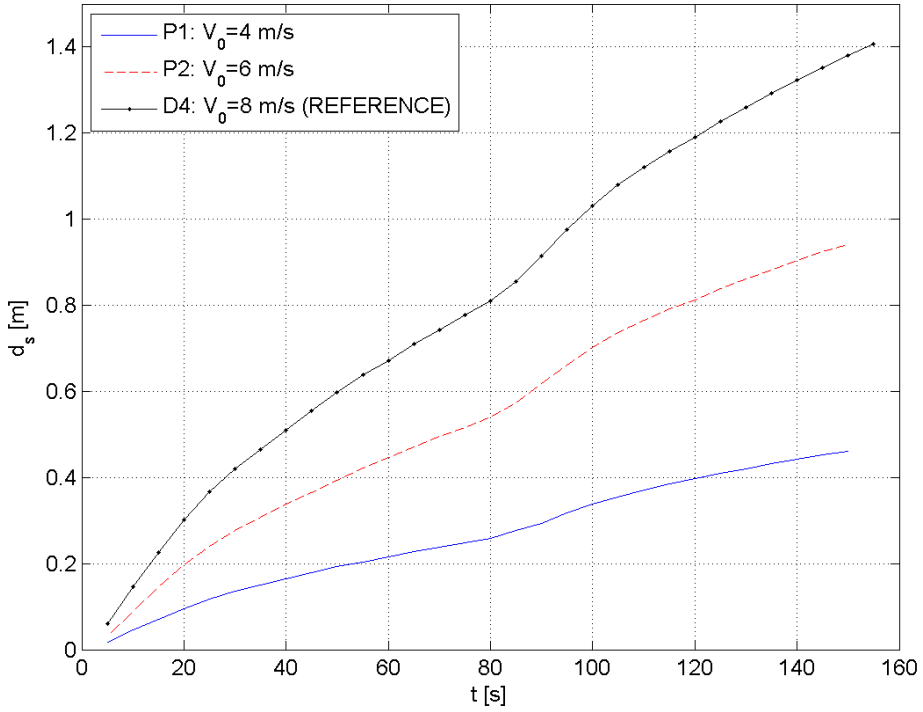

Figure 5.18 Maximum scour depth in time – 2 departures

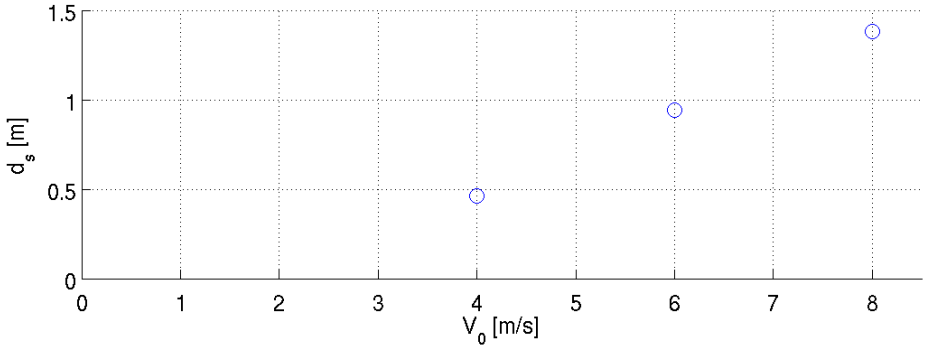

Figure 5.19 Maximum scour depth after 2 departures as function of efflux velocity

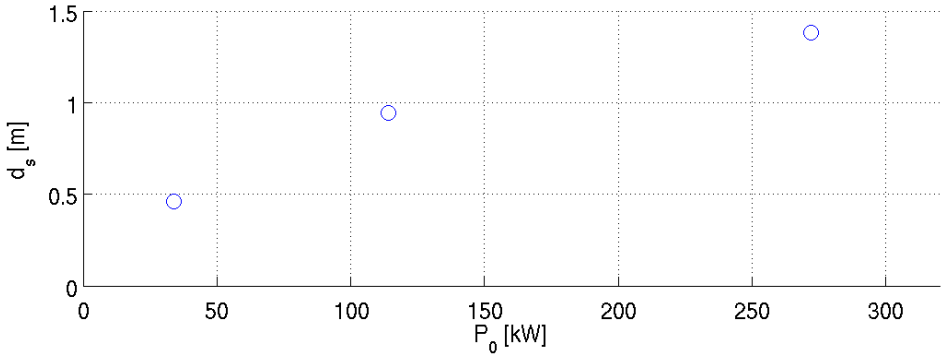

Figure 5.20 Maximum scour depth after 2 departures as function of applied power

5.4 Conclusions regarding sensitivity

5.4.1 Grain size diameter

Regarding the influence of the grain size diameter on the sensitivity of the model the following conclusions are drawn:

- The model is not very sensitive for changes in grain size diameter D_{50}. For a grain size diameter varying between $150\ \mu m < D_{50} < 1200\ \mu m$ the maximum scour depth varies from $1.06\ m < d_s < 1.43\ m$;
- The model is sensitive for changes in grain size diameter D_{15}. For a grain size diameter varying between $50\ \mu m < D_{15} < 140\ \mu m$ the maximum scour depth varies from $0.61\ m < d_s < 1.51\ m$;

- For *fine sand* ($D_{50} < 245\ \mu m$): scour depth is increasing for increasing grain size diameter;
- For *moderate sand* diameters ($245\ \mu m < D_{50} < 600\ \mu m$): the scour depth as function of grain size diameter is rather constant;
- For *coarse sand* ($D_{50} > 600\ \mu m$): the scour depth is decreasing for increasing grain size diameters;

- Regarding grain size diameter D_{50}, the model is most sensitive for varying grain size diameters in the regime of fine sand ($D_{50} < 245\ \mu m$);
- Regarding the soil grading: If the grading is high, i.e. a large amount of fine particles in the soil, the maximum erosion depth is decreasing considerably;
- For grain diameters in the range of sand the critical Shields parameter is inversely proportional to the maximum scour depth.

The sensitivity of the model for fine sediments explains partly the difference in measured scour depth and the calculated scour depth, since in the Port of Rotterdam the soil consists of fine particles namely, clay and silt.

5.4.2 Porosity

It can be concluded that the development of scour is more sensitive to changes in the relative difference in porosity (i.e. the porosity of the soil itself) than to the absolute difference in porosity (i.e. the dilatation of the soil during erosion). The higher the difference in porosity prior to erosion and the porosity of the loose soil, the less sensitive is the model due to this difference. The range of the maximum scour depth after two departures is from 1.05m to 1.75m.

The maximum erosion depth is governed by (1) the maximum porosity of the soil and (2) the minimum dilatation of the soil in order to bring the soil in the state of sufficient low porosity in order to erode. The simulations show that the scour depth is increasing with increasing porosity of the soil. Moreover, the scour depth is increasing when the difference between n_0 and n_1 becomes smaller. In case the statement of Van Rhee, that

the porosity of the loose soil can be estimated as the maximum porosity of the soil[8], is valid, one can state that the maximum scour depth is governed by the maximum porosity of the soil only.

5.4.3 Applied power

In case the efflux velocity V_0 is reduced with 50% (equivalent to a reduction of the power of 89%), the scour depth is reducing with 67 % from 1.41m to 0.46m.

[8] See section 2.4.1.3

6 Conclusions & Recommendations

In order to model the scour development in time due to a bow thruster of a vessel, departing from a vertical quay wall, a quasi-steady-state three dimensional (3D) numerical model is developed. The model is validated with full scale tests along a vertical quay wall, in the Port of Rotterdam. This chapter contains the conclusions following from the research objective and questions in section 6.1. The recommendations in section 6.2 suggest improvements of the model and potential future research.

6.1 Conclusions

The conclusions are subdivided into general conclusions regarding the numerical model itself, the velocity field induced by the bow thruster, the dimensions of the developed scour hole, the influence of different soil parameters on those dimensions and finally conclusions regarding the validation.

6.1.1 3D Numerical model

The objective of this research is *to establish a 3D numerical model which describes the scour development induced by thrusters after a certain number of departures of a vessel along the same location near a vertical quay wall***.**

The open source Computational Fluid Dynamics package OpenFOAM in combination with Matlab is used for the development of a 3D numerical model which simulates scour due to bow thrusters in time. A boundary adjustment technique is successfully applied in order to move the mesh near the bed.

The flow simulations, using the Realizable k-ε Model in OpenFOAM, provide the flow parameters near the bed in order to calculate the bed shear stress. In case the critical shear stress is reached the morphology plays a role and the bed changes. The occurring shear stress and the bed change itself is calculated in Matlab, by applying an empirical expression of [Van Rhee, 2010] for the erosion rate of sand. This expression is valid for both the high and low velocity regime of the flow. For each time step of 5 seconds the bed level is updated.

The development of the scour is studied for a maximum of six departures of the vessel along the same location near a vertical quay wall. In the sensitivity analysis two departures of the vessel are considered.

The effect of turbulence in the flow on the bed shear stress is taken into account by multiplying the turbulent kinematic viscosity with the velocity gradient along the bed. The turbulent kinematic viscosity models the transfer of momentum caused by the turbulent eddies.

6.1.2 Velocity field

What is the velocity field and the flow velocities near the non-erodible bed in the numerical model as function of keel clearance, distance between vessel and quay and operation time?

The efflux velocity of the bow thruster is modelled by mapping a circular velocity field on the boundary of the numerical domain with a constant velocity component of 8 m/s in longitudinal direction along the thruster axis. For small distances between quay and the vessel the model performs well regarding the near bed velocities. However, the radial spreading of the jet flow is underestimated due to neglecting the influence of vorticity and swirling flow induced by the propeller and due to a relative coarse grid. This results in an overestimation of the maximum near bed velocities near the quay and an underestimation of the near bed velocities further away from the quay wall. This deviation becomes significant for an increasing distance between vessel and quay. A similar deviation occurs for relative large and relative small keel clearances.

6.1.3 Dimensions of the scour hole

What are dimensions of the scour hole in the numerical model as function of time as result of the interaction between flow and sand bed, and is an equilibrium scour depth reached?

A maximum scour depth, after six departures of the vessel, of 2.2 meter is calculated. This is a conservative result compared with the measurements in the full scale test with MTS Noordzee, where a maximum scour depth of 1.85 meter is reached after 6 departures of the vessel.

Depending on the soil properties of sand the maximum scour depth after two departures of the vessel varies between 0.60m and 1.50 m. In the measurements with MTS Noordzee the scour depth is 80 cm after 2 departures.

The width of the scour hole (i.e. distance along the thruster axis perpendicular to the quay wall) in the model is maximum 9 meters after 6 departures.

An equilibrium depth is not reached after 6 departures of the vessel. No conclusions can be drawn regarding the equilibrium depth of the scour hole, since both, the numerical model and the full scale model, consider maximum 6 departures of the vessel.

6.1.4 Sensitivity

What is the interaction between flow and scour in the numerical model as function of different soil properties and applied power of the bow thruster?

The development of the scour is very sensitive for changes in the amount of fine sand (i.e. grain size diameter D_{15}) in the soil. A decrease in the grain size diameter leads to lower scour depths, due to an increasing hydraulic gradient, caused by dilatation of the soil during the erosion process, which hinders the erosion.

Beside this the porosity of the soil plays an important role. The higher the porosity, the more scour. The magnitude of the dilatation of the soil during the erosion process has a smaller influence on the development of the scour, in case the difference between the porosity prior to erosion (n_0) and the erosion of the loose soil (n_l) becomes larger.

The scour is rather insensitive for the applied power. However, this is not related to the numerical model but to the relation how the efflux velocity of the bow thruster is determined. The expression of the efflux velocity is a function of the cube root of the applied power. In fact the model is sensitive to the change of efflux velocity. Reducing the efflux velocity with 50%, results in a reduction of scour depth of 67%.

6.1.5 Validation

Do results of the numerical model regarding scour-hole dimensions agree with the measurements of the full scale tests in the Port of Rotterdam?

The numerical model is validated based on the full scale tests with MTS Noordzee. The numerical model gives conservative results compared to measurements. This could because of the following two reasons. (1) In the numerical model the empirical relation of [Van Rhee, 2010] is used which is calibrated for sand. However, on the location along the Parkkade where the full scale tests are performed the top layer of the soil consists of clay. (2) An overestimation of the near bed velocity close to the quay wall due to underestimation of the radial spreading of the thruster jet.

6.2 Recommendations

Several recommendations are given following from the conclusions. These recommendations are mainly related to improvement of the current numerical model.

6.2.1 Hydrodynamics

Improved modelling of the propeller induced flow in order to study the effect of radial spreading and turbulence of the flow on erosion.

Develop a numerical model (preferably in OpenFOAM) which involves the effect of the propeller in the bow thruster on the velocity field. This will probably introduce more turbulence and swirling flow which leads to a more realistic flow field. It is relative easy to couple a new, improved hydrodynamic model to the model developed in this thesis.

Derive a function for the turbulent mixing length for the jet near the bed in order to apply the formulation of [Hoan, 2008] or [Hofland, 2005].

In the current model local parameters near the bed for turbulence and flow velocity are used to calculate the bed shear stress. However, the turbulence in RANS models only represents the second order moments of the velocity components. This implies that velocities on a higher level above the bed can determine the higher order moments of the velocity fluctuations near the bed which represents the extreme forces on the particles.

That is why [Hoan, 2008] and [Hofland, 2005] proposed to average velocity and turbulence over the height. This height depends on the length scale of the turbulence. In case the length scale for this specific situation regarding the jet near the bed is known, one can apply the stability criteria which is validated by [Hoan, 2008] and [Hofland, 2005].

Mesh improvement near the bed in order to obtain sufficient low y^+ values to involve wall functions in the simulations.

Near the walls the gradients regarding velocity and turbulence properties are much higher compared to the core region of the flow. This means that the discretization procedures which are used in the core flow are not suitable for solving the near wall flow. In the current numerical model the cells near the bed are relative coarse, in the order of magnitude of centimetres, which results in large y^+ values (relative distance to the wall). Due to the coarse mesh, wall functions are not taken into account. In the wall functions a modification in the modelling of turbulent viscosity in cells next to the wall is made. Improving the mesh in order to involve wall functions, results in a better physical representation of the velocity gradients and turbulence near the wall.

6.2.2 Validation

Validate model with scour measurements of MTS Jade and [Schmidt, 1998].

The current model is only validated with the results of the full scale tests in the Port of Rotterdam with MTS Noordzee. However, there are more measurements available. In order to obtain a more extended validation the same model could be validated with the results of the MTS Jade. In addition [Schmidt, 1998] carried out physical modelling for a scale model of a vessel on a fixed location.

6.2.3 Bed protection design

Study whether current bed protections are not designed too conservative regarding the width of the bed protection.

In practice bed protections with a width of approximately 20 meters are applied in the Port of Rotterdam. Both the results from the numerical model and the full scale tests show that the width of the scour hole is much smaller than the width of the applied bed protections. For further research it might be valuable to study whether such a wide bed protection is really required. Based on this thesis and the full scale test in the Port of Rotterdam only, it seems that the bed protection is designed too conservative. However, it can be that this is not the case for two reasons. (1) In case bed protection is applied the flow field will behave different and the jet above the bed will propagate in a different way, which can cause erosion next to a narrow designed bed protection. (2) In this thesis only a bow thruster is applied, without taking into account the scour due to main propeller, which is in general located in the centre line of the ship further away from the quay wall.

References

Andersson, B. (2012). *Computational Fluid Dynamics for Engineers*. Cambridge University Press, New York.

Augustin, J. (2007). *Validation of different Design Criteria for Scour Protection Measures -MSc Thesis*.

Bisschop, F., Visser, P.J., Van Rhee, C., Verhagen, H. J. (2010). Erosion Due to High Flow Velocities: A Description of Relevan Processes. *International Conference on Coastal Engineering (ICCE)-No 32*, 1–10.

Blokland, T. (2013). *Praktijkproef Parkkade - Erosie door schroefstralen van binnenvaartschepen tegen kade*. Rotterdam Municipality Engineering Department.

Bredberg, J. (2000). *On the Wall Boundary Condition for Turbulence Models - Internal Report 00/4*. Chalmers University of Technology, Department of Thermo and Fluid Dynamics, Göteborg.

Brørs, B. (1999). Numerical Modeling of Flow and Scour at Pipelines. *J. Hydraul. Eng. 1999.125:511-523*, 511–523.

Hamill, G., Johnston, H., & Stewart, D. (1999). Propeller wash scour near quay walls. *J. Waterway, Port, Coastal, Ocean Eng.*, 170–175.

Hoan, N. T. (2008). *Stone Stability Under Non-uniform Flow - Phd Thesis*. Delft University of Technology.

Hoffmans, G. J. C. . (2012). *The Influence of Turbulence on Soil Erosion - Deltares Select Series Volume 10*. Delft: Eburon Academic Publisher.

Hofland, B. (2005 [March]6). *Rock "n" Roll: Turbulence-induced damage to granular bed protections - Phd Thesis*. Delft University of Technology.

Jacobsen, N. G. (2011). *A Full Hydro- and Morphodynamic Description of Breaker Bar Development - PhD Thesis*. Technical University of Denmark.

Lesser, G. R., Roelvink, J. a., van Kester, J. a. T. M., & Stelling, G. S. (2004). Development and validation of a three-dimensional morphological model. *Coastal Engineering*, *51*(8-9), 883–915.

Liang, D., Cheng, L., & Li, F. (2004). Numerical modeling of flow and scour below a pipeline in currents - Part II. Scour simulation. *Coastal Engineering*, *52*(1), 43–62.

Liu, X., & García, M. H. (2008). Three-Dimensional Numerical Model with Free Water Surface and Mesh Deformation for Local Sediment Scour. *J. Waterway, Port, Coastal, Ocean Eng., 134(4)*, (August), 203–217.

Mastbergen, D. R., & Van Den Berg, J. H. (2003). Breaching in fine sands and the generation of sustained turbidity currents in submarine canyons. *Sedimentology*, *50*(4), 625–637.

Meijer, D.G., Verhey, H.J. (1993), "Stroomsnelheden bij de oever veroorzaakt door boegschroeven", rapport Q1867, Waterloopkundig Laboratorium, Delft

Melling, G. (2013). CFD-based Methods for Numerical Modelling of Scour. In *Numerical Towing Tank Symposium, Poole, GB, 6pp*. University of Southampton.

Miedema, S. A. (2013). Constructing the Shields Curve - Part C: Cohesion by Silt. *WODCON XX: The Art of Dredging, Brussels, Belgium, 2013 - Proceedings*, 1–15.

Nielsen, B. (2005). *Bowthruster - Induced Damage- a physical model study on bowthruster-induced flow - MSc Thesis*. Delft University of Technology.

PIANC. (2012). *Guidelines for Berthing Structures, Related to Thrusters - Version 4.0*. Brussels: PIANC MARCOM WG48.

Roberts. (1998). Effects of Particle Size and Bulk Density on Erosion of Quartz PArticles. *J. Hydraul. Eng. 124(12), 1261–1267.*, (December), 1261–1267.

Römisch, K. (2012). Durch Schiffspropeller verursachte Kolkbildung. *HANSA International Maritime Journal-149. Jahrgang-2012-Nr.9*.

Ryan, D., & Hamill, G. a. (2011). Estimating propeller scour at quays alongside a berthing ship. *Proceedings of the ICE - Maritime Engineering*, *164*(2), 59–70.

Schmidt, E. (1998). *Leichtweiss-Institut für Wasserbau der Technische Universität Braunschweig - Mitteilungen Heft 143/1998 - Ausbreitungsverhalten und Erosionswirkung eines Bugpropellerstrahles vor einer Kaiwand*. Braunschweig.

Shields, A. (1936). Anwendung der Aehnlichkeitsmechanik und der Turbulenzforschung auf die Geschiebebewegung. *Mitteilungen der Preussischen Versuch- sanstalt furWasserbau und Schiffbau, Heft 26. Berlin NW87.*

Simoons, E. (2012). *Edge scour around an offshore wind turbine - MSc Thesis*. Delft University of Technology.

Van Blaaderen, E. (2006). *Modelling bow-thrusters induced flow near a quay wall - MSc Thesis*. Delft University of Technology.

Van Der Laan, T. (2005). Het ontwikkelen van een model voor boegschroefstralen bij verticale kademuren - MSc Thesis.

Van Doorn, R. (2012). *Bow Thruster Currents at Open Quay Constructions on Piles - MSc Thesis*. Delft University of Technology.

Van Rhee, C. (2010). Sediment Entrainment at High Flow Velocity. *J. Hydraul. Eng.*, *136*(September), 572–582. doi:10.1061/ ASCE HY.1943-7900.0000214

Versteeg, H. K. (1995). *An introduction to Computational Fluid Dynamics - The Finite Volume Method*. Harlow, United Kingdom: Longman Group Ltd.

Vuik, V. (2010). *Numerical modeling of sediment transport over hydraulic structures - MSc Thesis*. Delft University of Technology.

Vuik, J.C., Van Beek, P, Vermolen, F, Van Kan, J. (2007). *Numerieke Methoden voor Differentiaalvergelijkingen*. Delft: VSSD.

Whitehouse, R. J. S. (1998). *Scour at marine structures: a manual for practical application*. London: Thomas Telford Publications.

List of Symbols

Latin Symbols

A_1	Coefficient for in the formulation for the erosion velocity of Van Rhee where $A_1 = 3/4$ for single particle mode and $A_1 \approx 1.7$ for a continuum mode	[-]
C	Chezy coefficient	[$m^{1/2}/s$]
C_s	Roughness constant	[-]
C_μ	Dimensionless constant in the k-ε model	[-]
c	Cohesion	[Pa]
c_b	Near-bed volumetric concentration	[m^3/m^3]
D_*	Dimensionless particle diameter	[-]
D_0	Diameter of the propeller duct	[m]
D_{15}	Grain diameter where 15% of the grain mass has a smaller diameter	[m]
D_{50}	Grain diameter where 50% of the grain mass has a smaller diameter	[m]
D_p	Diameter of the propeller jet	[m]
d	Stone diameter	[m]
d_a	Characteristic size of detaching aggregates according to Mirtskhoulava	[m]
d_s	Maximum depth of the scour hole	[m]
E	- Entrainment rate or pick-up flux - Integration constant that depends on the roughness of the wall	[$kg/m^2/s$]
f_n	Percentage of maximum number of revolutions	[-]
G	Turbulence generation field	
g	Gravitational acceleration	[m/s^2]
h_p	Distance from propeller axis to the bed	[m]
K_s	Sand grain roughness height	[m]
K_T	Thrust coefficient or dimensionless relationship between propulsive force, number of revolutions and diameter of the propeller	[-]
k	Turbulent kinetic energy	[m^2/s^2]
k_l	Permeability of sediment of the bed at minimum compaction	[m/s]
k_s	Effective roughness	
L	Quay clearance, i.e. distance from the outflow opening of the thruster to the quay	[m]
$\widehat{\boldsymbol{N}}$	Unit normal vector	[-]
n_0	Porosity of the settled bed, i.e. the bed porosity prior to erosion	[-] or [%]
n_l	Bed porosity of the loose soil condition	[-] or [%]
P_0	Applied power of the bow thruster	[kW]
p	Pressure	[N/m^2]
$\boldsymbol{R}_p$	Reynolds number for the particles	[-]
r	Radial distance to the propeller axis	[m]
S	Settling flux	[$kg/m^2/s$]
$\Delta\widehat{\boldsymbol{U}}$	Displacement of the cell centres of the bed after erosion	[m]
$\widehat{\boldsymbol{U}}^n$	Bed level coordinate of cell centre before erosion	[m]
$\widehat{\boldsymbol{U}}^{n+1}$	Bed level coordinate of cell centre after erosion	[m]
U	Flow velocity	[m/s]

u_*	Shear velocity	[m/s]
V_0	Efflux velocity of the bow thruster	[m/s]
$V_{axis,0}$	Flow velocity along the jet axis	[m/s]
$V_{b,max}$	Maximum near bed velocity in front of a vertical quay wall	[m/s]
$V_{x,r}$	Flow velocity at location x,r	[m/s]
v_b	Near bed velocity	[m/s]
v_e	Erosion velocity of sand, i.e. velocity of the downward moving bed perpendicular to the bed	[m/s]
$v_{e,c}$	Erosion velocity of clay	[m/s]
v_{sed}	Velocity of the moving bed due to erosion of sedimentation	[m/s]
w_s	Settling velocity of the particles	[m/s]
x_s	Distance measured from quay wall to center of bow thruster	
y	Wall distance	[m]
y^+	Dimensionless wall distance	[-]

Greek Symbols

β	Angle of the bed slope	[°]
Δ	Relative density = $(\rho_s - \rho)/\rho$	[-]
ε	Energy dissipation rate	[m²/s³]
Φ_p	Dimensionless pick-up rate or erosion rate	[-]
Φ_p^1	Modified dimensionless pick-up rate in the formulation for the erosion velocity of Van Rhee	[-]
ϕ	Angle of internal friction of the soil	[°]
κ	Von Kármán constant	[-]
ν	Kinematic viscosity	[m²/s]
ν_t	Turbulent kinematic viscosity or eddy viscosity	[m²/s]
ρ	Density of water	[kg/m³]
ρ_s	Density of the (sand) particles	[kg/m³]
τ_b	Bed shear stress	[Pa]
$\Psi_{c,M}$	Critical Shields parameter for clay in the expression according to Mirtskhoulava	[-]
Ψ_s	Shields parameter	[-]
$\Psi_{s,cr}$	Critical Shields parameter	[-]
$\Psi_{s,cr}^1$	Modified critical Shields parameter in the formulation of the erosion velocity of Van Rhee	[-]

List of Figures

List of Tables

Abbreviations

2D	Two-Dimensional
2D-LDA	Two-Dimensional-Laser-Doppler-Anemometer
3D	Three-Dimensional
CFD	Computational Fluid Dynamics
CRP	Contra Rotating Propeller
LES	Large-Eddy Simulation
MTS	Motor Tank Ship
NAP	Normaal Amsterdams Peil (reference water level in the Netherlands)
RANS	Reynolds Averaging Navier Stokes

Appendix A. Related literature

A.1 Velocity distribution of free jet

The free velocity distribution is Gaussian or normal distributed around the axis as depicted in Figure A.1.

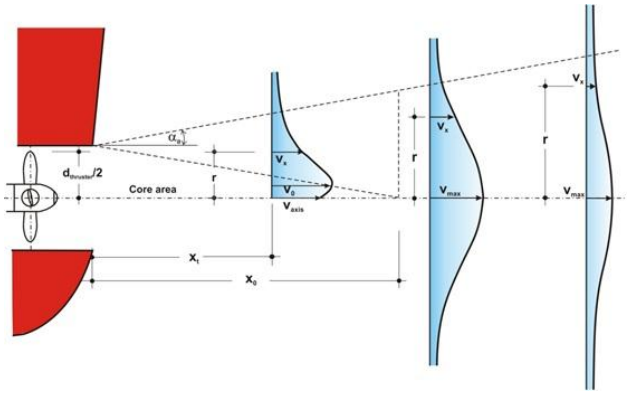

Figure A.1 Velocity distribution induced by a thruster

A general expression for the free jet is presented by Alberson et al. (1950). Based on the Albertson formulas the following flow distribution for propellers can be derived:

$$V_0 = C_1 f_n n_{max} D_p \sqrt{K_T} \quad \textbf{(A.1)}$$

And

$$V_{x,r} = A_3 \left(\frac{D_p}{x}\right)^a V_0 exp\left[-\frac{1}{C_2^2} \cdot \frac{r^2}{x^2}\right] f(rudder, confinement) \quad \textbf{(A.2)}$$

Where:

V_0 = efflux verlocity [m/s]
$V_{x,r}$= flow verlocity at location x,r [m/s]
f_n= percentage of maximum number of revolutions [-]
D_p= propeller diameter [m]
K_T= thrust coefficient or dimensionless relationship between propulsive force, number of revolutions and diameter of the propeller [-]
r= radial distance to the propeller axis [m]
C_1, C_2= coefficients
A_3= coefficient
a= exponent

Note that this formula is only valid in the absence of lateral boundaries or walls.

A.2 Bed velocity near vertical quay wall - German Method

The German methods according to [PIANC, 2012] as described in EAU and BAW are based on research by Fuehrer, Römisch & Engelke (1981), Schmidt (1998):

$$V_{axis,0}\begin{cases} V_0 & \frac{x}{D_0} < 1.9 \\ 1.9V_0\left(\frac{x}{D_0}\right)^{-1.0} & \frac{x}{D_0} > 1.9 \end{cases} \quad \textbf{(A.3)}$$

With $V_{axis,0}$ is the flow velocity along the jet axis and x is the distance along the jet axis.

Maximum flow velocity at the bed caused by the thruster jet perpendicular against the vertical wall is:

$$\frac{V_{b,max}}{V_0} = a_L 1.9\left(\frac{L}{D_0}\right)^{-1.0} \quad \textbf{(A.4)}$$

With L is the distance between outflow opening and quay wall corresponding to x_t in Figure 2.4. The value of α_L follows from Figure A.2.

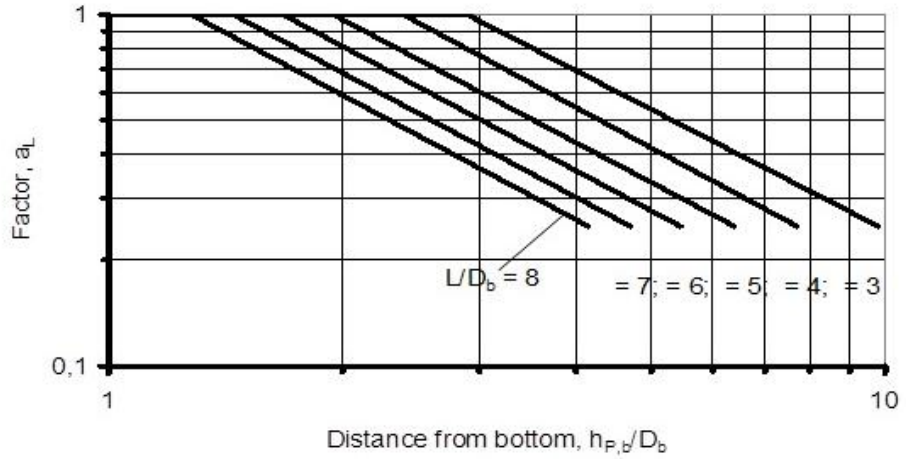

Figure A.2 Factor α_L as function of the wall and bottom distance

Where $h_{p,b}$ is the distance between propeller axis and sea bed and D_p is the diameter of the propeller jet.

A.3 Hydrodynamics – the Standard k-ε model

The k-ε model consists of two transport equations, one for the turbulent kinetic energy, k, and one for the energy dissipation ε

$$\frac{\partial k}{\partial t} + \langle U_j \rangle \frac{dk}{dx_j} = -\langle u_i u_j \rangle \frac{\partial \langle U_i \rangle}{\partial x_j} - \nu \left\langle \frac{\partial u_i}{\partial x_j} \frac{\partial u_i}{\partial x_j} \right\rangle + \frac{\partial}{\partial x_j} \left(\nu \frac{\partial k}{\partial x_j} - \frac{\langle u_i u_i u_j \rangle}{2} - \frac{\langle u_j p \rangle}{\rho} \right) \quad \textbf{(A.5)}$$

Where the physical interpretation is as follows:

$\frac{\partial k}{\partial t}$ Accumulation of k

$\langle U_j \rangle \frac{dk}{dx_j}$ Convection of k by the mean velocity

$\langle u_i u_j \rangle \frac{\partial \langle U_i \rangle}{\partial x_j}$ Production of k, large eddies extract energy from the mean flow

$\nu \left\langle \frac{\partial u_i}{\partial x_j} \frac{\partial u_i}{\partial x_j} \right\rangle$ Dissipation of k by viscous stress, whereby turbulent kinetic energy is transformed into heat.

$\nu \frac{\partial k}{\partial x_j}$ Molecular diffusion of k

$\frac{\langle u_i u_i u_j \rangle}{2}$ Turbulent transport by velocity fluctuations

$\frac{\langle u_j p \rangle}{\rho}$ Turbulent transport by pressure fluctuations

The notation for the velocity U_i in this representation is based on Reynolds statistical averaging methods for turbulent flows, in which the velocity is decomposed in a part that represents the mean velocity and a fluctuating part represented as:

$$U_i = \langle U_i \rangle + u_i \quad \textbf{(A.6)}$$

Because of the fact that the last four terms in equation (A.5) are unknown some approximations are introduced by [Andersson, 2012] which results in the modelled equation for k:

$$\frac{\partial k}{\partial t} + \langle U_j \rangle \frac{dk}{dx_j} = \nu_T \left[\left(\frac{\partial \langle U_i \rangle}{\partial x_j} + \frac{\partial \langle U_j \rangle}{\partial x_i} \right) \frac{\partial \langle U_i \rangle}{\partial x_j} \right] - \varepsilon + \frac{\partial}{\partial x_j} \left(\left(\nu + \frac{\nu_T}{\sigma_k} \right) \frac{\partial k}{\partial x_j} \right) \quad \textbf{(A.7)}$$

Where:

σ_k is a model coefficient known as the Prandtl-Schmidt number

ν_T is the turbulent kinematic viscosity

The modelled energy dissipation rate is modelled with a second transport equation which can be written as:

$$\frac{\partial \varepsilon}{\partial t} + \langle U_j \rangle \frac{d\varepsilon}{dx_j} = C_{\varepsilon 1} \nu_T \frac{\varepsilon}{\kappa} \left[\left(\frac{\partial \langle U_i \rangle}{\partial x_j} + \frac{\partial \langle U_j \rangle}{\partial x_i} \right) \frac{\partial \langle U_i \rangle}{\partial x_j} \right] - C_{\varepsilon 2} \nu_T \frac{\varepsilon^2}{\kappa} + \frac{\partial}{\partial x_j} \left(\left(\nu + \frac{\nu_T}{\sigma_k} \right) \frac{\partial k}{\partial x_j} \right) \quad \textbf{(A.8)}$$

Where the physical interpretation of the terms is as follows:

$\frac{\partial \varepsilon}{\partial t}$	Accumulation of ε
$\langle U_j \rangle \frac{d\varepsilon}{dx_j}$	Convection of ε by the mean velocity.
$C_{\varepsilon 1} \nu_T \frac{\varepsilon}{\kappa} \left[\left(\frac{\partial \langle U_i \rangle}{\partial x_j} + \frac{\partial \langle U_j \rangle}{\partial x_i} \right) \frac{\partial \langle U_i \rangle}{\partial x_j} \right]$	Production of ε
$C_{\varepsilon 2} \nu_T \frac{\varepsilon^2}{\kappa}$	Dissipation of ε
$\frac{\partial}{\partial x_j} \left(\left(\nu + \frac{\nu_T}{\sigma_k} \right) \frac{\partial k}{\partial x_j} \right)$	Diffusion of ε

A.4 Stability parameters

An important issue in sediment transport is the stability of the sand particles. The stability parameters are mainly assessed with help of [Hoan, 2008].

Governing variables

A transport formulation of stones or sand should be available in order to calculate the (amount of) sediment transport or bed damage level. This amount of damage and/or sediment transport is function of different variables involved. [Hoan, 2008] made an overview of the dominant governing variables regarding stones which is presented in Table A.1.

Table A.1 Dominant governing variables [Hoan, 2008]

Governing varibles	Expression	Dimension
Bed shear stress	$\tau = \rho u_*^2$	N/m²
Velocity	u, v, w	m/s
Turbulence	$\kappa, \sigma(u), \sigma(v), \sigma(w)$	m²/s²
Stone size	D_{n50}	m
Gradation of the stones	d_{85}/d_{15}	-
Shape of the stones	$SF = a/\sqrt{bc}$	-
Specific submerged density of stone	$\Delta = (\rho_s - \rho)/\rho$	-

The ratio between load and strength is used in many formulations to determine the threshold of movement of the particle. In here the load is often the bed shear stress induced by the flow velocity of the water and the strength is mainly function of the stone size. One of the classical formulations is the one of Shields (1936) for uniform flow. This approach is used and adapted later on by different researches of which an overview is presented below.

Shields

The Shields parameter is dependent on the load, which is the bed shear stress, and the strength, which is the submerged weight of the particle. The bed shear stress is in reality often not the only load, since in many practical applications turbulence also plays an important role. The Shields parameter is given by:

$$\Psi_s = \frac{\tau_b}{\rho \Delta g d} = \frac{u_*^2}{\Delta g d} \tag{A.9}$$

in which d is the stone diameter.

Jongeling et al.

The parameter of Jongeling et al. is described in [Hoan, 2008] and similar to the Shields parameter, but with the difference that the output of RANS models can be used as input for this parameter in order to include the effects of turbulence. The parameter is written as:

$$\Psi_{WL} = \frac{\langle \left(\bar{u} + \alpha\sqrt{k}\right)^2 \rangle_{hm}}{\Delta g d} \tag{A.10}$$

Where k represents the turbulent kinetic energy, α is an empirical turbulence magnification factor, and $\langle ... \rangle_{hm}$ is a spatial average over a distance of hm above the bed. For further detailed information is referred to [Hoan, 2008], section 2.4.3.

The turbulent kinetic energy is defined as

$$k = \frac{1}{2}(\overline{u'^2} + \overline{v'^2} + \overline{w'^2}) \quad \textbf{(A.11)}$$

Hofland

[Hofland, 2005] suggested a method to determine the stability of the bed protection using the output of a 3D RANS model and the stability parameter is represented by:

$$\Psi_{Lm} = \frac{\max\left[\langle \bar{u} + \alpha\sqrt{k} \rangle_{LM} \frac{L_m}{z}\right]^2}{\Delta g d} \quad \textbf{(A.12)}$$

In which Lm is the Bakhmetev mixing length ($Lm = kz\sqrt{1 - z/h}$), $\langle ... \rangle_{Lm}$ is a moving average with varying filter length Lm and z is the distance from the bed.

Hoan

[Hoan, 2008] proposed and validated a new expression for the stability parameter using the turbulence quantity $\sigma(u)$. This stability parameter provides a better quantification of the hydraulic loads exerted on the bed, compared to the stability parameters of Hofland, Jongeling et al. and Shields in non-uniform and turbulent flow. The final expression for the formulation of the proposed stability parameter is as follows:

$$\Psi_{u-\sigma[u]} = \frac{\langle [\bar{u} + \alpha\sigma(u)]^2 \times \sqrt{1 - z/h} \rangle_h}{\Delta g d} \quad \textbf{(A.13)}$$

Where $\alpha = 3$ is an empirical constant which give the most accurate results.

$\bar{u}$ is the mean velocity and is computed as:

$$\bar{u} = \frac{1}{N}\sum_{i=1}^{N} u(i) \quad \textbf{(A.14)}$$

Where N is the number of samples.

$\sigma(u)$ represents the turbulence intensity and is in fact equal to the standard deviation of u:

$$\sigma(u) = \sqrt{\frac{1}{N}\sum_{i=1}^{N}[u(i) - \bar{u}]^2} \quad \textbf{(A.15)}$$

Entrainment rate

The entrainment rate is related to the turbulence near the bed. [Hoan, 2008] states that Mosselman and Akkerman (1998) distinguish two ways of defining mobility of particles:

- Entrainment rate (E): the number of pick-ups (n) per unit time (T) and area (A);
- Bed load transport (q_s): the number of particles that is transported through a cross-section per unit time.

Those mobility parameters are defined as follows:

$$E = \frac{nd^3}{AT} \tag{A.16}$$

and

$$q_s = \frac{nd^3}{BT} = E \times l \tag{A.17}$$

Where B is the section width and l is the displacement length. In the study of [Hoan, 2008] the damage of the bed is quantified instead of the amount of erosion. For this the author used the dimensionless entrainment rate Φ_E and is determined as:

$$\Phi_E = \frac{E}{\sqrt{\Delta g d_{n50}}} \tag{A.18}$$

A.5 Erosion velocity – sand

[Mastbergen & Van Den Berg, 2003] studied breaching in fine sands, where amongst others the breaching process is analysed quantitatively. Breaching is caused due to negative pore pressures that is induced by rapid erosion processes due to flow or due to gravity in case of steep slopes. In order to investigate this subject, the influence of negative pore pressures on the pick-up rate of non-cohesive sediment particles on a slope has been assessed.

An expression for the sand bed erosion velocity perpendicular on the bed, v_e, for high erosion rates or fine sand with relatively low permeability is derived by Mastbergen and Van den Berg and is written as:

$$v_e = \sqrt{\frac{-A_2\left(\Psi_s - \Psi_{s,cr}\right)^m D_*^n}{(1-n_0)\frac{\sin(\phi-\alpha)}{\sin\phi}} v_s v_{wal}} = \sqrt{\frac{A_2\left(\Psi_s - \Psi_{s,cr}\right)^m D_*^n k_l \sqrt{\Delta^3 g D_{50}}}{\Delta n}} \quad \textbf{(A.19)}$$

where $A_2 = 0.018$ is a dimensionless coefficient, D_* is the dimensionless grain size (Bonnefile) parameter, n_0 is the actual porosity of the sand bed, ϕ is the angle-of-repose of the sand, α is the local bed slope angle, v_s is the Shields velocity for sand grains, v_{wal} is the wall velocity, n is the power in the erosion function, m is another power in the erosion function, k_l is the permeability of the loose sand bed, D_{50} is the median grain size and Δn is the porosity increase of the sand bed from undisturbed to loose conditions.

This expression is validated by erosion tests in sand using high-pressure water jets, however the very high flow velocities due to the water jets are not investigated. A comparison between the computed values and the erosion tests is depicted in Figure A.3 with $A_2 = 0.018$, $\Psi_{s,cr}$=0.06, a sea water temperature of 15°C and f_0=0.1. Data obtained from Van Rijn (1984a, 1993): D_{50}=130, 190, 790 and 1500 μm with $\bar{u}$ = 0.5 -1.3 m/s; and Winterwerp et al. (1992): D_{50} = 120 and 225 μm with $\bar{u}$ =1-3.5m/s.

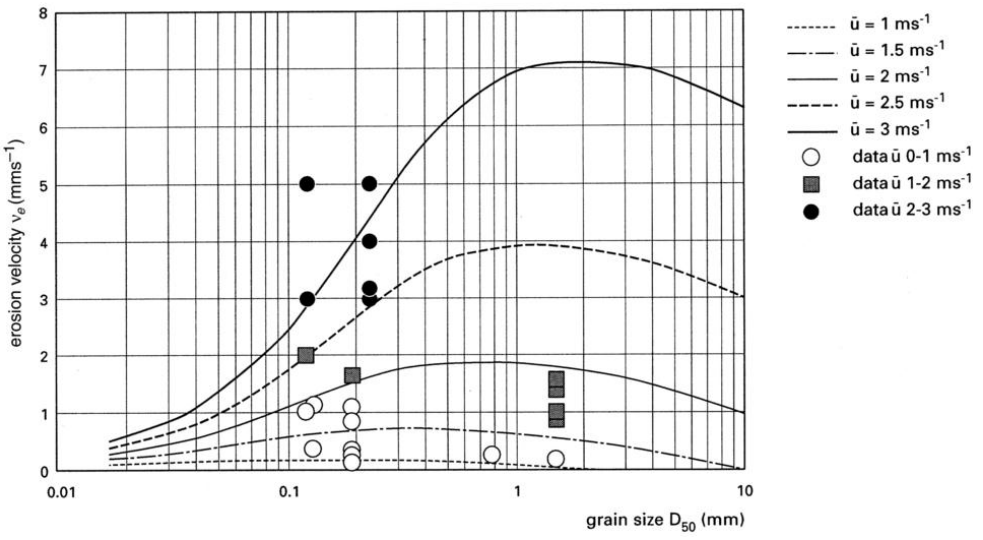

Figure A.3 Erosion velocity in sand as a function of grain size and flow velocity [Mastbergen & Van Den Berg, 2003]

A.6 Erosion velocity - clay

In many studies curves like Shields used are described, but mainly neglecting the effect of cohesion or in other words, only lift and drag forces are taken into account. In cohesive materials the particles are not only subjected to those forces but also to inter-particle attraction or repulsion forces such as van der Waals forces and electro chemical forces. [Miedema, 2013] developed, verified and validated a model which includes additional attraction forces between particles mentioned before.

[Hoffmans, 2012] presented a method to calculate the erosion velocity of clay, based on the work of Mirtskhoulava (1988,1991) which is simplified by Hoffmans and Verheij (1997). The expression for the cohesive sediments is

$$v_{e.c} = \log\left(\frac{8.8h}{d_a}\right)\sqrt{0.4(\Delta g d_a + 0.6C_{f,M}/\rho} \quad \textbf{(A.20)}$$

With

$$C_{f,M} = 0.035c \quad \textbf{(A.21)}$$

In which $C_{f,M}$ is the fatigue rupture strength of clay which is linearly related to the cohesion c and d_a $(= 0.004\,m)$ is the characteristic size of detaching aggregates according to Mirtskhoulava. By using

$$r_0 = \alpha_0 \frac{u_*}{U_0} = \alpha_0 \frac{\sqrt{g}}{C} \quad \textbf{(A.22)}$$

where g is the acceleration due to gravity, u_* is the bed shear velocity and α_0 (= 1.2) is a coefficient and the Chézy coefficient, defined as

$$C = \frac{\sqrt{g}}{\kappa}\ln\left(\frac{12h}{k_s}\right) \quad \textbf{(A.23)}$$

Eq. (A.20) becomes

$$v_{e.c} = \alpha_0 r_0^{-1}\sqrt{\Psi_{c,M}(\Delta g d_a + 0.6C_{f,M}/\rho)} \quad \textbf{(A.24)}$$

with

$$\Psi_{c,M} = (\kappa/2.3)^2 \cdot 0.4 = 0.012 \quad \textbf{(A.25)}$$

In which κ (=0.4) is the Von Kármán constant and k_s $(\approx 1.5d_a)$ is the effective roughness.

A.7 Sediment transport theory

In the sediment transport theory bed load transport and/or suspended sediment transport plays a role. The bed load transport and suspended sediment transport are quantifications for the amount of sediment transport. Bed level changes are calculated based on the gradient of the transport capacity for the bed load.

The bed load transport is the transport of sediment along the bed. The particles are still in contact with the bed and shear stress is important. In the suspended load the sediment particles are suspended in the water column.

The sediment transport theory is applied by several researchers. [Liu & García, 2008] developed a 3D numerical model with free water surface and mesh deformation for local sediment scour. Also [Jacobsen, 2011] applied the same approach for the bed level change due to breaking waves. In both cases the hydro- and morphodynamics are fully interacting in the model. The consequence of a fully interacting model is that from numerical point of view it is challenging to elaborate a stable model, which requires numerical and mathematical manipulation. Beside that the morphological relations which are available to determine the sediment transport are validated for relative low flow velocities, which are valid for example in coastal areas, but not for jet flow induced by ship propulsion systems.

Liu and Garcia (2008)

[Liu & García, 2008] developed a three-dimensional numerical model with free water surface and mesh deformation for local sediment scour. Regarding the entrainment rate E several models are presented in the literature study based on a comparison of eight relations against data made by Garcia and Parker (1991). In this comparison Van Rijn's formulation is included, but formulated in a different way. The entrainment rates for the compared relations are all expressed dimensionless. E can be written in dimensionless form as

$$\tilde{E} = \frac{E}{w_s} \qquad \textbf{(A.26)}$$

Where w_s is the sediment fall velocity. Three of the existing sediment entrainment models are listed by [Liu & García, 2008] and presented below in a table which is depicted in Table A.2[9].

Table A.2 Sediment entrainment models [Liu & García, 2008]

Authors	Model	Parameters
García and Parker (1991)	$\tilde{E}=AZ_u^5/1+A/0.3Z_u^5$	$A=1.3\times10^{-7}\quad Z_u=U_{*s}/v_sR_{ep}^{0.6}$
van Rijn (1984)	$\tilde{E}=0.015d_{50}\Psi^{1.5}/Z_bD_*^{0.3}$	$D_*=d_{50}[R-1/g\mu^2]^{1/3}\quad \Psi=(\theta/\theta_c-1)\quad Z_b=0.05H$
Smith and McLean (1977)	$\tilde{E}=0.65\gamma_0(\theta/\theta_c-1)/1+\gamma_0(\theta/\theta_c-1)$	$\gamma_0=2.4\times10^{-3}$

[9] Note that in Table A.2 the parameters θ and θ_c are used for the (critical) Shields parameters which is in this report denoted as Ψ_s and $\Psi_{s,cr}$ respectively.

In which Z_b is the reference level very near bed to avoid singularity, which are 5% of the water depth from the bed for the expressions of Garcia and Parker (1991) and Van Rijn (1984). For the expression of Smith and McLean an expression is used for Z_b which can be written as

$$Z_b = 26.3\left(\frac{\Psi_s}{\Psi_{s,cr}} - 1\right)d + k_s \qquad \textbf{(A.27)}$$

where k_s is the equivalent roughness height of the bed.

It is possible to simplify the deposition rate E by setting it equal to the sediment settling velocity times the near-the-bed concentration, by using the concept of turbulence diffusivity and set the vertical sediment entrainment flux as

$$E = \frac{\nu_t}{\sigma_c}\frac{\partial c}{\partial y} \qquad \textbf{(A.28)}$$

which has been used by [Brørs, 1999] and [Liang, Cheng, & Li, 2004]. Here ν_t is the eddy viscosity or kinematic viscosity and σ_c the turbulent Prandtl-Schmidt number for c.

Bed Morphology

There are several methods to update and compute the bed elevation η.

[Liu & García, 2008] proposed to describe the sediment continuity by the Exner equation, since the bed elevation changes are based on the continuity of sediment. The Exner equation can be written as

$$\frac{\partial \eta_b}{\partial t} = \frac{1}{1-n_0}[-\nabla \cdot \mathbf{q}_b + D - E] \qquad \textbf{(A.29)}$$

where η_b is the bed elevation, n_0 is the porosity of the bed, $\mathbf{q}_b$ is the bed-load transport rate vector which components are given by eq. (A.31) D is the deposition rate given by

$$D = w_s c_b \qquad \textbf{(A.30)}$$

The bed-load transport in different directions are given by

$$q_i = q_0\frac{\tau_i}{|\tau|} - C|q_0|\frac{\partial \eta}{\partial x_i}, \qquad i = 1,2 \qquad \textbf{(A.31)}$$

where q_i is the dimensional bed-load transport flux component and q_0 is the dimensional bed-load transport flux. [Liang et al., 2004] also described the Exner equation in their scour model and states that the Exner equation uses mass balance of sediment material in the bed load layer.

Another approach is proposed by [Liang et al., 2004] which is based on mass balance of sediment over the whole water column and can be written as

$$\frac{\partial \eta_b}{\partial t} = \frac{1}{1-n_0}\left[-\frac{\partial (q_T)}{\partial x} - \frac{\partial}{\partial t}\left(\int_{\eta=\eta_b}^{\eta_b+H} c\ d\eta\right)\right] \qquad \textbf{(A.32)}$$

where q_T is the total sediment transport rate that comprises bed load q_b and suspended sediment transport rate q_s.

Liang et al. recommended to use eq.(A.32) to calculate the bed level change because from numerical point of view it is more stable than eq.(A.29) which involves only the bed-load transport. Beside this in the research of Liang et al. it is also found that the scour predicted using eq.(A.29) developed faster than those observed in the experiments.

A.8 Scour hole prediction – analytical expressions

In 2007 a method for predicting the scour hole depth is elaborated in a technical note of Van Oord about scour protection near quay walls and slopes [Augustin, 2007]. The method is according to Westrich & Kobus 1974, which is later on applied by Rajaratnam and is described below. The resulting equations do not contain a time factor so the equations are only valid for a fully developed scour hole. Beside this the method is only valid for scour development without boundaries due to e.g. quays or other hydraulic structures.

Westrich and Kobus 1974, Rajaratnam and Beltaos 1977

Westrich and Kobus 1974 studied the scour hole depths due to jets perpendicular to the bottom. In order to do so, two different forms of scour holes are defined. In the first form there is an equilibrium stage between eroding forces and soil's strength to withstand them. The second form there is equilibrium between the eroded soil by the jet and the soil that slides down into the scour hole.

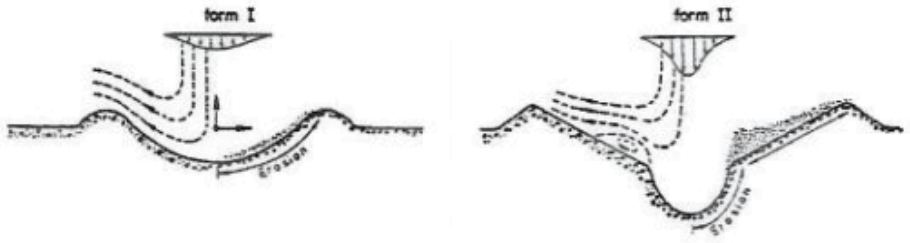

Figure A.4 Form I and II of scour holes

Taking into account the jet velocity, fall velocity of particles, relative distance (z/D), impulse parameter and time parameter Westrich and Kobus found two constant values for the ratio of the jet velocity and the fall velocity for both forms.

$$\frac{u_0}{w} = 1.5 \rightarrow Form\ I$$

$$\frac{u_0}{w} = 2.9 \rightarrow Form\ II$$

Rajaratnam and Beltaos 1977 combined their own theory for horizontal jets and Westrich and Kobus. This resulted in a relation between the depth of the scour hole and the densimetric Foude number which is the ratio of inertial to buoyancy forces. This number is dimensionless and can be interpreted as a measure of the buoyancy of a jet. In this case the densimetric Froude number is dependent on the distance from the propeller to the bottom (i.e. keel clearance):

$$\frac{h_{hole}}{z} = f\left(\frac{Fr_0}{\frac{z}{D}}\right) \qquad \textbf{(A.33)}$$

And also between the radius of the scour hole and the distance:

$$\frac{r_{hole}}{z} = f\left(\frac{\frac{Fr_0}{z}}{D}\right) \quad \textbf{(A.34)}$$

Where: Fr_0 is the densimetric Froude number:

$$Fr_0 = \frac{u_0}{\sqrt{g \cdot d \cdot \frac{\rho_s - \rho_w}{\rho_w}}} \quad \textbf{(A.35)}$$

Based on these results Rajaratnam & Aderibigbe 1996 defined an erosion parameter E_{cr} using relationship between z and D to determine whether the scour hole will develop according to the mechanism of form I or II:

$$E_{cr} = \frac{u_0 \cdot \left(\frac{D}{z}\right)}{\sqrt{g \cdot d \cdot \frac{\rho_s - \rho_w}{\rho_w}}} \quad \textbf{(A.36)}$$

Römisch 2012

[Römisch, 2012] formulates expressions for amongst others the scour hole depth near a vertical quay wall for bow thrusters. Tests showed that the development of the scour hole due to jets can be divided into two phases. In the first phase of low hydraulic load the depth of the scour hole increases very fast with increasing jet load. When the jet load increased further, the development of the scour hole is less intensive. For each phase an expression is drawn up for a thruster perpendicular to a quay wall.

$$\frac{h_{hole,B}}{d_{85}} = \begin{cases} C_m \cdot 0.1 \cdot \left(\frac{B}{B_{cr}}\right)^{13} \; for\ phase\ 1, & 1.0 < \frac{B}{B_{cr}} < 1.4 \\ C_m \cdot 4.6 \cdot \left(\frac{B}{B_{cr}}\right)^{2.25} \; for\ phase\ 2, & \frac{B}{B_{cr}} > 1.4 \end{cases} \quad \textbf{(A.37)}$$

Where: C_M = 0.3 for manoeuvring vessels

C_M = 0.1 for stationary vessel (i.e. vessel at rest)

B= stability coefficient (similar to densimetric Froude number)

$$B = \frac{v_b}{(d_{85} \cdot g \cdot \frac{\rho_s - \rho_w}{\rho_w})} \quad \textbf{(A.38)}$$

B_{cr}= 1.20 according to Fuehrer and Römisch 1995

Hamill et al. 1999

[Hamill et al., 1999] investigated in the laboratory scouring action of the wash generated by a number of propellers in the confines of quay structures. Empirical equations have been developed for the maximum scour depth, for any given exposure period, for both free expanding jets and those in close proximity to harbour structures. This research is based on Römisch 1975, Blaauw et al. 1978 and Verhey et al. 1987, which gave insight into methods to approximate the maximum scour depth and is extended by Hamill 1988 into scour due to propellers on a sandy bed. In here the development in time is also developed. The maximum scour depth is a function of:

- efflux velocity calculated as suggested by Blaauw et al. 1978 with $V_0 = nD_p\sqrt{K_T}$, where K_T is thrust coefficient or dimensionless relationship between propulsive force, number of revolutions and diameter of the propeller.
- median sediment grain size;
- propeller diameter;
- clearance distance between the propeller tip and the seabed;
- density of water;
- difference between mass density of the sediment and the fluid;
- and the kinematic viscosity of the fluid.

The research of Rajaratnam 1981 showed that for high Reynoulds numbers the effect of viscosity could be neglected. In the investigation of Hamill (1988) therefore the effect of viscosity also was neglected and the maximum scour depth can be rewritten as:

$$\frac{\varepsilon_m}{D_p} = f\left[Fr_0, \frac{D_p}{d_{50}}, \frac{C}{d_{50}}\right]$$

This means that the maximum scour depth depends on:

1. Densimetric Froude number;
2. Ratio of the propeller diameter to the sediment grain size;
3. Ratio of the clearance to the sediment grain size.

Beside this Hamill 1988 proposed an expression for maximum scour depth which varies as a logarithmic function in time:

$$\varepsilon_m = \Omega[\ln(t)]^{\Gamma}$$

With time in seconds and the scour depth calculated in millimetres.

Where the coefficients are defined based on unobstructed propeller was, i.e. for free expanding jets:

$$\Gamma = 4.113\left(\frac{C}{d_{50}}\right)^{0.742}\left(\frac{D_p}{d_{50}}\right)^{-0.522} {F_{r0}}^{-0.682}$$

And

$$\Omega = 6.9 \times 10^{-4}\left(\frac{C}{d_{50}}\right)^{-4.63}\left(\frac{D_p}{d_{50}}\right)^{3.58} {F_{r0}}^{4.535}$$

Because in this case the presence of a quay wall is not taken into account Hamill et al. 1999 decided to extend the work by doing experiments to include the effect of the confinement of the wash by a vertical, perpendicular quay wall.

The experiments showed that for scouring action of unconfined propeller wash the following equation is valid:

$$\varepsilon_m = k\Omega[\ln(t)]^{\Gamma}$$

For the coefficients new (empirical) expressions are developed based on the measurements:

$$\Omega = \Gamma^{-6.38}$$

Where

$$\Gamma = \left(\frac{C}{d_{50}}\right)^{0.94} \left(\frac{D_p}{d_{50}}\right)^{-0.48} {F_{r0}}^{-0.53}$$

With 70% of the data found to lie within 45% of the predicted value, with k taking a value of 38.97. Those equations are only applicable for depths of seabed below the propeller in the range of 0.5-2.5 times the propeller diameter.

The equations above, only define the maximum scour depth, but do not tell anything about the location where this maximum depth occurs. The following equation predicts the location, i.e. the distance from the propeller face to the position of the maximum depth in the fully developed profile:

$$X_{mu} = Fr_o^{0.94} C$$

Where X_{mu} =the distance from the propeller phase to the position of maximum scour in the final eroded profile [m];

C = the propeller clearance distance.

For each experiment the distance from the propeller face to the position of maximum scour in the final eroded profile X_{mu} (in meters), was determined.

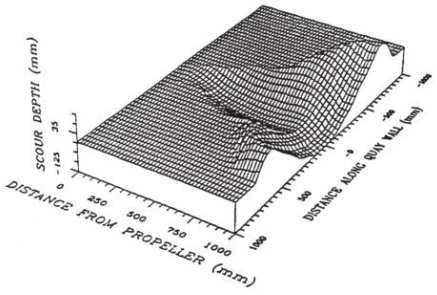

Figure A.5 Isometric view of Scour at Quay wall [Hamill et al., 1999]

In the final phase of the research the effect of confinement (i.e. in this case a vertical quay wall) is taken into account. Figure A.5 illustrates the effect of the confinement on the bathymetry. In all cases the maximum scour depth near a quay wall is higher than in the unconfined situation. That is why Hamill et al. assumed that the maximum scour depth in the confined situation is the superposition of the maximum scour depth in unconfined situation and the change in maximum scour depths in the confined situation. The equation below can be used to estimate the *change* in maximum scour depth of scour in the final eroded profile due to the introduction of a quay wall into the propeller wash:

$$\left(\frac{\varepsilon_{mc\infty} - \varepsilon_{mu\infty}}{\varepsilon_{ma\infty}}\right) + 1 = 1.18\left(\frac{X_w}{X_{mu}}\right)^{-0.2}$$

Where: $\varepsilon_{mc\infty}$ = confined maximum scour depth;

$\varepsilon_{mu\infty}$ = unconfined maximum scour depth;

$\varepsilon_{ma\infty}$ = unconfined scour depth measured relative to the propeller axis;

X_w = wall distance.

The relation above is based on the experiments and depicted in Figure A.6.

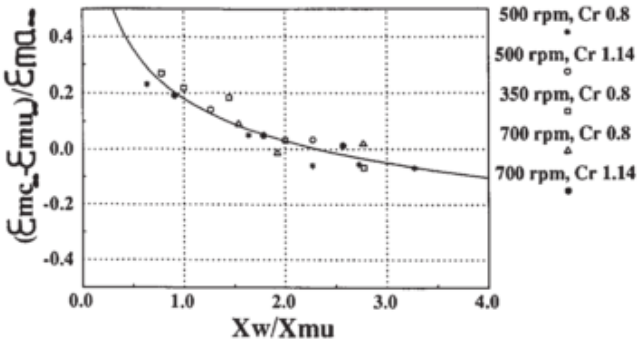

Figure A.6 Unified trend in additional scour data for number of speeds of rotation and clearance ratios

In the research of Hamill et all 1999 the effect of the rudder is not taken into account. The effect of the angle of the rudder are later on researched in Ryan and Hamill 2011 [Ryan & Hamill, 2011]

Appendix B. Experimental tests

B.1 Full scale test Rotterdam

Below the procedure of the full scale tests in the Port of Rotterdam is described briefly with help of pictures during the full scale tests with inland vessel the MTS Jade in Figure B.1 to Figure B.5.

Figure B.1 MTS Jade moored near quay

Figure B.2 MTS Jade departing from the quay

Figure B.3 Turbulent flow induced by main propeller

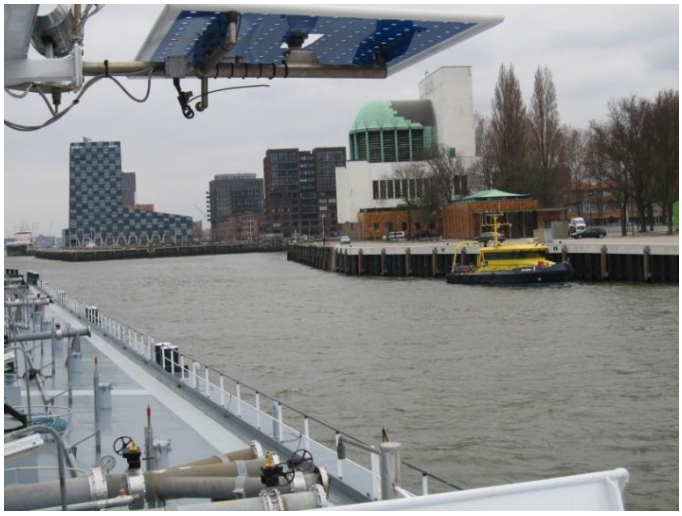

Figure B.4 Survey boat measuring scour depth near quay

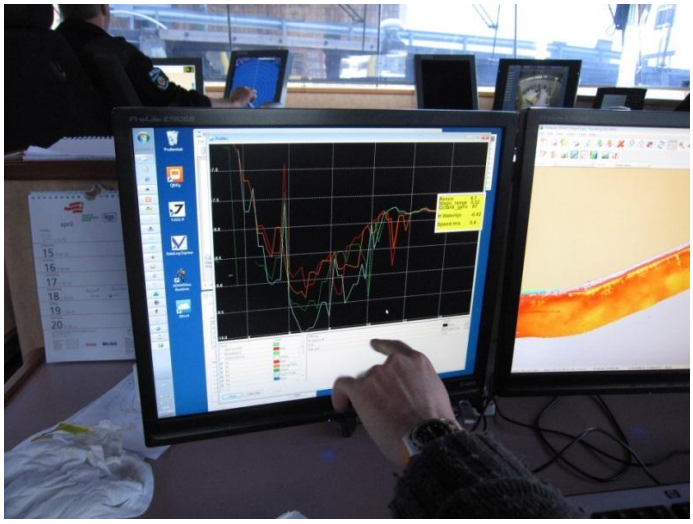

Figure B.5 Raw data resulting from multi-beam measurements on the survey boat

Location

The full scale tests were performed in front of the Parkkade between bollard (in Dutch: 'Bolder') 5 and bollard 11 as depicted in Figure B.6.

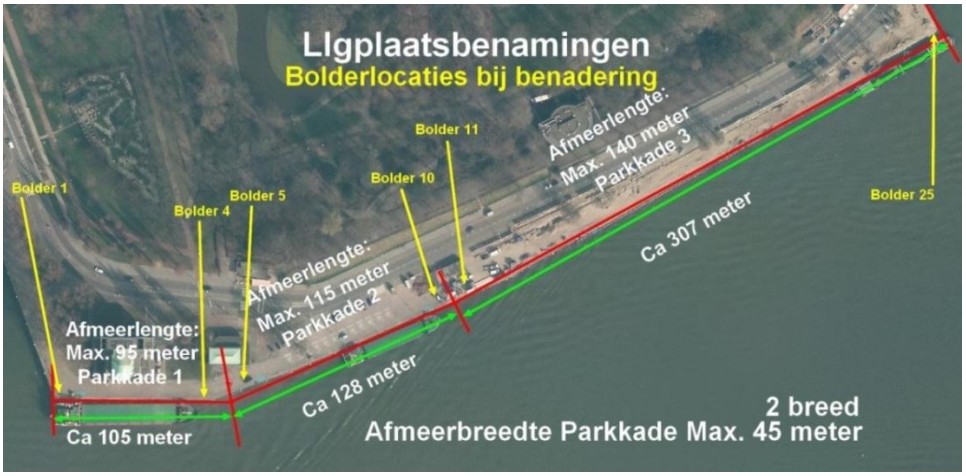

Figure B.6 The Parkkade in the Port of Rotterdam with approximate bollard location

Specification of the inland vessels

Below the main specifications of the vessels MTS Jade and MTS Noordzee are given respectively. This information is obtained with help of the website www.vlootschouw.nl.

MTS Jade (Tanker) (see Figure B.8)

Europe number	2326538
Name of company	Jade VOF, Rotterdam
Length	135.00 meter
Beam	20.00 meter
Draught	4.60 meter
Tonnage	9007 ton
Cubage	10.600 m^3
Engine	2 x MTU 12 V 4000 M 60, 1324kW/1800 hp, 1800 rpm

Main propeller: Two azimuthal main propellers, each consisting of two Contra Rotating Propellers (CRP) of type VZ-1250-R and 1250 kW power with 1800 rpm (for each propeller) (see Figure B.7).

Thrusters:

- Veth-Compact-Jet bow thruster of Type CJ-1200 with electro engine of 405 kW power with 1800 rpm.
- Veth-Jet bow thruster of Type 4-K-1200 (four channel type) with electro engine of 405 kW power with 1800 rpm.

Remark: Note that MTS Jade is equipped with two different bow thrusters.

Figure B.7 Contra Rotating Propeller from Veth

Figure B.8 MTS Jade

MTS Noordzee (Tanker) (see Figure B.9)

Europe number	2313102
Name of company	United Barge Owners 45 BV, Rotterdam
Length	110.00 meter
Beam	13.50 meter
Draught	4.20 meter
Tonnage	4200 ton
Cubage	4440 m³
Engine	Caterpillar 3516 (B) DI-TA electronic, 1492 kW/2028 hp, 1600 rpm

Thruster: Two Veth-Jet bow thrusters of type 4-K-1200 (four channel type) with electric motor of 320 kW power with 1800 rpm.

Main propeller: one 5 bladed propeller 1910 mm with a duct of type optima and a diameter of 1,916 mm.

Figure B.9 MTS Noordzee

Soil properties

Regarding the soil properties only the measurements are depicted which locates from geographical point of view nearest to the location of MTS Noordzee.

First the results from a soil sample are given, regarding the composition of the soil, the porosities and density. After that the distribution of the grain size diameters of sand are given based on a soil sample at -10 NAP (which is about 2 meters below bed level). At last the results from a triaxial test are given. In short:

- Figure B.10 and Figure B.11: Soil composition over depth;
- Figure B.12: Grain size distribution;
- Figure B.13: Triaxial test.

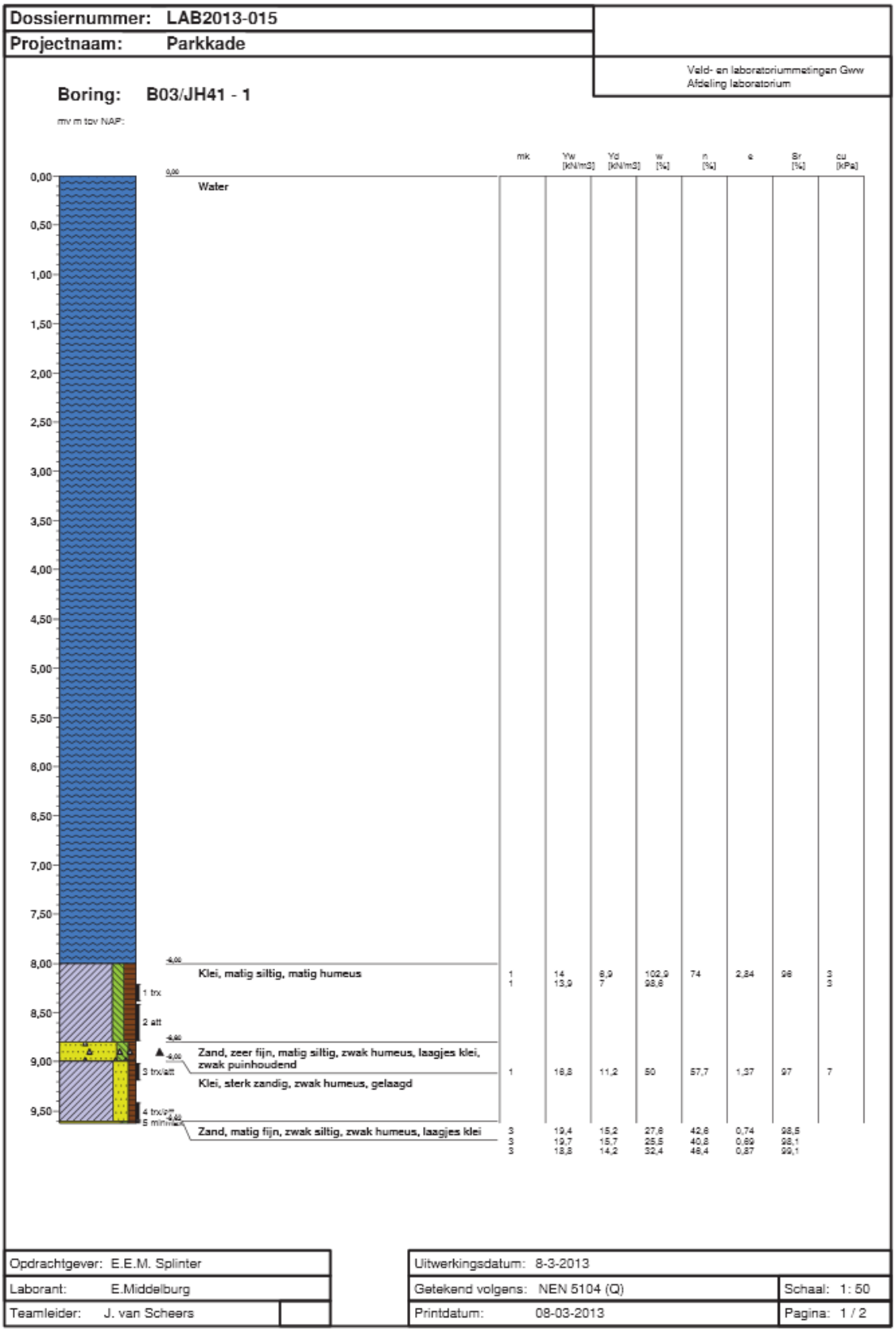

Figure B.10 Soil composition

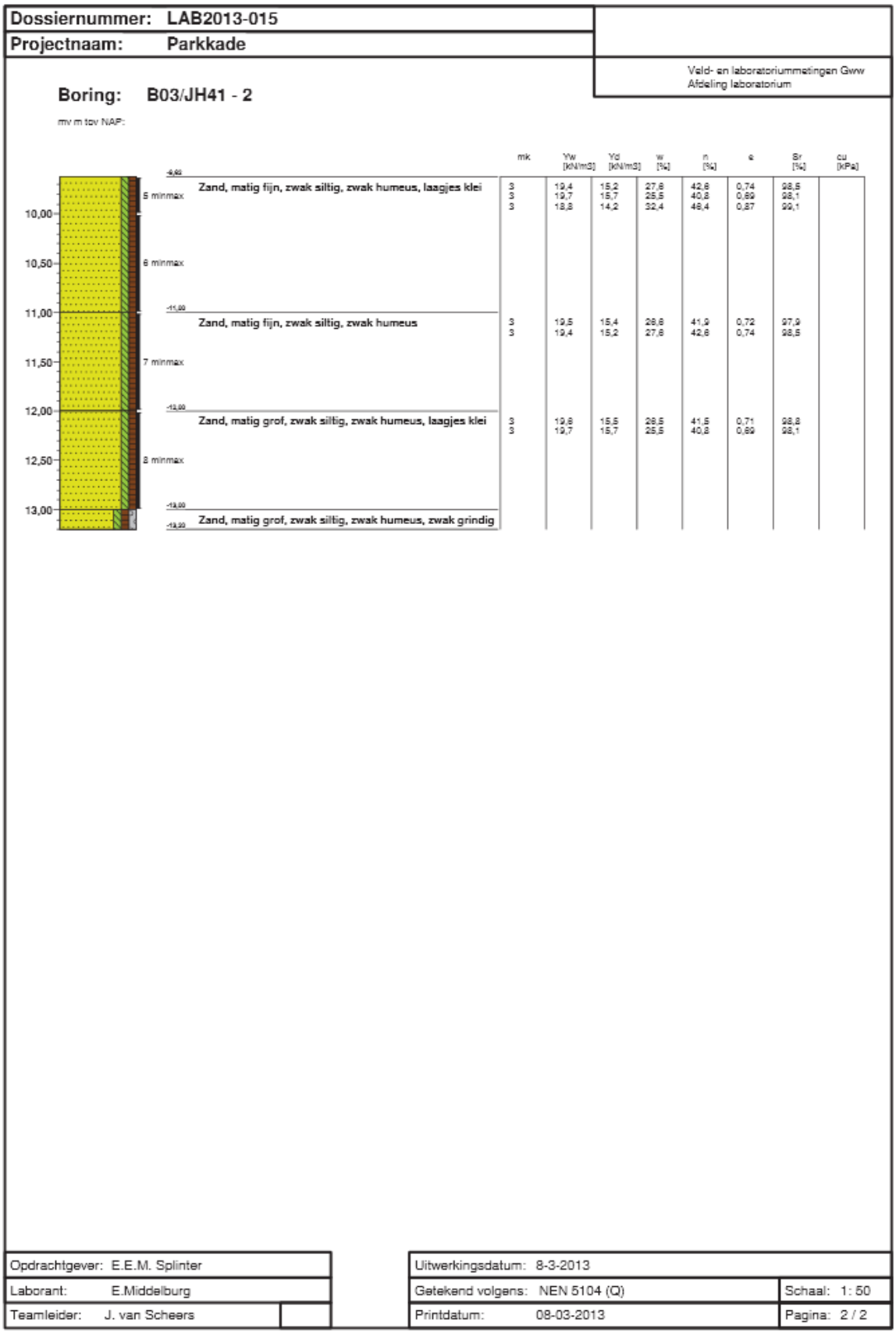

Figure B.11 Soil composition

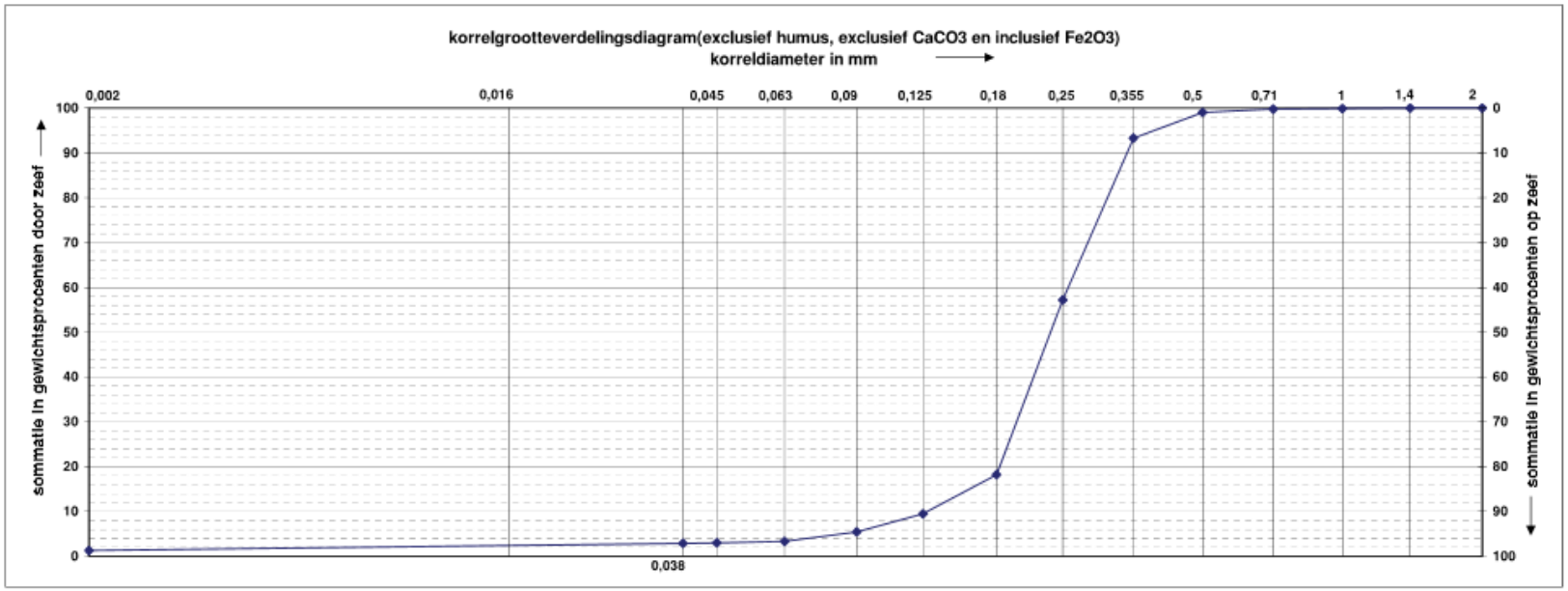

samenstelling monster (inclusief humus, CaCO3 en Fe2O3)

identificatie monster	grind >2 mm %	zand 0.063-2mm %	silt 0.002-0.063mm %	lutum <0.002 mm %	humus %	CaCO3 %	D50 mm	M50 (0.063-2mm) mm	D60/D10 (0.063-2mm)	grondsoort volgens NEN5104
10-11m-NAP	0,0	93,0	2,0	1,2	0,4	3,4	0,235	0,239	1,80	Z(239)s1, h1, g1 ,Ca3

Tabel uitgedrukt in massapercentages van de stoofdroge grond

opdrachtgever:	K.Hulsbos	monsterklasse (NEN5119):	3	datum:	12-3-2013	boringnummer:	JH41
laborant:	E.Middelburg	teamleider:		mapnr.:	2013-015	hoogteligging: bodem	tov NAP: -8,00 m

GEMEENTEWERKEN ROTTERDAM
INGENIEURSBUREAU

Veld- en Laboratoriummetingen Gww

project: Parkkade mvj13009

KORRELGROOTTEVERDELING

Figure B.12 Grain size distribution

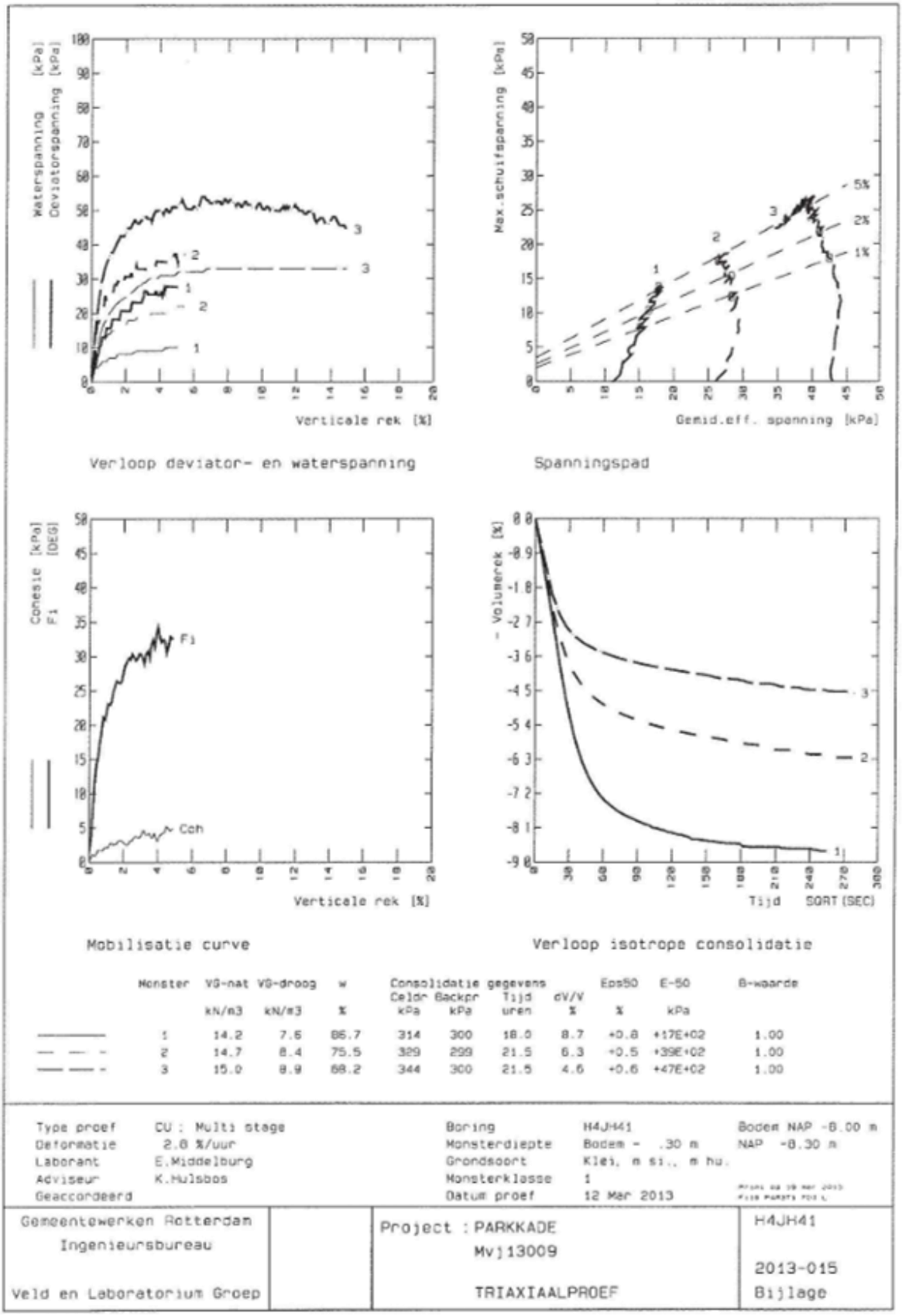

	Monster	VG-nat	VG-droog	w	Consolidatie gegevens Celdr	Backpr	Tijd	dV/V	Eps50	E-50	B-waarde
		kN/m3	kN/m3	%	kPa	kPa	uren	%	%	kPa	
———	1	14.2	7.6	86.7	314	300	18.0	8.7	+0.8	+17E+02	1.00
— — —	2	14.7	8.4	75.5	329	299	21.5	6.3	+0.5	+39E+02	1.00
———	3	15.0	8.9	68.2	344	300	21.5	4.6	+0.6	+47E+02	1.00

Type proef	CU : Multi stage	Boring	H4JH41
Deformatie	2.0 %/uur	Monsterdiepte	Bodem - .30 m
Laborant	E.Middelburg	Grondsoort	Klei, m si., m hu.
Adviseur	K.Hulsbos	Monsterklasse	1
Geaccordeerd		Datum proef	12 Mar 2013

Bodem NAP -0.00 m
NAP -0.30 m

Gemeentewerken Rotterdam Ingenieursbureau		Project : PARKKADE Mvj13009	H4JH41 2013-015
Veld en Laboratorium Groep		TRIAXIAALPROEF	Bijlage

Figure B.13 Triaxial test

B.2 Phsyical model [Schmidt, 1998]

Dimensions of scale model

Abb. A-5: Modellschiff im Maßstab M = 1:45

Abb. A-6: Modellschiff im Maßstab M = 1:18

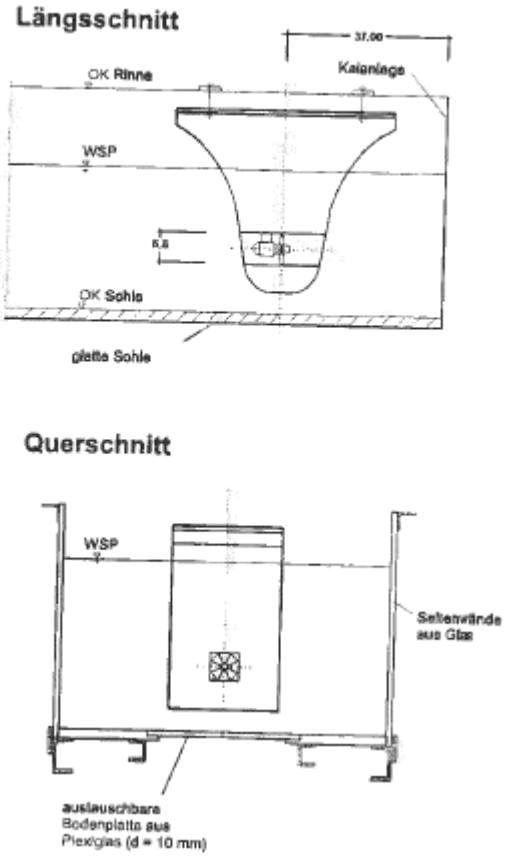

Abb. A-1: Versuchsrinne im Maßstab M = 1:45

Abb. A-2: Querschnitt durch den Modellpropeller M = 1:45

Velocity field for different keel- and quay clearances

Anlage 10

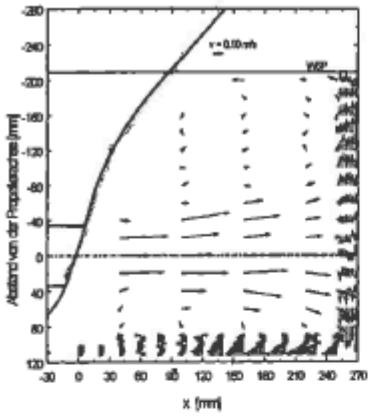

a) h_p = 11,3 cm

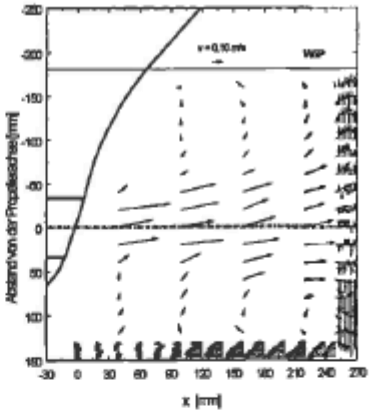

b) h_p = 14,8 cm

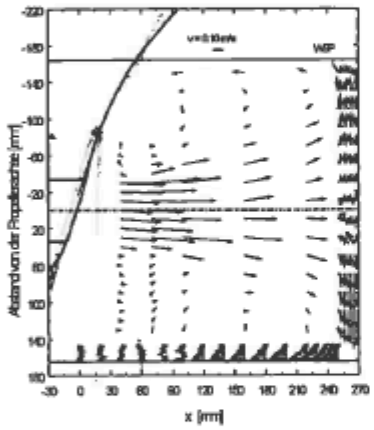

c) h_p = 16,5 cm

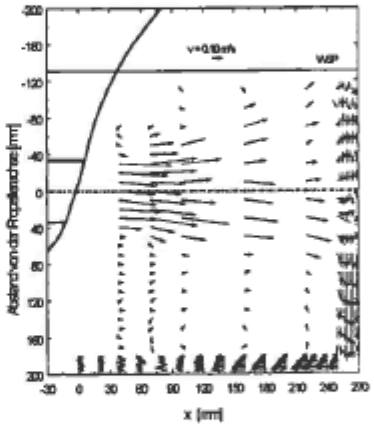

d) h_p = 19,8 cm

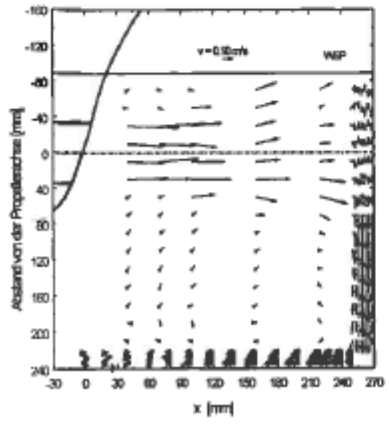

e) h_p = 23,8 cm

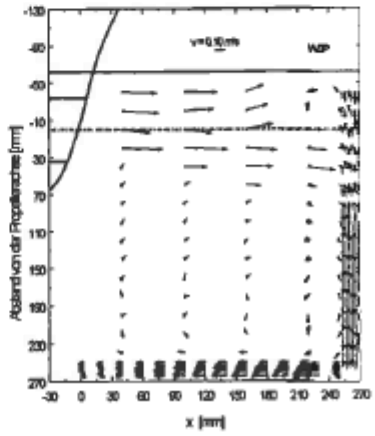

f) h_p = 26,7 cm

Appendix C. Software & CFD

This appendix gives an overview of the software which is considered for modelling the local scour due to bow thrusters.

Delft3D

Delft3D is a software suite developed by Deltares to make 3D calculations for flows, sediment transport, waves, water quality, morphological developments and ecology. Integrated in this is also the development of these processes in time.

The interaction between sediment and water and the development in time is integrated in the software what makes the modelling feasible and accessible. However, the flow velocities in coastal, river and estuarine areas are in general not so high, i.e. up to about 2 m/s. The flow velocities induced by bow thrusters can reach much higher values up to 8 m/s. The formulations and equations applied in Delft3D are mainly based on classical morphology for larger time scales and smaller velocities. Beside this vertical accelerations are assumed to be small compared to gravitational accelerations. This means that Delft3D is designed to model large scale flow of e.g. estuaries, rivers and lakes of which the horizontal length and time scales are much larger than the vertical scales [Lesser, Roelvink, van Kester, & Stelling, 2004].

In the MSc thesis [Simoons, 2012] where the edge scour around an offshore wind turbine is modelled with amongst others Delft3D, similar conclusions are drawn regarding Delft3D used for scour modelling. First of all is concluded that the model results in Delft3D-Flow in this specific thesis needs more research for a correct calculation of edge scour development with Delft3D. Second, even in case the model results would be perfect, considerable or even unacceptable computational times need to be overcome.

In other words, it is possible and feasible to model the thruster jet and the scour in time in Delft3D, but the quantitative results might be doubtful, mainly due to simplification of the flow field. In case Delft3D will be used qualitative results should be assessed and are more significant in order to answer the research questions than the quantitative results. For the physical and numerical details behind Delft3D-FLOW is referred to [Lesser et al., 2004].

Deft

Deft is an incompressible flow solver developed at Delft University of Technology. The same approach as [Hoan, 2008] suggested might be applicable in this case. Hoan computed with Deft the flow properties and on its turn this flow properties are the input for the scour calculation. Hoan developed a Shields like stability parameter for non-uniform flow which can be used in combination with the output of CFD RANS models. The scour can be modelled by using mobility parameter to quantify the hydraulic loads exerted on the bed.

ANSYS CFX and ANSYS FLUENT

ANSYS CFX and ANSYS FLUENT are commercial CFD models, in which sediment transport can be studied by analysing the trajectories of particles and is capable of simulating 2D and 3D multiphase flow. CFX is not available in the TU Delft and Deltares, but FLUENT is available at 3ME faculty of TU Delft.

According to [Vuik, 2010] FLUENT represents the difference between bed-load transport and suspended-load transport correct, but is seems that FLUENT is not able to reproduce incipient motion. This means that for large ratios of w_s/u_* and for bed load transport the results of the model should be treated carefully. However it is not expected this will be a problem. In practice bed load transport will not play a major role because the main part of the sediment will be in suspension, due to the high flow velocities of the jet.

From practical point of view it is not suitable to use FLUENT since there is no support from Deltares during the thesis regarding this package.

FinLab

FinLab is developed in TU Delft and is a 3D non-hydrostatic free-surface flow model aiming at applications of small scale flow models around hydraulic engineering problems,. The sedimentation and erosion of bed material in complex 3D flows can be modelled as well with FinLab. Disadvantage of using this model is that no support from Deltares is available since it is not used within the company.

Appendix D. Results of numerical model with non-erodible bed – physical model

Case 2.1

The geometrical properties of case 2.1 are:

L	[mm]	270
h_P	[mm]	113
V_0	[m/s]	0.50

The velocity field of the numerical model and Schmidt's physical model can be compared looking at Figure D.1 and Figure D.2.

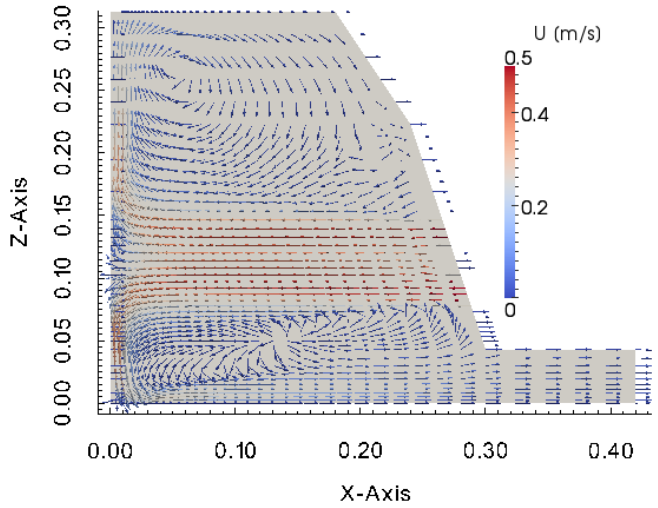

Figure D.1 Velocity field numerical model Case 2.1 [m/s] with jet with zero velocity core

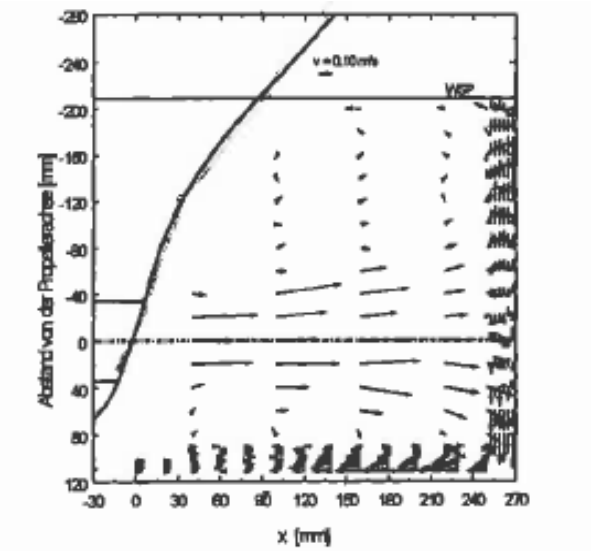

Figure D.2 Velocity field according to Schmidt 1998, h_p=113mm

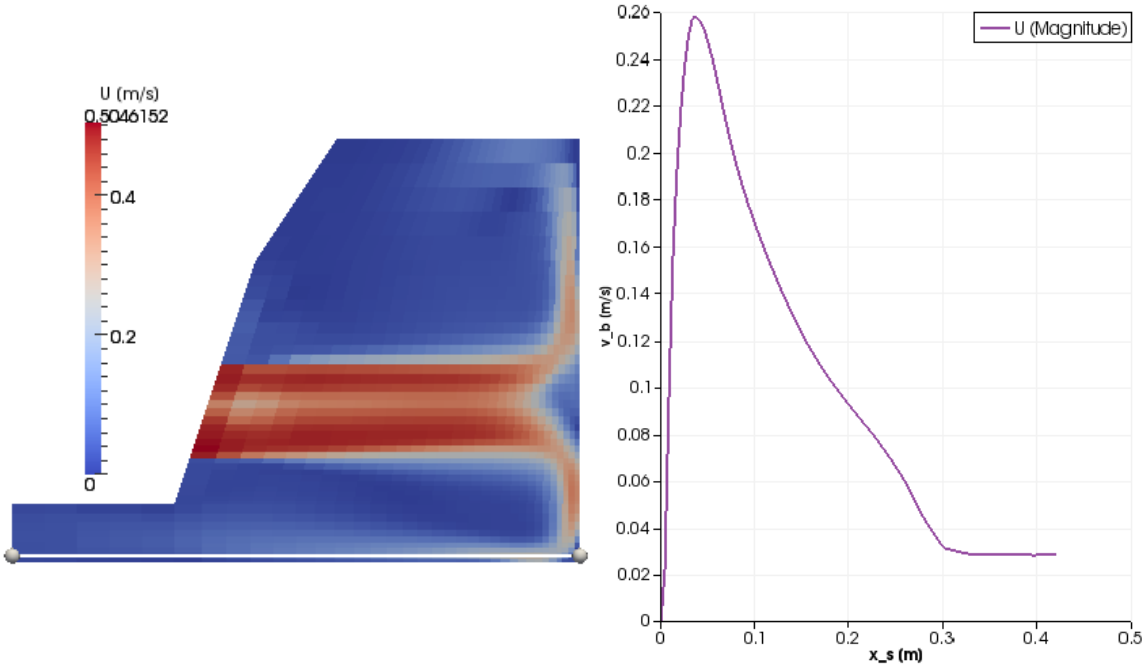

Figure D.3 Velocity field in Z-X plane and near bed velocities plotted over line X= 0.005 m

Table D.1 Bed velocities Case 2.1 compared with physical model of Schmidt

SCHMIDT		**MODEL t=30s**			
		Without zero velocity core		With zero velocity core	
x_s [cm]	v_b/V_0 [-]	v_b [m/s]	v_b/V_0 [-]	v_b [m/s]	v_b/V_0 [-]
2	0.29	0.192	0.38	0.204	0.41
3	0.38	0.218	0.44	0.226	0.45
5	0.4	0.224	0.45	0.228	0.46
7	0.38	0.208	0.42	0.21	0.42
9	0.37	0.183	0.37	0.184	0.37
11	0.33	0.164	0.33	0.163	0.33
13	0.31	0.15	0.30	0.146	0.29
15	0.27	0.139	0.28	0.131	0.26
17	0.17	0.126	0.25	0.115	0.23
19	0.15	0.11	0.22	0.108	0.22
21	0.08	0.051	0.10	0.099	0.20

x_s is the horizontal distance measured perpendicular from the quay wall (see Figure D.4)

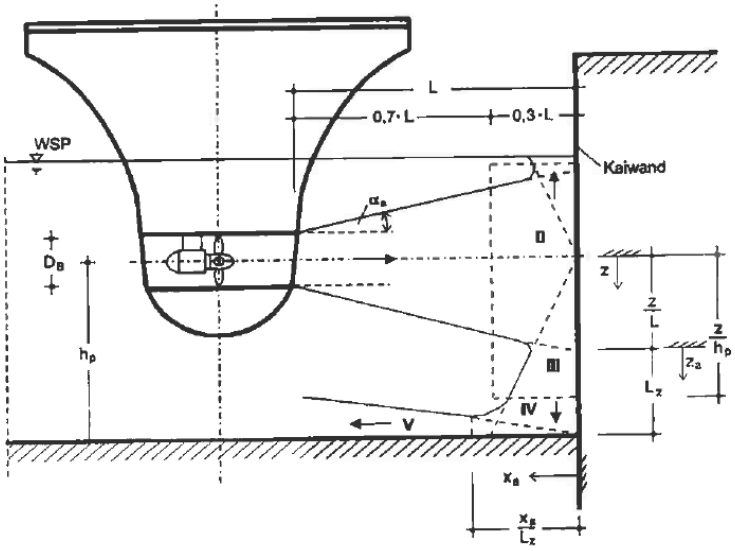

Figure D.4 Schematization of the velocity field near a vertical quay wall

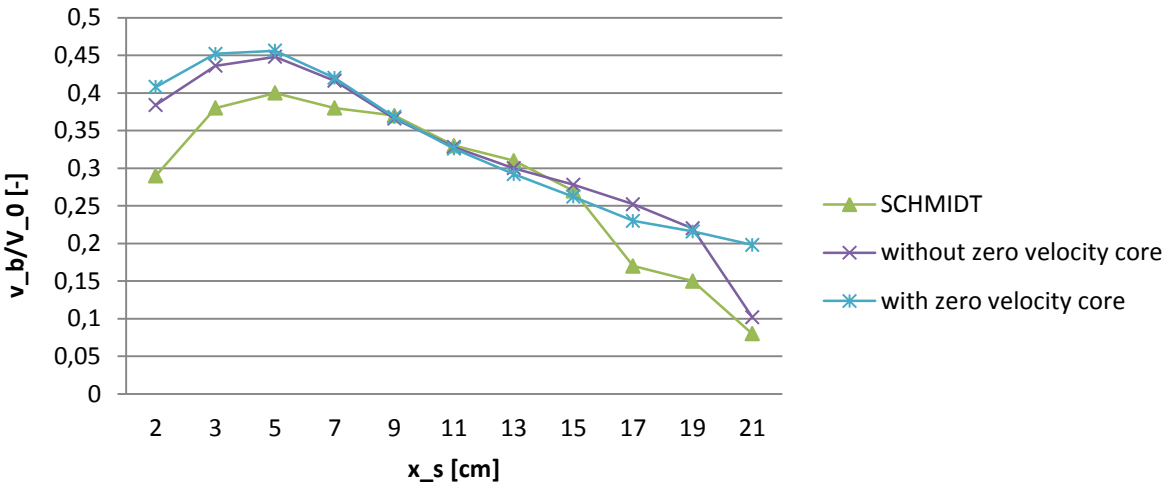

Figure D.5 Bed velocities Case 2.1 compared with physical model of Schmidt

Case 2.2

The geometrical properties of case 2.2 are:

L	[mm]	270
h_p	[mm]	164
V_0	[m/s]	0.5

Table D.2 Bed velocities Case 2.2 compared with physical model of Schmidt

SCHMIDT		NUMERICAL MODEL t=30s			
		Without zero velocity core		With zero velocity core	
x_s [cm]	v_b/V_0 [-]	v_b [m/s]	v_b/V_0 [-]	v_b [m/s]	v_b/V_0 [-]
2	0.22	0.212	0.42	0.122	0.24
3	0.30	0.231	0.46	0.153	0.31
4	0.34	0.232	0.46	0.17	0.34
5	0.35	0.225	0.45	0.173	0.35
7	0.33	0.204	0.41	0.164	0.33
9	0.31	0.179	0.36	0.145	0.29
11	0.27	0.158	0.32	0.13	0.26
13	0.29	0.144	0.29	0.119	0.24
15	0.23	0.132	0.26	0.109	0.22
17	0.16	0.12	0.24	0.099	0.20
19	0.17	0.11	0.22	0.091	0.18
21	0.07	0.101	0.20	0.083	0.17

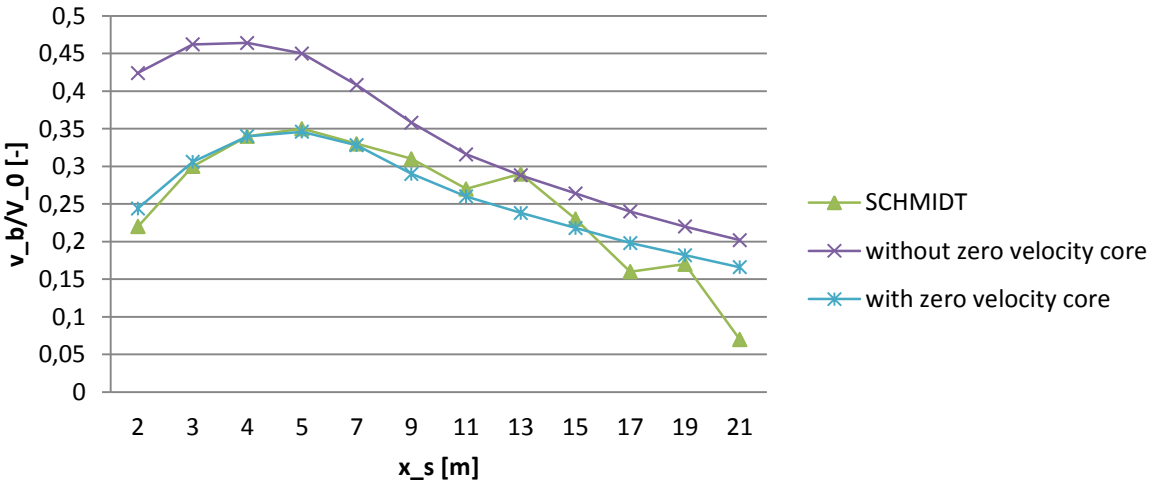

Figure D.6 Bed velocities Case 2.2 compared with physical model of Schmidt

Case 2.3

The geometrical properties of case 2.3 are:

L	[mm]	270
h_P	[mm]	238
V_0	[m/s]	0.50

Table D.3 Bed velocities compared with physical model of Schmidt

SCHMIDT		NUMERICAL MODEL			
		Without zero velocity core		With zero velocity core	
x_s [cm]	v_b/V_0 [-]	v_b [m/s]	v_b/V_0 [-]	v_b [m/s]	v_b/V_0 [-]
2	0.15	0.046	0.09	0.035	0.07
3	0.23	0.082	0.16	0.066	0.13
4	0.25	0.111	0.22	0.09	0.18
5	0.27	0.129	0.26	0.106	0.21
7	0.27	0.138	0.28	0.112	0.22
9	0.26	0.128	0.26	0.104	0.21
11	0.24	0.114	0.23	0.094	0.19
13	0.23	0.104	0.21	0.085	0.17
15	0.22	0.097	0.19	0.079	0.16
17	0.18	0.092	0.18	0.072	0.14
19	0.17	0.086	0.17	0.064	0.13
20	0.14	0.083	0.17	0.056	0.11
21	0.14	0.08	0.16	0.049	0.10

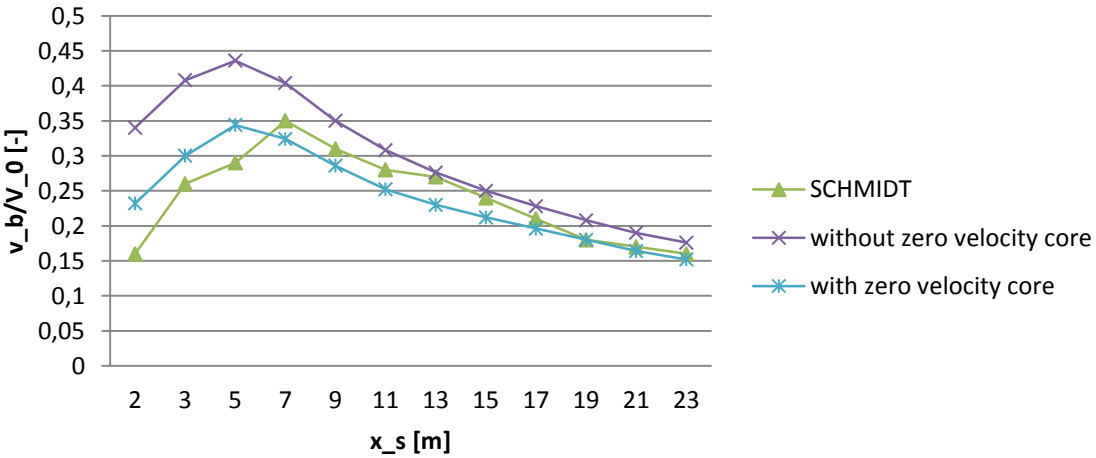

Figure D.7 Bed velocities Case 2.3 compared with physical model of Schmidt

Case 2.4

The geometrical properties of Case 2.4 are:

L	[mm]	270
h_P	[mm]	148
V_0	[mm]	0.5

Table D.4 Bed velocities compared with physical model of Schmidt

SCHMIDT		NUMERICAL MODEL			
		Without zero velocity core		With zero velocity core	
x_s [cm]	v_b/V_0 [-]	v_b [m/s]	v_b/V_0 [-]	v_b [m/s]	v_b/V_0 [-]
2	0.26	0.185	0.37	0.155	0.31
3	0.34	0.21	0.42	0.183	0.366
5	0.4	0.215	0.43	0.194	0.388
7	0.39	0.199	0.398	0.18	0.36
9	0.39	0.174	0.348	0.157	0.314
11	0.36	0.156	0.312	0.14	0.28
13	0.34	0.142	0.284	0.126	0.252
15	0.31	0.13	0.26	0.114	0.228
17	0.26	0.119	0.238	0.104	0.208
19	0.19	0.11	0.22	0.095	0.19
21	0.12	0.1	0.2	0.087	0.174

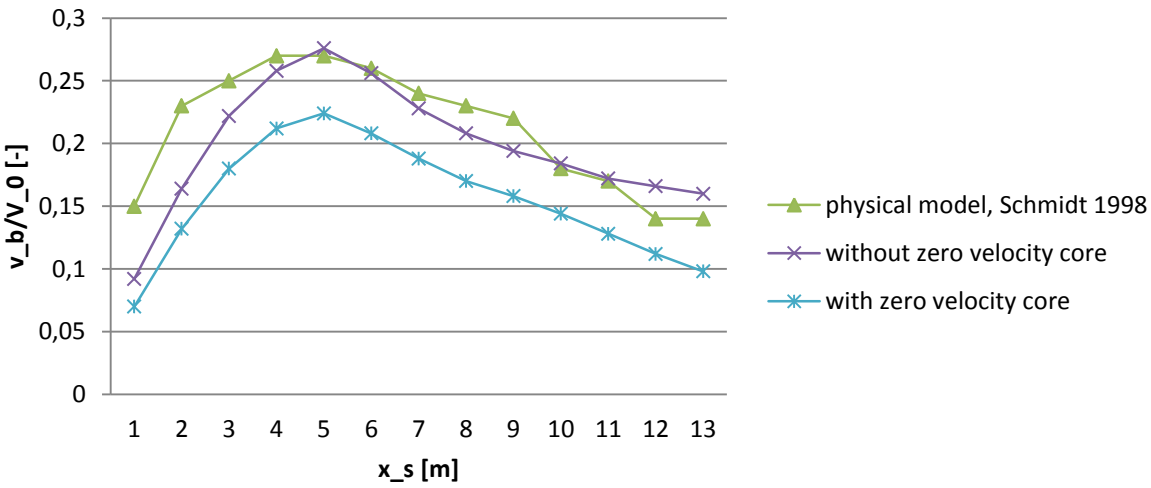

Figure D.8 Bed velocities compared with physical model of Schmidt 1998

Case 2.5

The geometrical properties of Case 2.5 are:

L	[cm]	37
h_p	[cm]	14.8
V_0	[m/s]	0.5

Table app D.5 Bed velocities compared with physical model of Schmidt

SCHMIDT		NUMERICAL MODEL			
		Without zero velocity core		With zero velocity core	
x_s [cm]	v_b/V_0 [-]	v_b [m/s]	v_b/V_0 [-]	v_b [m/s]	v_b/V_0 [-]
2	0.18	0.161	0.32	0.144	0.29
3	0.23	0.195	0.39	0.177	0.35
5	0.27	0.212	0.42	0.194	0.39
7	0.32	0.198	0.40	0.181	0.36
9	0.31	0.176	0.35	0.161	0.32
11	0.31	0.158	0.32	0.144	0.29
13	0.32	0.143	0.29	0.13	0.26
15	0.27	0.13	0.26	0.117	0.23
17	0.24	0.118	0.24	0.105	0.21
19	0.24	0.107	0.21	0.095	0.19
21	0.21	0.098	0.20	0.087	0.17
23	0.18	0.09	0.18	0.08	0.16

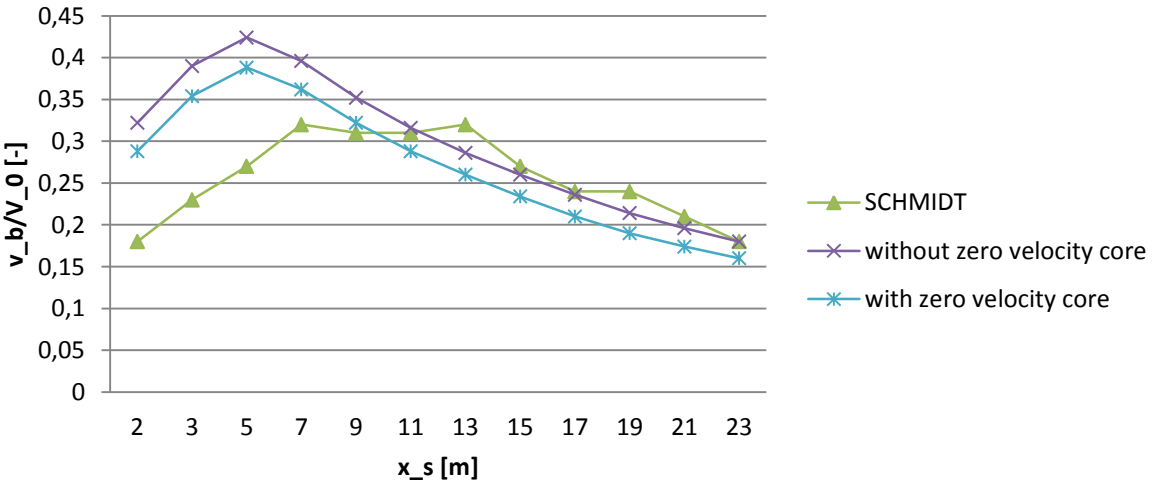

Figure D.9 Bed velocities compared with physical model of Schmidt 1998

Case 2.6

The geometrical properties of Case 2.6 are:

L	[cm]	49.5
h_P	[cm]	14.8
V_0	[m/s]	0.5

Table D.6 Bed velocities compared with physical model of Schmidt

SCHMIDT		NUMERICAL MODEL			
		Without zero velocity core		With zero velocity core	
x_s [cm]	v_b/V_0 [-]	v_b [m/s]	v_b/V_0 [-]	v_b [m/s]	v_b/V_0 [-]
2	0.11	0.19	0.38	0.105	0.21
3	0.15	0.209	0.42	0.137	0.27
5	0.19	0.215	0.43	0.163	0.33
7	0.21	0.206	0.41	0.157	0.31
9	0.22	0.176	0.35	0.142	0.28
11	0.2	0.151	0.30	0.128	0.26
13	0.22	0.137	0.27	0.116	0.23
15	0.23	0.129	0.26	0.105	0.21
17	0.21	0.12	0.24	0.094	0.19
19	0.19	0.108	0.22	0.085	0.17
21	0.19	0.093	0.19	0.077	0.15
23	0.21	0.072	0.14	0.07	0.14

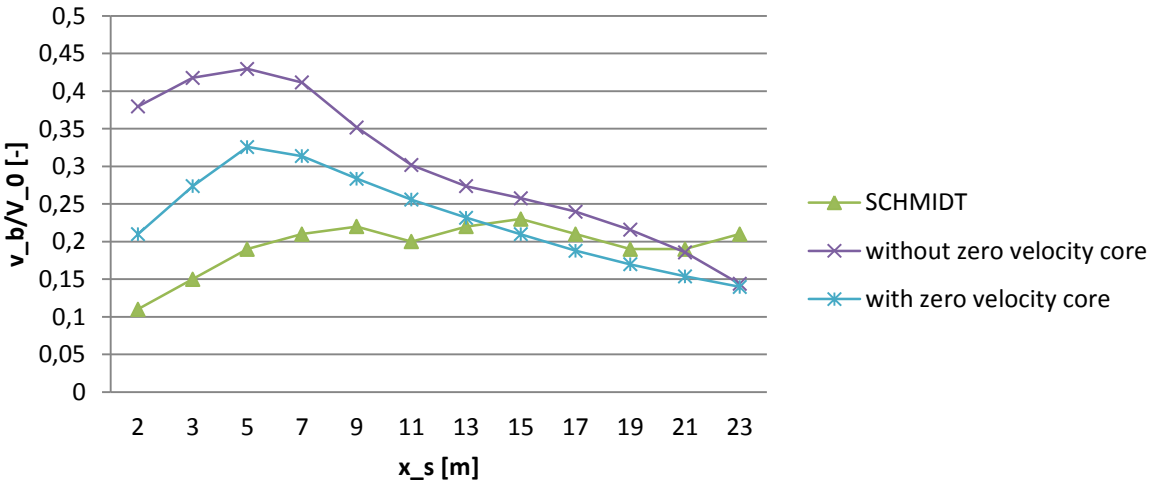

Figure D.10 Bed velocities compared with physical model of Schmidt 1998

Case 2.7

The geometrical properties of Case 2.7 are:

L	[cm]	37
h_P	[cm]	16.5
V_0	[m/s]	0.5

Table D.7 Bed velocities compared with physical model of Schmidt 1998

SCHMIDT		MODEL			
		Without zero velocity core		With zero velocity core	
x_s [cm]	v_b/V_0 [-]	v_b [m/s]	v_b/V_0 [-]	v_b [m/s]	v_b/V_0 [-]
2	0.16	0.17	0.34	0.116	0.23
3	0.26	0.204	0.41	0.15	0.30
5	0.29	0.218	0.44	0.172	0.34
7	0.35	0.202	0.40	0.162	0.32
9	0.31	0.175	0.35	0.143	0.29
11	0.28	0.154	0.31	0.126	0.25
13	0.27	0.138	0.28	0.115	0.23
15	0.24	0.125	0.25	0.106	0.21
17	0.21	0.114	0.23	0.098	0.20
19	0.18	0.104	0.21	0.09	0.18
21	0.17	0.095	0.19	0.082	0.16
23	0.16	0.088	0.18	0.076	0.15

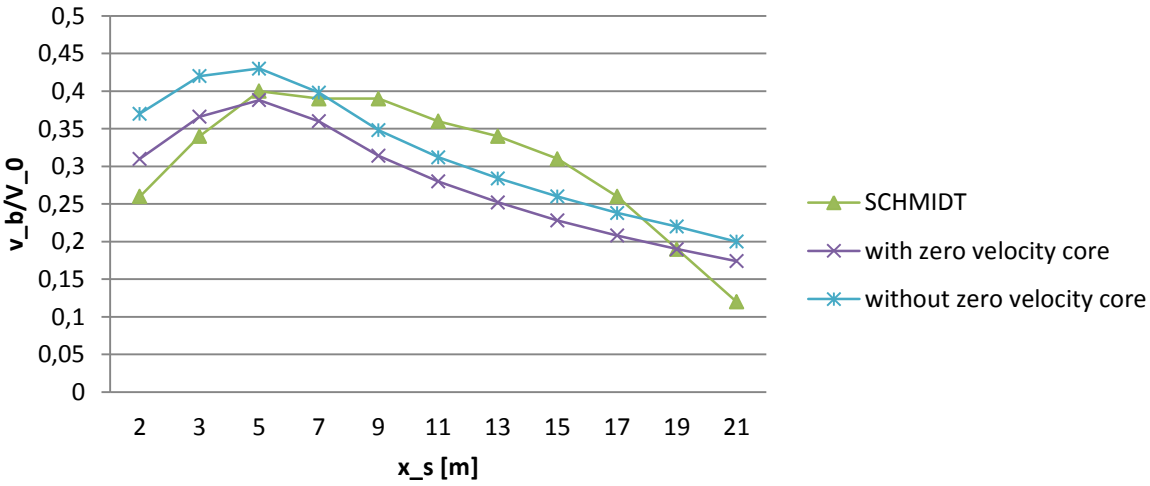

Figure D.11 Bed velocities compared with physical model of Schmidt 1998